The Thesis Committee for Luca Magenes
Certifies that this is the approved version of the following thesis:

Fatigue Assessment of High Mast Illumination Poles Using Field Measurements

APPROVED BY
SUPERVISING COMMITTEE:

Supervisor:

Todd Helwig

Karl Frank

Fatigue Assessment of High Mast Illumination Poles Using Field Measurements

by

Luca Magenes B.S.

Thesis

Presented to the Faculty of the Graduate School of

The University of Texas at Austin

in Partial Fulfillment

of the Requirements

for the Degree of

Master of Science in Engineering

The University of Texas at Austin

August 2011

Dedication

I dedicate my work to my family and to Valeria for the continuous love and support during these two years.

Acknowledgements

I would like to acknowledge Dr. Helwig and Dr. Frank for the support and motivation, my friends and colleagues Jeremiah Fasl and James Kleineck for the substantial contribution to this work, the sponsor of the project Texas Department of Transportation, and personally Michael Smith and Steve Eveland for the support during the field instrumentation trips. I also would like to thank Vasileios Samaras and Matt Reichenbach for taking part in one of the field trips and each one that helped me out in every little thing during the past two years at Ferguson Lab.

August 2011

Abstract

Fatigue Assessment of High Mast Illumination Poles Using Field Measurements

Luca Magenes, M.S.E.

The University of Texas at Austin, 2011

Supervisor: Todd A. Helwig

Failures of high mast illumination poles (HMIPs) in recent years have raised concerns on the long-term fatigue performance of the poles by various transportation officials around the US. The thesis documents a study sponsored by the Texas Department of Transportation focused on the fatigue behavior of in-service HMIP systems. This study is an extension of previous investigations on the fatigue behavior of the poles that have demonstrated that many poles have poor performance and fail in fatigue before the AASHTO category E' limit. Galvanized specimens were also tested and some of them showed evidence of initial cracking, impacting the fatigue performance such that the galvanized poles behaved worse than the uncoated specimens.

Ultrasonic Testing (UT) has shown several poles around the state of Texas contain cracks in the welds between the shaft and base plate. To further investigate the performance of the poles in-service, a field study was initiated to measure the wind speed and direction, as well as the corresponding stresses in the pole shaft. This thesis presents results from the field investigation.

A data acquisition system was developed to gather wind data and induced stresses. The system was powered by a solar panel and can be remotely accessed via a wireless modem. Data collected throughout the year details the intensity and number of stress cycles experienced by the poles, and could be correlated with the measured wind velocity. Using the field data, more accurate estimates of expected fatigue life for the poles were made. The study provides TxDOT with valuable data on the performance of in-service poles so that the most critical fatigue cases can be identified and proper decisions can be made on the appropriate inspection or repair schedule.

Table of Contents

List of Tables

List of Figures

Chapter 1 Introduction

1.1 Description of the problem

High Mast Illumination Poles (HMIPs) as shown in Figure 1,1. are multisided, hollow, cantilever poles that are typically used to provide light to highway intersections and other urban environments. The poles are typically 70 to 175 ft (22m to 54m) tall that are anchored to a foundation and support a lighting frame on top. The details and specifications for the design of these poles typically vary among different states.

Fig. 1.1 High Mast Illumination Poles in Houston, TX (courtesy of http://www.mckeehen.net/)

Following collapses of HMIPs in the US, The Texas Department of Transportation (TxDOT) began a campaign of ultrasonic inspections of in-service poles. TxDOT currently has pole designs with either 8-sided or 12-side pole shafts, depending on the pole height and design wind speed. The connection details between the shaft and the base plate can either be a full penetration weld or might also use a ground sleeve, which is a doubler plate that goes around the shaft as shown in Figure 1.2 (left). Though no collapses have occurred in Texas, several poles have been found with cracks at the shaft to base plate connection. The twelve-sided, 150 ft (46 m) high pole, designed for 80 mph (36 m/s) wind speed without a ground sleeve performed very poorly in laboratory tests (Pool, 2010). In these poles, the shaft is connected to the base plate with a full penetration weld that has a 3/8" (9.5 mm) root opening as shown in Figure 1.2 (right). Cracks were most prevalent near the bends of the shaft, at the top of the weld toe as shown in the photograph taken through the microscope in Figure 1.3. TxDoT has found that 100% of the inspected poles with these design features possessed cracks at one or more bends.

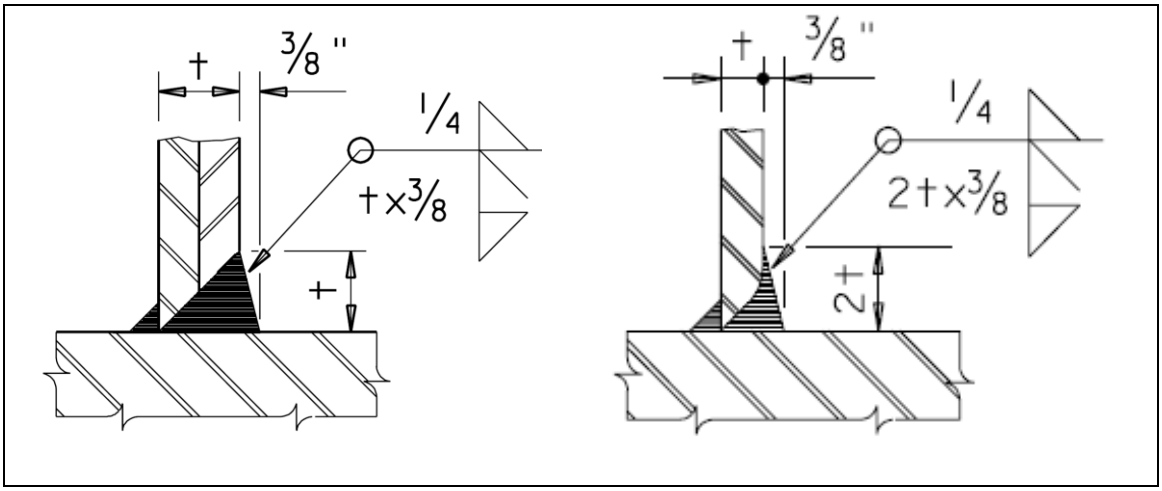

Fig. 1.2. Section view of the shaft to base plate connection, with the external collar (left) and without the external collar (right)

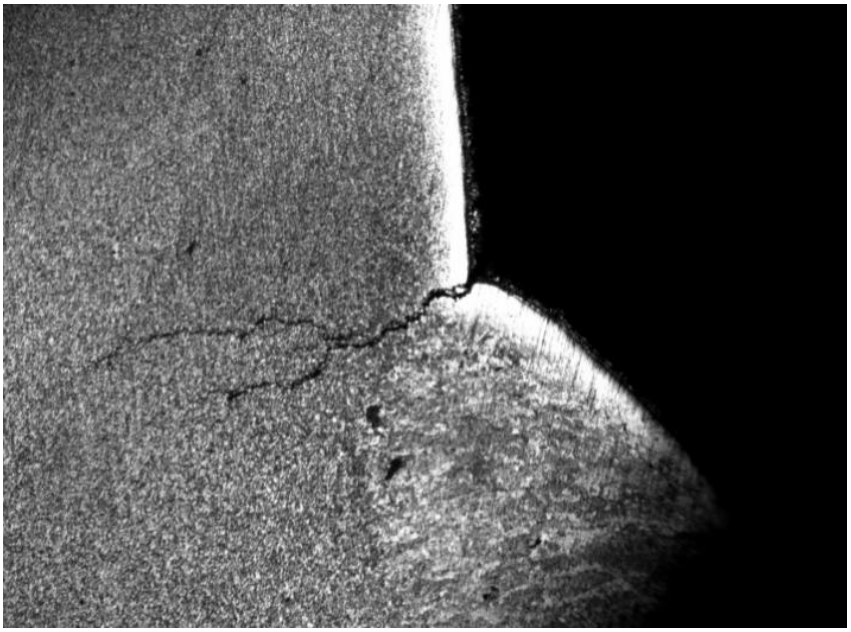

Fig. 1.3 Microscope picture of the crack location

1.2 High Mast Illumination Poles Failures

There have been a number of collapses of HMIPs reported around the US. A 140 ft tall HMIP along Interstate 29 in Sioux City, Iowa fractured at the shaft to baseplate joint in November of 2003 as shown in Figs. 1.4 and 1.5. The pole had a 1 ¼" thick baseplate, and a 3/16" thick shaft with a twelve-sided section.

Fig. 1.4. HMIP collapse in Sioux City, Iowa (MTC, 2007)

Fig. 1.5. Baseplate of the Collapsed HIMP in Sioux City, Iowa (Warpinski, 2007)

In November 2005 the 150 ft tall HMIP shown in Fig. 1.6 collapsed in Rapid City, South Dakota. The pole had a 1 ¾" thick baseplate and a 3/8" thick shaft. The pole had been installed only two years prior to the collapse.

Fig.1.6. HIMP Collapse in Rapid City, South Dakota (Rapid City Journal)

Fractures have also been reported on in illumination poles for recreational parks, schools, and outdoor stadiums. Many of these poles have heights ranging from 70 ft. to 135 ft. Nine incidents of these Stadium lighting poles have been confirmed by the Costumer Product Safety Commission from 2000 to 2006. One involved a pole falling through a roof of a school

gymnasium (Fig. 1.7), causing significant property damage. CPSC also confirmed that 50 other poles with this design developed fracture or cracks next to the weld joint with the base plate similar to the crack shown in Fig. 1.8.

Fig.1.7. Collapse of a stadium sighting Pole over a gymnasium (Left), and in a practice field (Right) (CPSC website)

Fig.1.8. Cracks above the weld toe in stadium sighting poles (CPSC website)

A common factor in these collapses is the crack location on the shaft directly above the weld toe. Previous investigations have confirmed the fatigue behavior of such cracks (Rios, Stam, Pool).

1.3 Scope of the study

The research documented in this thesis is part of a larger study focusing on both the cracking behavior during the galvanizing process as well as the in-service behavior of poles monitored

through field instrumentation. Results from the study during the galvanizing process are presented by Kleineck (2011), while this thesis focuses on the field monitoring.

The focus of the field instrumentation is to measure the response of HMIP's subjected to wind events at various locations throughout the state of Texas. The data targeted in the instrumentation included the speed and direction of the wind along with the corresponding stresses in the pole shaft. The wind and strain data can be compared to laboratory test results to provide a better estimate of the remaining fatigue life. Several High Mast Illumination Poles were instrumented around the State of Texas. The poles designs are similar, featuring a total height of 150 ft and a base diameter of 33″. The 3/8″ thick pole shafts were 12-sided and had a 33″ thick based diameter welded to a 3″ thick baseplate. One of the goals of the instrumentation was to monitor the behavior at various times through the year to obtain a better measure of the long-term performance. This long term data provides an indication of the amount of loading that the structures are subjected to during their service lives so that a fatigue life estimate can be carried out for the poles. The data is correlated to load test results obtained from previous work conducted at Ferguson Structural Engineering Laboratory at The University of Texas at Austin. Wind direction and velocity were also recorded so that a correlation between stress on the structure and the aerodynamic excitation could be made.

The data gathered over time was used to define a stress history that can be used to estimate an equivalent average stress that the HMIP will be subjected to during its service life. The use of this data with load test results are used to provide a good estimate of the remaining fatigue life for the poles of various designs and differing support conditions. These estimates will help TxDOT identify the most critical HMIP's that might require replacement, repair, or more frequent ultrasonic inspections. The experience gathered from this long-term instrumentation will also contribute to the development of reliable, remote data acquisition systems for long-term structural monitoring.

Chapter 2 Previous Research

2.1 Introduction

There have been a number of previous investigations on the behavior of HMIP systems. Because there have been a number of problems reported on the fatigue behavior of HMIP baseplate connections, much of the recent research has focused on the fatigue performance of various connection details. Previous research pointed out how the HIMP failures occurring around the US were fatigue type failures (Rios, 2007), and that the cracking initiated at the shaft to baseplate connection, at the bends of the shaft (Rios, 2007). This chapter provides a summary of the recent research as well as other background information necessary for understanding the material presented later in this thesis. The research discussed in this thesis is part of a series of research investigations that have been conducted at the University of Texas over the past several years. The following subsections focus on the results of these past studies. An overview of the dynamic behavior of HMIP sections along with background information on the impact of wind loads on pole sections is then provided.

2.2 University of Texas HMIP Research

The work that has been conducted at the University of Texas has focused heavily on the fatigue performance of various HMIP connection details. The work has included laboratory studies as well computational investigations. These studies demonstrated the impact of the base plate geometry and weld details on the fatigue performance. The research also showed that the galvanizing process that is used to improve the corrosion performance leads to small cracks in the welds between the shaft to base plate connection. These cracks have a significant impact on the long term fatigue performance of the HMIP connections and are the primary focus of the current stage of the research. The study on the cracking has focused on the behavior during galvanizing that has been discussed by Kleineck (2011) and the work documented in this thesis that is dedicated towards the behavior under wind loading in field conditions.

2.1.1 Fatigue Performance - Phase I

The research in fatigue testing of High Mast Illumination Poles at the Univeristy of Texas at Austin started in 2006. Specimens 14 ft long HMIP base sections designed with three different baseplate to shaft connection details where investigated that are referred to as the socket detail, the Texas detail, and the Wyoming detail. The connection details that were studied consist of the following:

- The socket connection is realized inserting the shaft in the base plate hole, and then fillet welded internally and externally as shown in Figure 2.1.
- The "Texas" detail is realized butting up the pole shaft to the baseplate, and welding internally with a fillet weld. A weld access hole is therefore necessary in the base plate. After the fillet weld is made, a full penetration weld is made between the shaft and the base plate from the outside.
- The "Wyoming" connection detail still uses a full penetration weld, but a backing bar is used on the inside of the shaft.

High Mast specimens with a 16 sided section were fatigue tested in the laboratory. The specimens had a base shaft diameter of 24", and featured different connection details, variable baseplate thickness, and different numbers of anchor bolts. The test setup consisted of two specimens that were attached back to back to a stiff reaction box as shown in Figure 2.2. The baseplates of the two specimens were connected at the middle of the setup to the reaction box, that was connected to a hydraulic ram that reacted on a load frame anchored to a reaction floor. The specimens were loaded at a frequency of 1.75 Hz in displacement control. The test was interrupted when a reduction of 10% in the force to obtain the maximum displacement was measured. The maximum displacement imposed was determined in such a way to cause a nominal stress range at the base plate section of 12 ksi. Results from these tests showed that:

- The "Texas" and Wyoming details had good performance, satisfying AASHTO fatigue category E' requirements
- The socket connection detail had a poor fatigue performance, far below AASHTO category E'
- Thicker base plate and higher number of bolts significantly increased the fatigue performance of the specimens

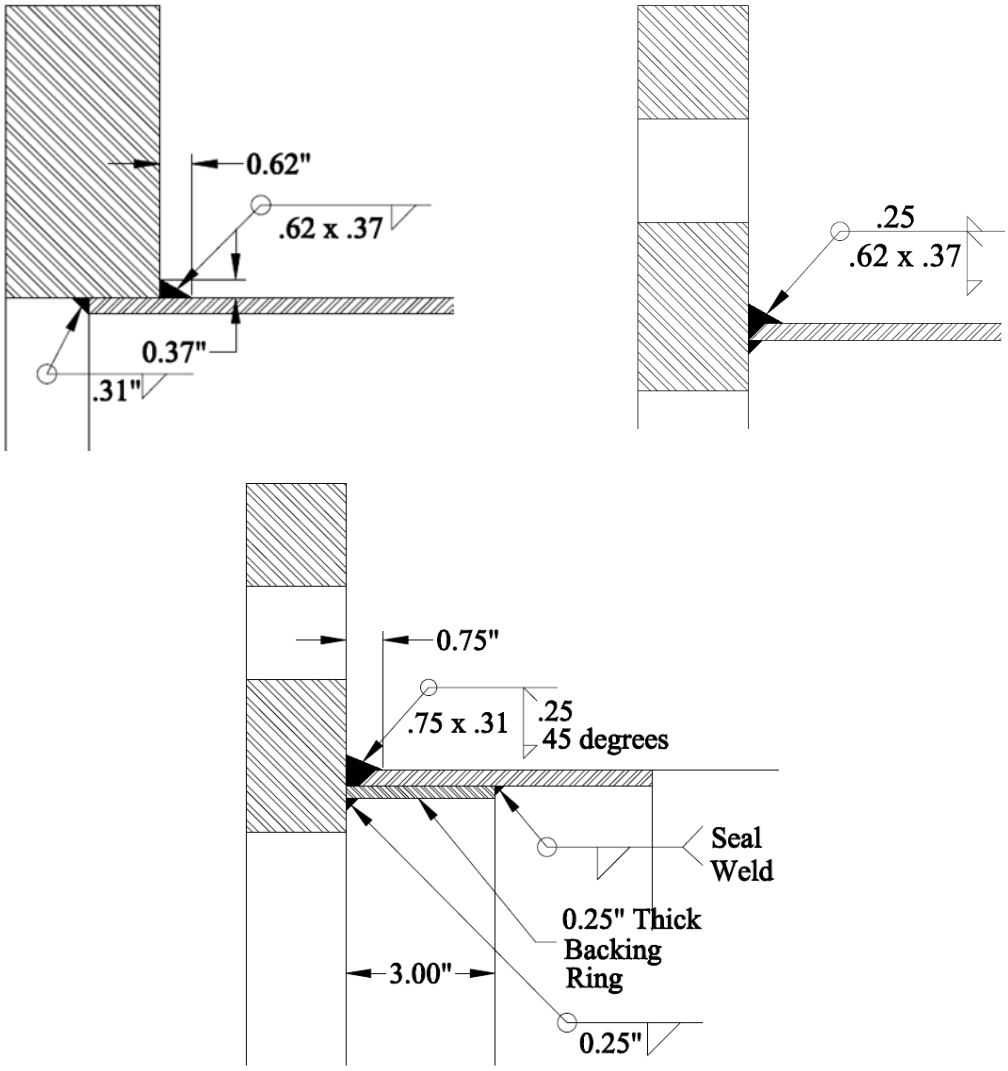

Fig. 2.1. Socket connection (top left), Texas connection (top right), Wyoming connection (bottom) (Rios, 2007)

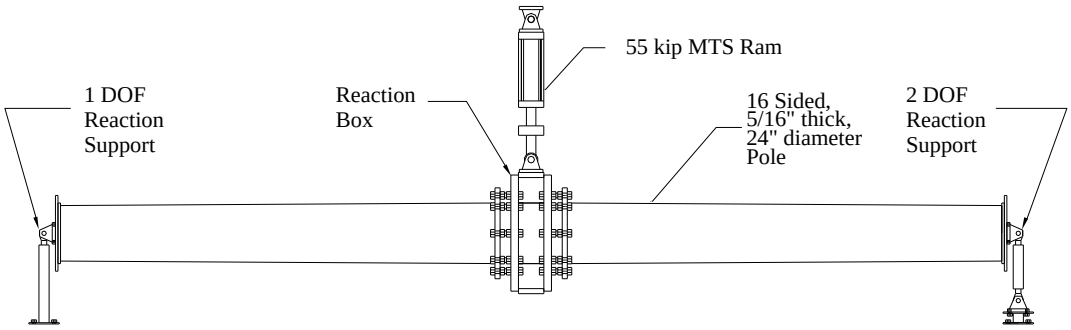

Fig. 2.2. Load Testing Setup (Rios, 2007)

2.1.2 Fatigue Performance - Phase II

The second phase of the fatigue testing were documented by Stam, 2009. Specimens tested in this phase of the study were fabricated and load tested with the same basic setup from the first phase of testing. The specimens utilized slightly modified details from the previous investigations. Some were fabricated with the use of an external collar that is referred to as a ground sleeve. The ground sleeve, depicted in Figure 2.4, serves as a doubler plate around the shaft.

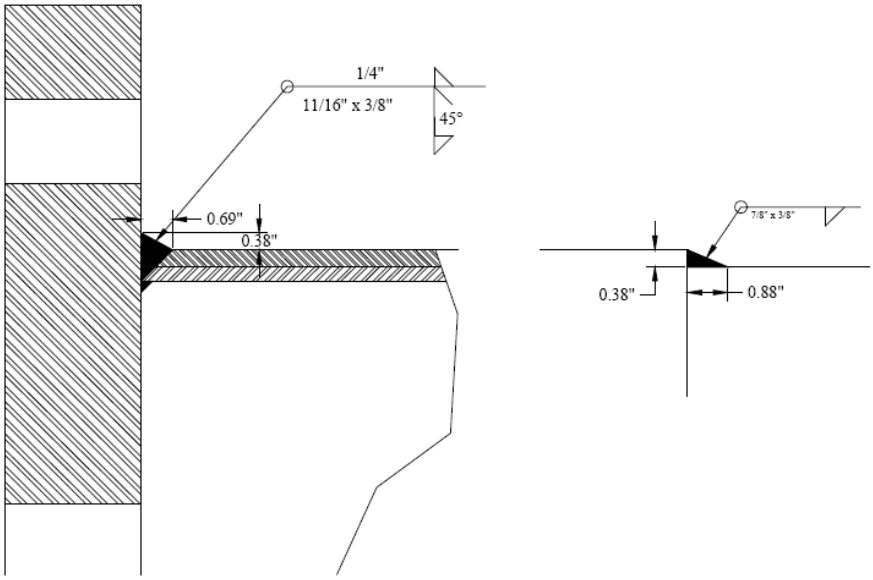

Fig. 2.3 Texas detail with External Collar (Stam, 2009)

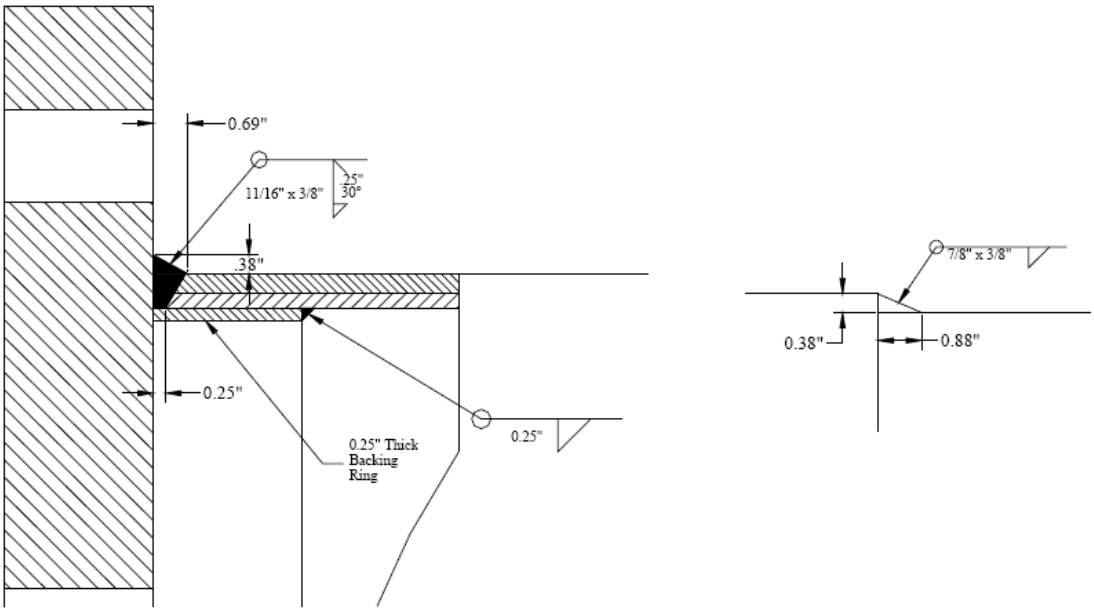

Fig. 2.4 Wyoming detail with External Collar (Stam, 2009)

Conclusions that were made from the second phase of testing consisted of the following:

- The Texas detail performance improved with External Collar and did not develop fatigue cracking even after passing AASHTO category C
- The Socket connection with a 3" thick base plate satisfied the AASHTO category D requirements
- Both the Texas and Wyoming details benefited from the reduction of baseplate inner diameter

The second phase of the research also included a three-dimensional finite element model that was developed in ABAQUS. The model was used to conduct a parametrical study to investigate the variations in the Stress Concentration Factor (SCF). The SCF provides a measure of the amplification of the nominal stresses at hotspots and provides an indication of the impact on the fatigue performance. The SCF were obtained by normalizing hotspot stresses ($\sigma_{Hotspot}$) with the nominal stresses ($\sigma_{Nominal}$):

$$SCF = \frac{\sigma_{Hotspot}}{\sigma_{Nominal}} \qquad \text{(Eq. 2.1)}$$

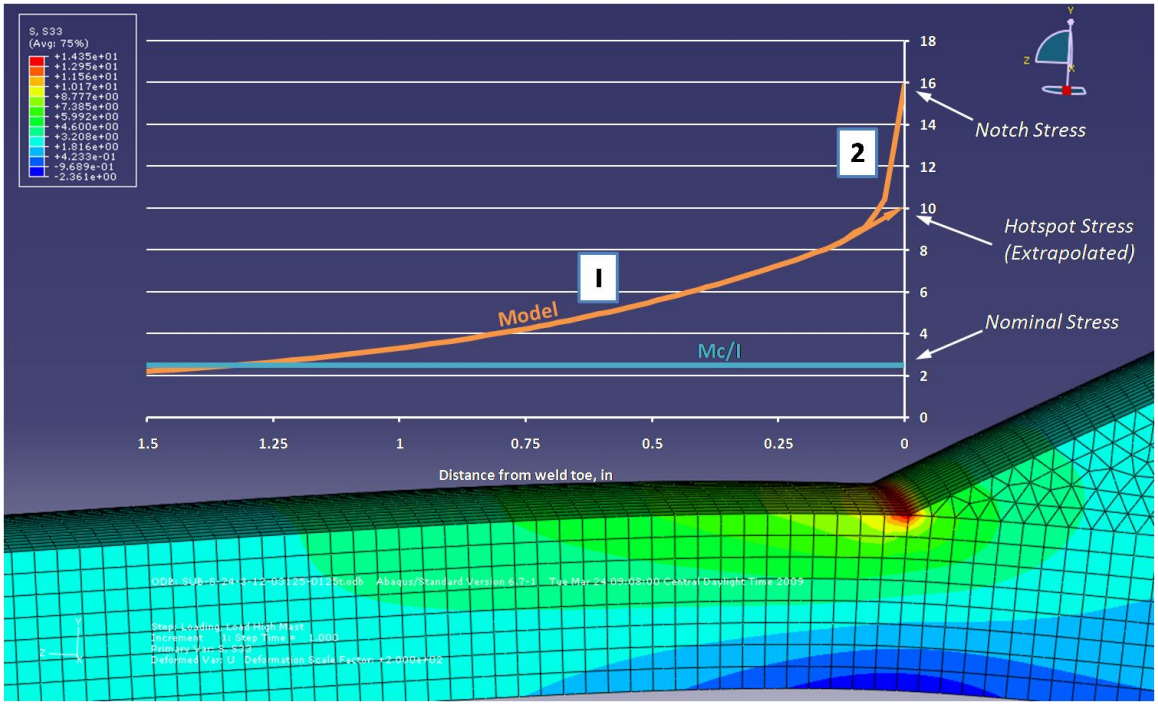

Fig. 2.5. Extrapolation of Hotspot Stress from Finite Element Model (Stam, 2009)

From the FEM parametric study the following conclusions where made:

- Increasing the shaft diameter or the shaft thickness results in a lower hotspot stress
- Adding anchor rods results in a SCF reduction when the connection is flexible (no external collar and thin base plate). The SCF does not change significantly with the number of anchor bolts when the 3 in. thick base plate was used.
- A smaller diameter of the internal baseplate diameter results in a smaller SCF
- Adding an external collar to a socket detail can reduce the SCF by up to 40%

2.1.3 Fatigue Performance – Phase III

The specimens that were fabricated and tested in the third phase of the study featured a 12 sided hollow section with a 33" base diameter. A 3" thick base plate with 12 anchor bolts was used and the shaft wall thickness was 5/16". The connection details studied in this phase focused on the Texas detail shown previously in Figure 2.1 and the Texas detail with external collar shown previously in Figure 2.2a. These specimens match the connections of the HMIP's that were instrumented on the field on the present study and widely used throughout the state of Texas. Therefore the results from these tests provide valuable information of the long term fatigue performance of the Texas poles in service. These information is useful for the evaluation of the fatigue performance that are presented in Chapter 5.

One of the specimens in the phase III testing was load tested prior to galvanization, in what is called "black" state. This test was performed to investigate the effect of galvanization on the fatigue performance of the HMIP. Concerns about the hot dip galvanizing process possibly causing micro cracking above the weld toe had been raised by Koenigs (2003). Koenigs investigated the fatigue performance of traffic signal mast arms, and noticed how galvanized connections exhibited a reduced fatigue life as compared to the non-galvanized connections.

A "field" repair procedure and a "shop" repair procedure were also developed. These were practical solutions for TxDOT to implement on in-service poles that were cracked. The shop repair procedure requires an extended preparation of the welding with a grind depth of half of the shaft thickness, and a length of two inches past the crack extent. The weld process is a flux core arc weld (FCAW). The field repair procedure was developed for poles already in service that are

found to be cracked. The surface preparation is similar to the one for shop repair, but the welding is a shielded metal arc welding (SMAW). More information about the welding procedures is provided by Pool (2010). Two HIMP specimens were repaired following each of these procedures and load tested.

Table 2.1 shows the list of specimens from the phase III testing. The "black" specimen that was load tested, but never failed, is not shown in the table.

Table 2.1 – Phase III HMIP fatigue testing specimens (Pool ,2010)

Specimen Code	Arm Diameter (in)	Arm Thickness (in)	Base Plate Thickness (in)	# of Bolts	Connection Detail	Galv.	Peened	Manufacturer
33-3-12-TX-SG-A	32.625	0.3125	3	12	Texas	Yes	No	Structural Metals
33-3-12-TX-SB-B	32.625	0.3125	3	12	Texas	Yes	No	Structural Metals
33-3-12-TX-VG-A	32.625	0.3125	3	12	Texas	Yes	No	Valmont
33-3-12-TX-VG-B	32.625	0.3125	3	12	Texas	Yes	No	Valmont
33-3-12-TX-VG-A (flip)	32.625	0.3125	3	12	Texas	Yes	No	Valmont
33-3-12-TX-VG-B (flip)	32.625	0.3125	3	12	Texas	Yes	No	Valmont
Field Repair	32.625	0.3125	3	12	Texas FCAW Repaired	Yes	No	Valmont
Shop Repair	32.625	0.3125	3	12	Texas SMAW Repaired	Yes	No	Structural Metals
33-3-12-TXEC-SG-A	32.625	0.3125	3	12	Texas w/ External Collar	Yes	No	Structural Metals
33-3-12-TXEC-SG-B	32.625	0.3125	3	12	Texas w/ External Collar	Yes	No	Structural Metals

Figure 2.6 shows the results of the load testing performed in Phase III. Both the specimens with the external collar connection did not fail to the test. The "shop" repaired specimen also never failed.

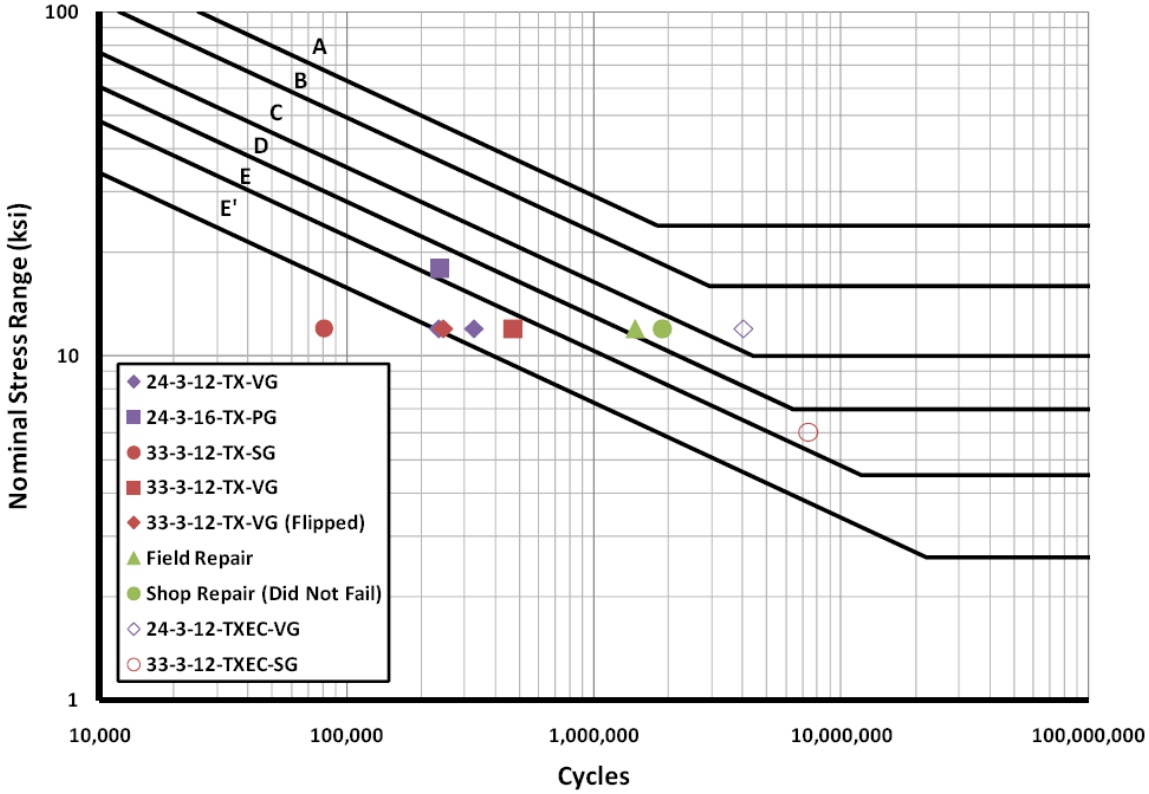

Fig. 2.6. Extrapolation of Hotspot Stress from Finite Element Model (Pool, 2010)

Conclusions that were reached from the Phase III study are as follows:

- The ultrasonic inspections performed on every pole before testing indicated that only poles that had been galvanized had initial cracking.
- The likely source of the cracking was from the galvanizing process.
- Initial cracking significantly reduces the fatigue performance of the poles with the Texas standard detail.
- The external collar provides improved fatigue performance of poles compared to poles without the external collar.

The conclusions from this study reflect exactly what it has been seen in the field from the ultrasonic inspections carried out by TxDOT on in-service HMIP around the state of Texas.

2.2 Thermal investigation during Galvanization

Initial cracks can propagate in-service due to wind loads acting on the HMIP's, significantly reducing the fatigue life of the poles and increasing the potential for collapse. The concerns raised by previous investigations about the initial cracking found after galvanizing, lead to a new phase of the project. The thermal study during galvanization is aimed to determine the causes of the initial cracking in HMIPs and is summarized by Kleineck (2011).

Fig. 2.7. HMIP specimen entering the zinc bath

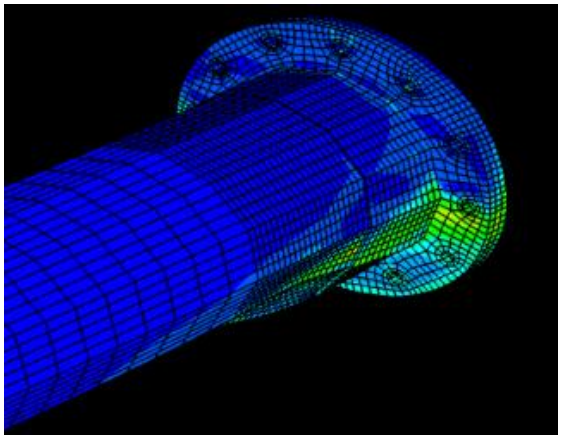

Fig. 2.8. FEM for Thermal Sudies

HMIPs are protected from corrosion by the hot galvanizing coating, which is formed by dipping the pole into a molten zinc bath at a temperature of approximately 840 °F (450 °C). The thermal stresses generated in the steel during this process were investigated with a three-dimensional finite element model developed with the software ABAQUS. The model recreates the molten zinc bath with a semi-space in which the steel element is subjected to heat transfer by conduction and convection. Measurements at galvanizing plants during the process were taken to study the behavior and also to provide validation data for the finite element model. The temperature of the steel was monitored in multiple locations during the galvanization of HMIP specimens. The measurements showed high temperature gradients between the baseplate and the shaft, that could result in high stresses in the material. In addition to demonstrating the behavior of the HMIP's during galvanizing, the data was used to validate the finite element model of the galvanizing process. Some of the modeling aspects that the data was used to help define were the coefficients

for the heat transmission equations, the correct angle at which the HMIP is dipped in the zinc bath, and the speed at which it is lowered in. Once the response from the model matched the conditions measured on-site, a parametric study was conducted to determine what parameters intervene in the likelihood of the HMIP to develop initial cracks.

Other important results were obtained by Ultrasonic Testing (UT) of the specimens. The specimens were inspected using UT techniques before an after galvanizing. The specimens were designed with similar geometries, but some had an external collar connection, while some did not. In the current TxDOT design for poles that are 150 ft tall, with a design wind speed of 80 mph, the shaft wall is 5/16" thick. The results (Tab. 2.2.) show how the use of an external collar reduces the amount of cracking caused by galvanizing.

Table 2.2. Ultrasonic Tests Results after Galvanization

Specimen Name	Shaft Wall Thickness (in)	Baseplate Thickness (in)	External Collar	Bends Cracked (%)	$\sum$ Crack Lengths (in)
33-3-12-TX-SG-C	5/16	3		100	27.6
33-3-12-TX-SG-SB	5/16	3		58	8.3
33-3-12-TXEC-SG-SA	5/16	3	√	58	7.7
33-3-12-TXEC-SG-B	5/16	3	√	25	8
33-3-12-TXEC-SG-SC	5/16	3	√	17	5

These results will be discussed in chapter 5, in correlation with the data obtained from the field. They will be used to define a fatigue performance of the in-sevice poles that are found to be cracked.

2.3 Wind Effects on High Mast Illumination Poles

HMIP are slender tall structures, with multisided or circular hollow sections, which are mainly subjected to wind loads. These loads are caused by buffeting from natural wind gusts and vortex shedding. Vortex shedding involves the generation of pressure differences normal to the wind direction, which cause the structure to oscillate transverse to the wind. The following sub-sections provide a brief discussion about wind engineering concepts.

2.3.1 Vortex Shedding

Vortex shedding occurs when alternating vortices are created on opposite sides of an object. The creation of vortexes next to the object depends on the regime of flow, which is determined by the Reynolds number R_e:

$$R_e = \frac{U \cdot D}{\nu} \qquad \text{(Eq. 2.2)}$$

Where, U is the wind velocity

D is the diameter of the cross section

ν is the coefficient of kinematics fluid viscosity (1.56×10^{-4} ft^2/sec for air)

Vortex shedding occurs with $300 < R_e < 3.5 \times 10^5$, and the regime is fully turbulent.

For vortex shedding to excite the structure, the vortex frequency has to be close to a natural frequency of the structure. When this happens, the structure will be locked-in a resonant state with the vortex shedding. The critical wind speed for vortex shedding is given by:

$$U_{Lock-in} = \frac{f_n \cdot D}{S_t} \qquad \text{(Eq. 2.3)}$$

Where, $U_{Lock-in}$ is the wind velocity for Lock-in

D is the diameter of the cross section

S_t is the Strouhal number, a constant that depends on the cross section shape.

To determine the dynamic load acting on the HMIP due to vortex shedding a model developed by Scanlan can be used (Simiu and Scanlan, 1996). The model assumes that the vortex shedding excitation is a sinusoidal process, and thus the forcing function is a harmonic.

The maximum displacement occurred during vortex shedding excitation depends on the mass and damping properties of the structure. The Scruton number S_c combines these two properties in a unique quantity:

$$S_c = \frac{m \cdot \zeta}{\rho \cdot D^2} \qquad \text{(Eq. 2.4)}$$

Where, m is the mass per unit length

ζ is the critical damping ratio

ρ is the air density

D is the diameter of the cross section

The following empirical relationship can be used to determine the maximum displacement under vortex shedding excitation as a function of the Strouhal number and the Scruton number (Simiu and Scanlan, 1996):

$$\frac{y_0}{D} = \frac{1.29}{[1 + 0.43 \cdot (8\pi^2 \cdot S_t^2 \cdot S_c)]^{3.35}} \qquad \text{(Eq. 2.5)}$$

Where, y_0 is the maximum displacement

S_t is the Strouhal number

S_c is the Scruton number

D is the diameter of the cross section

2.3.2 Buffeting

The term buffeting indicates an unsteady loading caused by the wind on the structure, by flow velocity fluctuations. The dynamic excitation of the structure due to buffeting increases with the flow speed, and it is not limited to the natural frequencies of the structure as in vortex shedding.

2.3.3 Static Parameters

The static action of the wind under steady conditions can be simplified by a drag force F_D acting in the direction parallel to the wind, and a lift force $F_L$acting transversally to the wind. The drag coefficient C_D and the lift coefficient C_L need to be defined:

$$C_D = \frac{F_D}{\frac{1}{2} \cdot \rho \cdot U^2 \cdot A} \quad \text{(Eq. 2.6)}$$

$$C_L = \frac{F_L}{\frac{1}{2} \cdot \rho \cdot U^2 \cdot A} \quad \text{(Eq. 2.7)}$$

Where, ρ is the air density

U is the wind velocity

D is the diameter of the cross section

2.3.4 AASHTO Wind Design Specifications

The AASHTO Specifications (AASHTO, 2001) target a design life of 50 years for luminary support structures.

The design wind pressure P_z is computed as:

$$P_z = 0.00256\, K_z\, G\, V^2 I_r C_D \quad \text{(psf)} \quad \text{(Eq. 2.8)}$$

Where, K_z is the height exposure factor, which is equal to 1.37 for a height of 150 ft

G is the gust effect factor, which shall be taken as a minimum of 1.14, or calculated following more complex procedures presented in ASCE 7 (ASCE, 2005).

V is the basic wind speed (80 mph, or 100 mph for the HMIPs considered in this study)

I_r is the wind importance factor, which is taken as 1 for a design life of 50 years

C_D is the drag coefficient, and for a dodecagonal ranges from 0.79 to 1.20 as demonstrated in the graph shown in Fig.2.9.

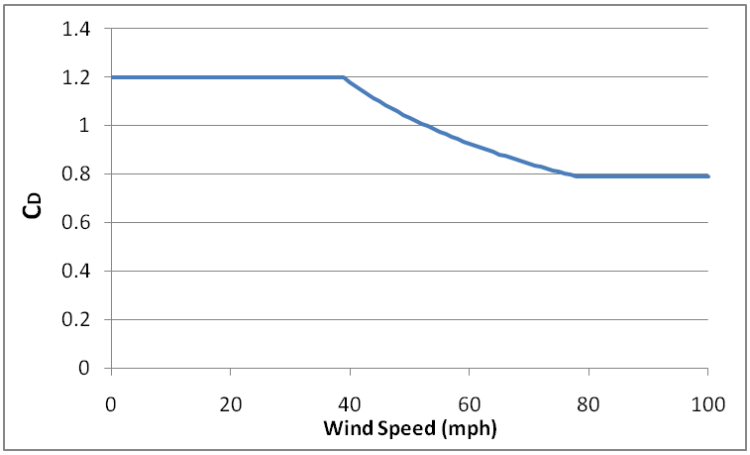

Fig. 2.9. Drag Coefficient for a Dodecagonal section as suggested by (AASHTO, 2006)

AASHTO only requires that the vortex shedding action is considered for non-tapered structures, or structures having a taper (diameter diffenece over length) less than 0.14 in/ft. The taper of the HMIP considered in this study is roughly 0.17 in/ft, thus vortex shedding design is not required.

The equivalent static wind pressure range for fatigue is then calculated as:

$$P_{VS} = 5.2\, C_D I_F \qquad \text{(psf)} \qquad \text{(Eq. 2.9)}$$

Where, I_F is the fatigue importance factor, which is taken as 1.0 for HMIPs installed on major highways

C_D is the drag coefficient, and for a dodecagonal ranges from 0.79 to 1.20 as shown in Fig.2.9.

For non-tapered poles, the fatigue design is carried out considering the vortex shedding critical wind speed V_C for the first natural mode of the structure, which is $U_{Lock-in}$ from equation 2.3. AASHTO suggests the Strouhal number to be taken as 0.18 for circular sections, and 0.15 for multisided sections. The equivalent static pressure range to be used for the design of vortex shedding induced loads is:

$$P_{VS} = \frac{0.00118\, V_C^2\, C_D I_F}{2\,\beta} \qquad \text{(psf)} \qquad \text{(Eq. 2.10)}$$

Where, V_C is the vortex shedding critical wind speed for the first natural mode of the structure

β is the critical damping ratio, which is conservatively taken as 0.005

I_F and C_D as defined in equation 2.9.

2.3.1 Iowa Study

An interesting study funded by the Iowa Department of Transportation (IDT) and Midwest Transportation Consortium (MTC) was carried out at Iowa State University (Warpinski, 2006) (MTC, 2007). Failures of HMIPs occurred in Iowa, as shown in Chapter 1. These failures demonstrated a lack of knowledge in design specifications such as AASHTO. The study developed with a field investigation on in-service poles, wind tunnel testing, and analytical modeling of the induced wind loads, was aimed to reevaluate the current equations used for the design of HMIPs.

Wind tunnel tests were performed on a 12-sided cylinder to calculate aerodynamic parameters. The testing model was a 20" long wooden cylinder with a 12-sided cross section. The model was secured transversally to the wind flow (Fig. 2.10) by mean four chains attached to coil springs. Two leaf springs where also used to fix the model in the wind direction. To measure the drag coefficient the coil springs where replaced by fixed supports, to restrain the model in the wind direction. The force was measured by transducers at the extremities of the springs.

The Strouhal number was measured to be 0.2, which is different from the value specified in AASHTO. The drag coefficient was measured at flow regimes with R_e ranging from 2.5×10^4 to 2.25×10^5, and was found to vary from 1.4 to 1.6 (Fig.2.11.)

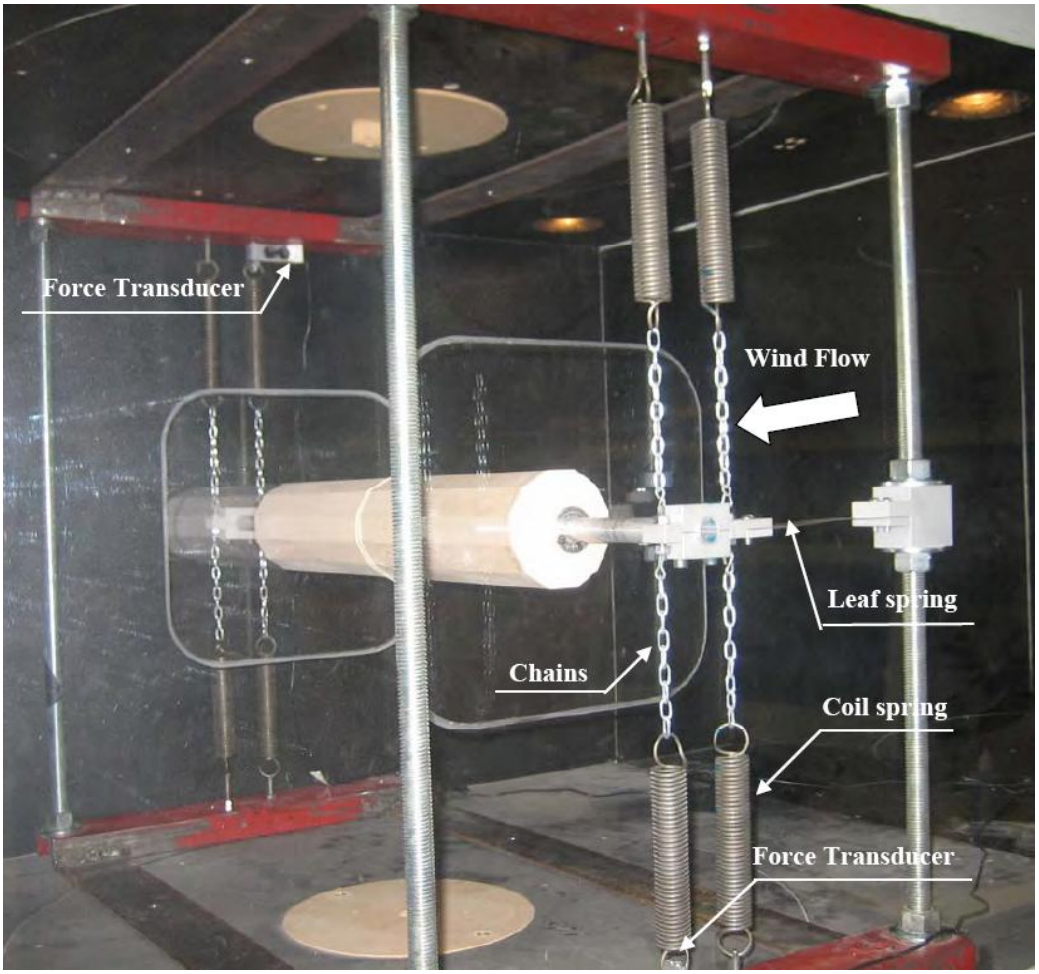

Fig.2.10. Wind Tunnel Testing Setup from the Iowa Study (MTC, 2007)

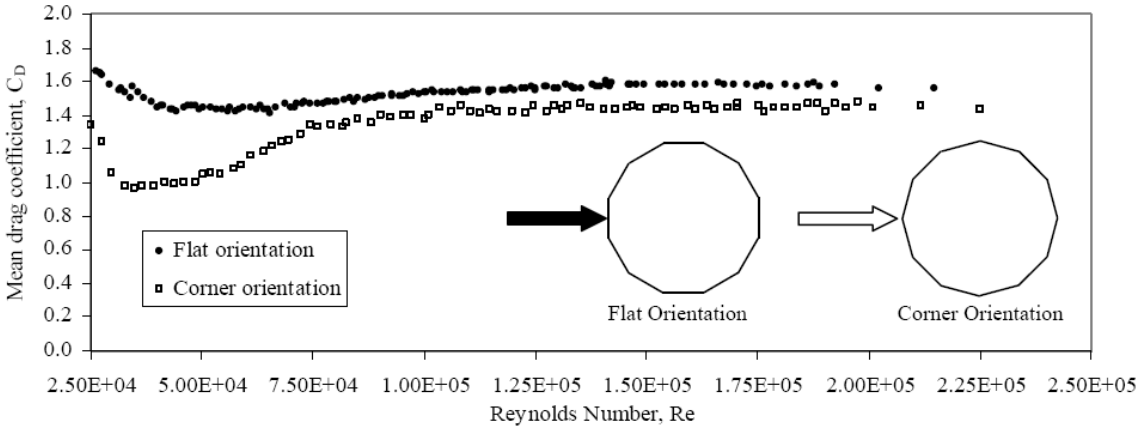

Fig. 2.11. Measured Drag Coefficient for a 12-sided section (MTC, 2007)

Field instrumentation and monitoring was performed on two HMIP in Northern Iowa, in high wind locations. One of the HMIP's was located in Sioux City and another in Mason City. The HIMPs were 148 ft tall, with a 12-sided cross section, a 0.313 in thick shaft having base diameter (measured flat side to flat side) of 28.5" and a top diameter of 8.77" (0.14in/ft taper). The base plate was 1.25 in thick and was anchored to the foundation by six 2.25 in diameter bolts.

The instrumentation consisted of anemometers, accelerometers and strain gages. One of the poles was instrumented with three anemometers distributed along the height of the structure and six strain gages. For the second pole, one anemometer, four accelerometers and fourteen strain gages were used.

The accelerometers allowed a measurement of the natural frequencies of the pole: 0.388Hz, 1.34Hz, 3.41Hz, 6.70 Hz, respectively for the first four modes of vibration (MTC, 2007).

The damping ratio was measured using a pluck test, which consists in exciting the structure with an impulsive force and measuring the dynamic response. This was done pulling and releasing a cable attached to the pole at a suitable height. Table 2.3 shows the measured modal frequencies of the pole, obtained by a Fast Fourier Transform (FFT) of the recorded motion. Also shown are the frequencies calculated analytically from a Finite Element Modeling (FEM) of the Structure (Warpinski, 2007). The values of the damping ratio were found to be lower than the value specified by AASHTO for design calculations.

Tab. 2.3. Modal Frequencies and Damping Ratios (MTC, 2007)

Mode	FEA	FFT	Difference	Damping ratio [86]
1	0.338	0.305	10.82%	0.60%
2	1.337	1.294	3.32%	0.17%
3	3.407	3.333	2.22%	0.27%
4	6.702	6.396	4.78%	0.30%

From the long term field monitoring it was observed that buffeting excitation was prevalently in the first natural mode of the HMIP, while vortex shedding excitation was observed in the second

mode of vibration. The critical wind velocity for vortex shedding in resonance with the second mode was computed to be approximately 6.5 mph. Vortex shedding induced vibrations were observed at a wind speeds ranging from 3 to 8mph. The strain gage measurements showed that the maximum vortex shedding induced stress range exceeded the constant amplitude fatigue limit of 2.6 ksi, as defined for AASHTO Category E' detail. The pole had a socket type connection that is classified with the lowest fatigue performance, and has been observed to perform poorly in fatigue (Stam, 2009). Figure 2.12 shows how the stress level in the wind transverse direction has a peak at the vortex shedding critical velocity of approximately 6.5 mph.

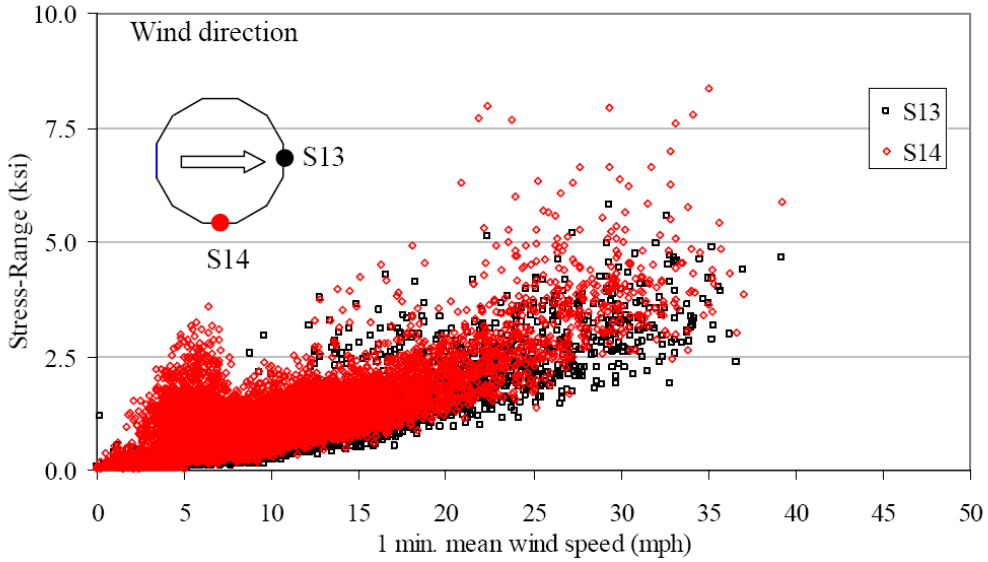

(g) Channels S13 and S14 at 5.75 ft from base

Fig. 2.12. Measured Stress Range vs. Wind Speed from Iowa Study (MTC, 2007)

The highest stress range measured during the long term instrumentation was 12.6 ksi, at a height of 5.75 ft from the base plate. High stresses were caused by buffeting in the first mode of vibrations in presence of wind speeds higher than 20 mph. Since the cumulative frequency of occurrence of wind stronger than 20 mph was lower than 5% on a period of 15 months, buffeting was not believed to b contribute significantly to fatigue damage of the pole. Figure 2.12 shows the average wind speed frequency of occurrence at the instrumented site.

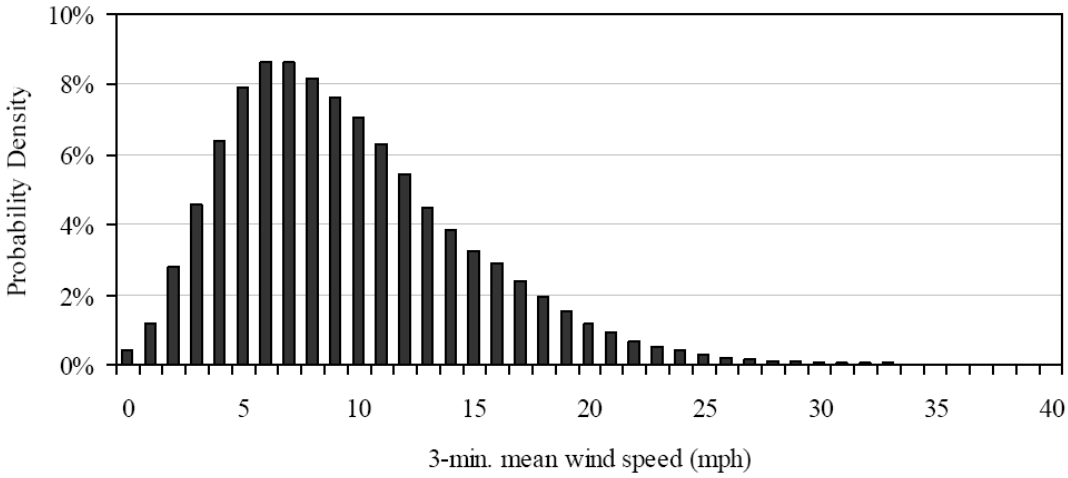

(a) Probability density

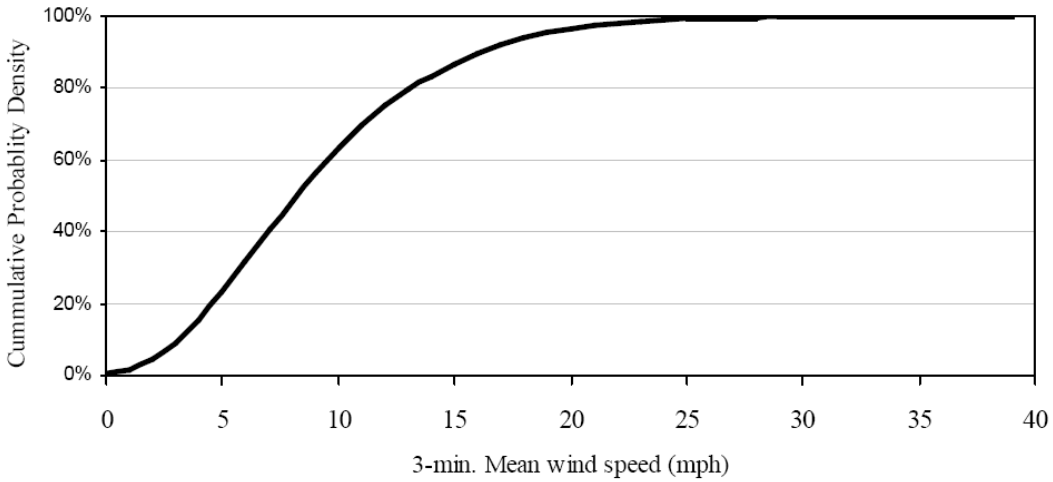

(b) Cumulative probability density

Fig. 2.13. Probability Distributions of Mean Wind Speed in Sioux City (MTC, 2007)

A mathematical dynamic model was then developed for the combined response to buffeting and vortex shedding (Chang et al., 2009). Figure 2.13 shows the predicted stress range on the pole in parallel and perpendicular to the wind direction.

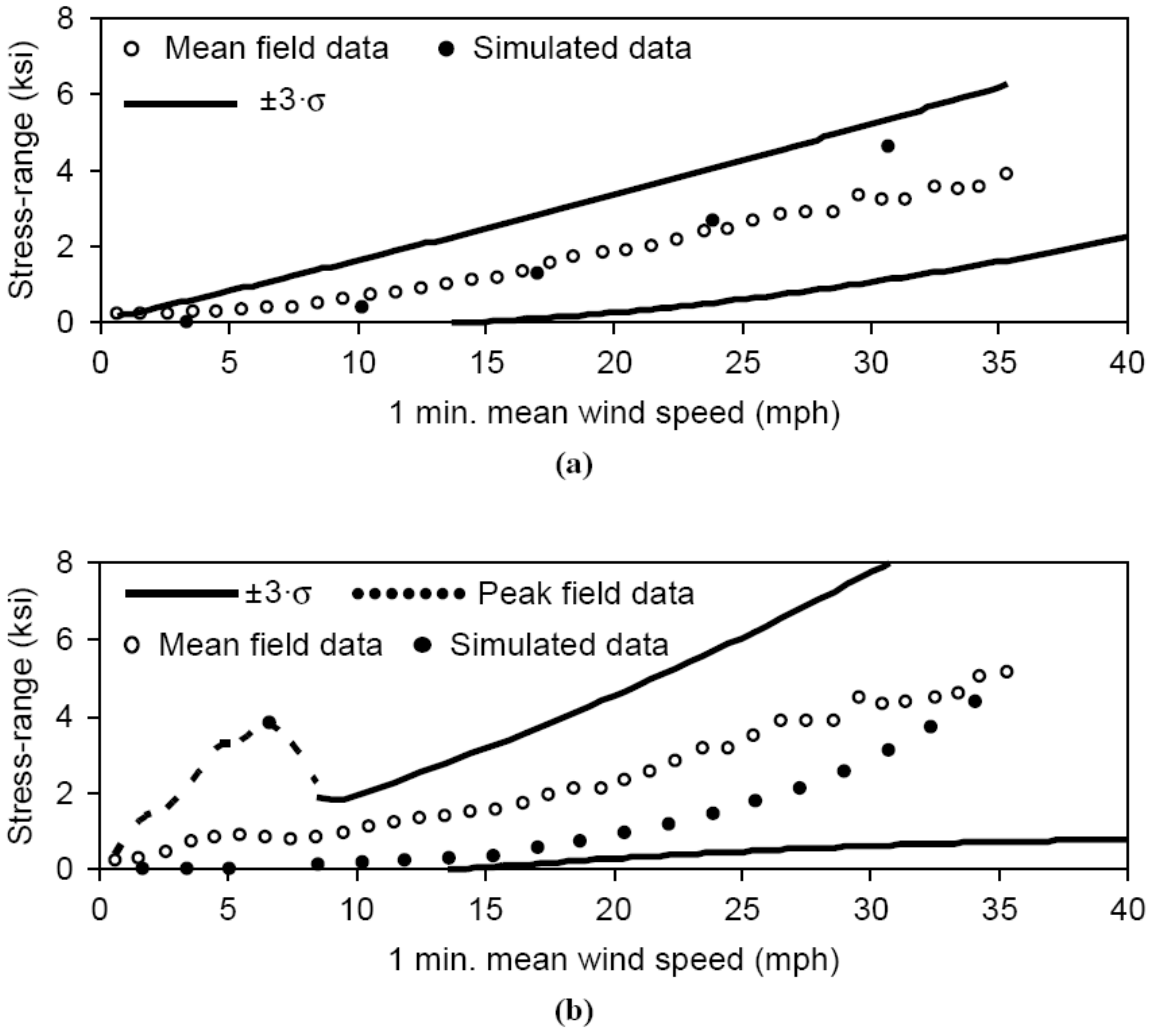

FIGURE 7 Simulated stress ranges: (*a*) along-wind response and (*b*) across-wind response.

Fig. 2.13. HMIP analytical model response (Chang et al., 2009).

In Chapter 5, these results are discussed and compared with the results of the field measurements obtained from studies of HMIP's in Texas.

Chapter 3 Filed Instrumentation

3.1 Objective of the Instrumentation

The objective of the field instrumentation was to collect long term stress and wind data from multiple poles located around the state of Texas. Four Poles were instrumented and monitored with a system that was accessible via a modem with a cellular link. Energy harvesting was necessary to recharge the batteries that powered the system.

A total of five HMIPs were instrumented at four sites around the state of Texas as indicated in the wind activity map shown in Figure 3.1. The activity map winds indicated on the map represent the average wind speeds throughout the year. The instrumented locations include the following sites:

1. Austin, Mo-Pac @ Parmer Ln.
2. El Paso, IH-10 @ Brown St.
3. El Paso, US-54 @ Hercules St.
4. Corpus Christi, IH-37 @ SH-286
5. Lubbock, US-62 @ SH-289

The site locations were selected in an attempt to capture the wide range of exposure conditions in the state of Texas. The Austin location was primarily selected for convenience to evaluate the system; however the location is also representative of the conditions found in several areas around the state. The El Paso site included poles with significant cracking positioned in the desert mountains of Texas. Lubbock is located in the Texas high plains. The relatively flat region experiences significant wind throughout the year. The final location that was selected was in Corpus Christi, which is an area representative of the Texas Coast. Figure 3.2 shows the base section of the instrumented HMIP in Austin. Although the connection detail in the five poles varied, the basic geometry of the poles were similar. The poles had twelve-sided shafts with a base diameter of 33" and a height of 150 ft. The pole in Corpus Christi had the external collar

connection between the shaft and base plate, while the other poles had the standard Texas connection with the full penetration weld.

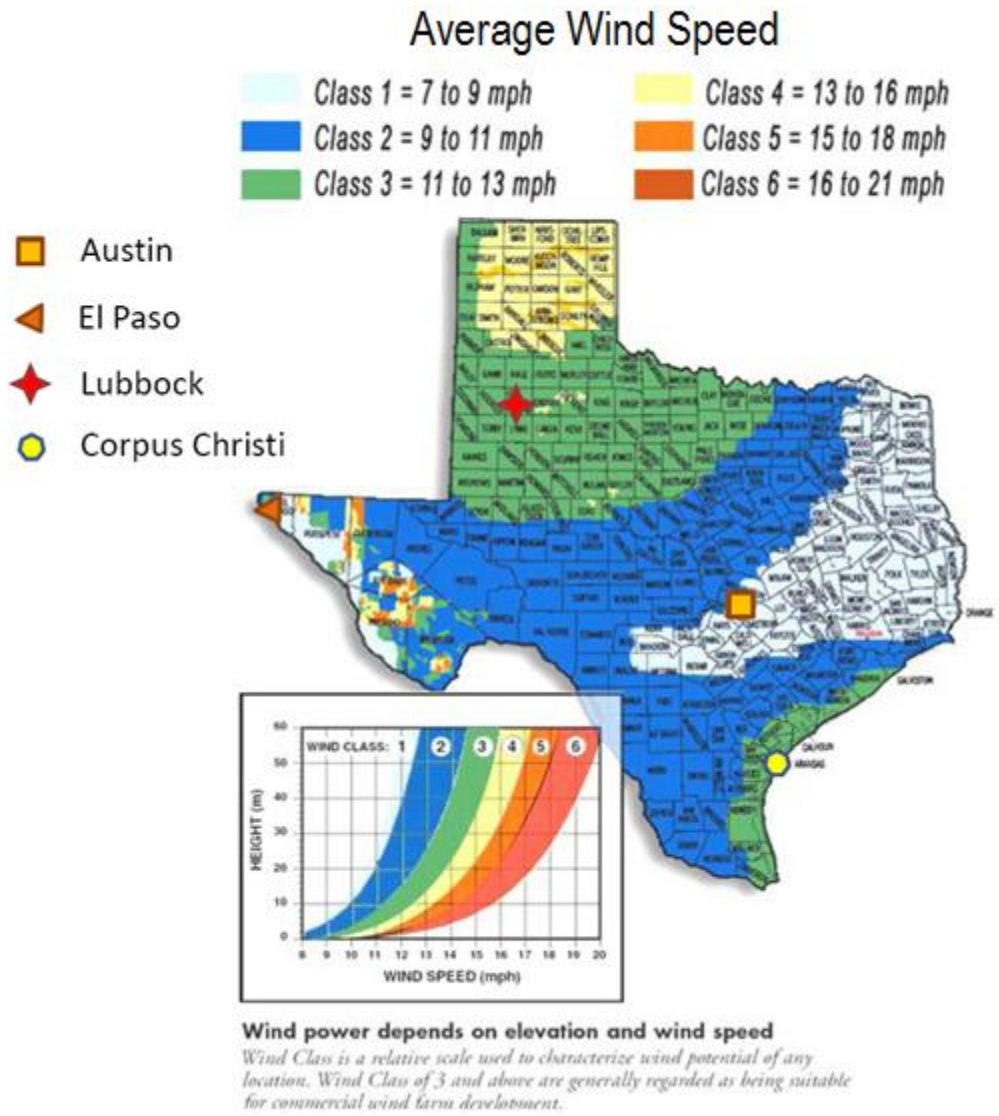

Fig. 3.1. Location of instrumented HMIPs on a wind activity map (www.whisperenergy.com)

Fig. 3.2. Typical 12 Sided Pole instrumented (Austin, TX).

3.2 Hardware

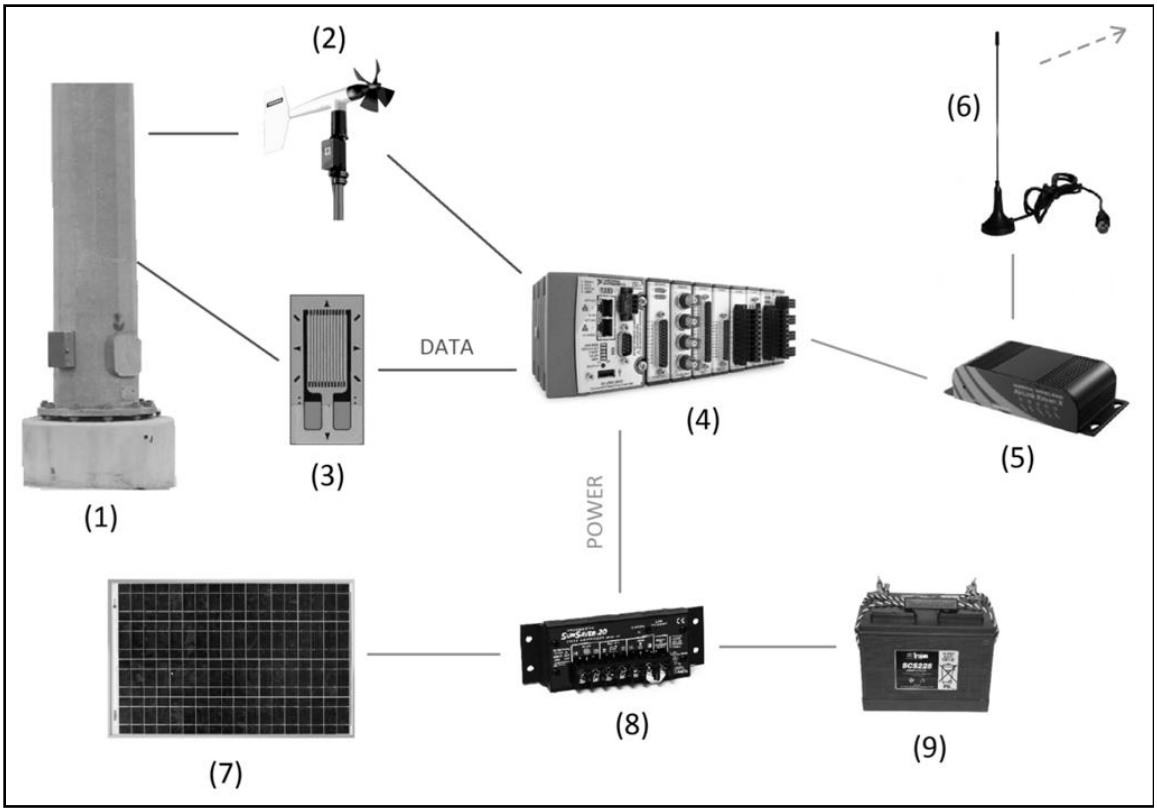

Fig. 3.3. Scheme of the Instrumentation: (1)High Mast Pole, (2)Anemometer, (3)Strain Gages, (4)DAQ, (5)Wireless Modem, (6)Antenna, (7)Solar Panel, (8)Charge Controller, (9)Battery

The instrumentation that was used in the field included sensors, data acquisition, a power source, and an energy harvesting system for recharging. Figure 3.3 shows a schematic representation of the instrumentation setup. The sensors included strain gages and an anemometer that were attached to the HMIP (1). The strain gages (3) provided a measure of the stresses induced from wind acting on the pole, while the anemometer (2) provided the corresponding wind speed and direction. The sensors were monitored with a data acquisition system (DAQ) (4) that was programmed to record, process and store the data. A wireless modem (5) with an antenna (6) was provided so that the system could be configured remotely and data could be downloaded. The system was powered by a 12V battery (9), which was charged by a solar panel (7). A charge controller (8) was provided to control the charge transfer between the solar panel, battery, and the

data acquisition system. A plan view (Fig.3.4) of the setup in the El Paso Pole on IH-10 shows the location of the anemometer brace and the four strain gauges on orthogonal faces named N,S,E,W. A discussion of each of the components of the system is provided in the following subsections.

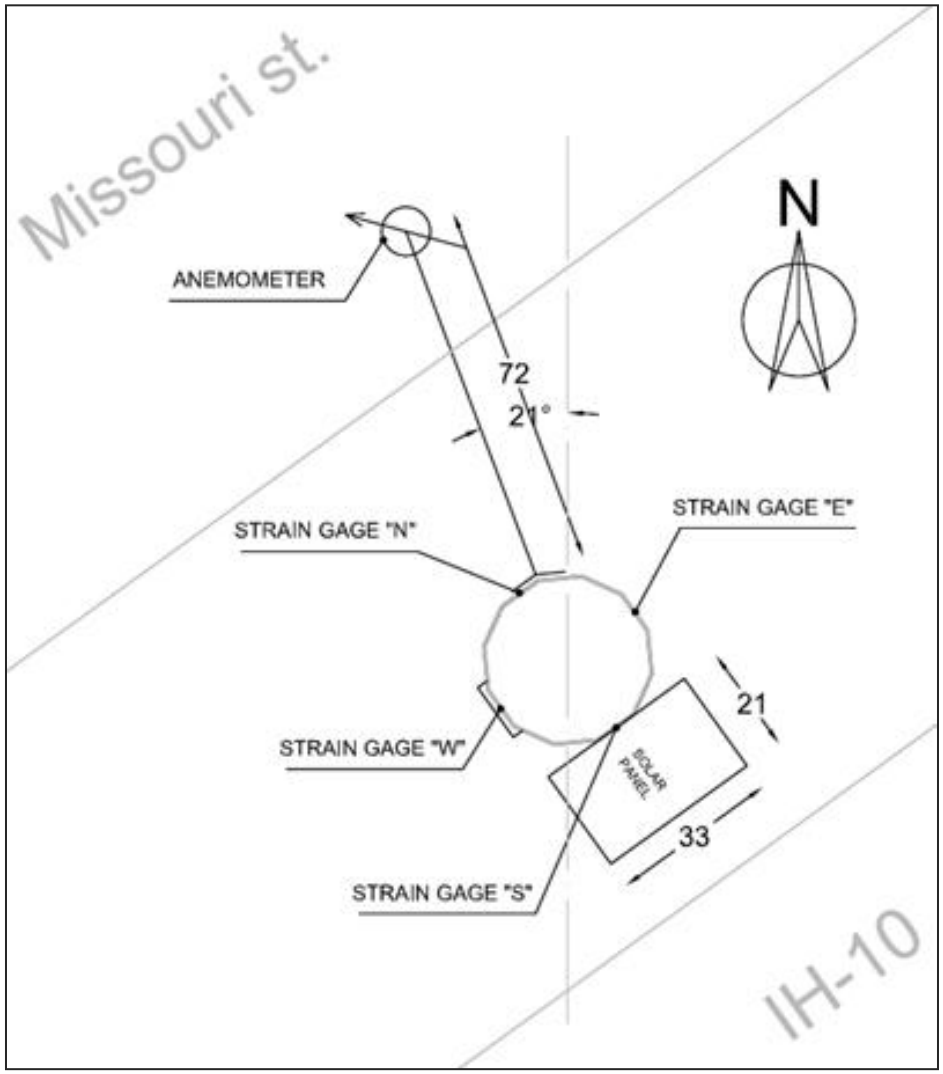

Fig. 3.4. Plan view of the instrumentation on IH-10 (El Paso, TX)

3.2.1 Stress Measurement

Foil strain gages with a 350 ohm resistance were installed on the HMIPs to measure wind-induced stresses. Four gages were installed on orthogonal faces of the pole at a height of 76" (193 cm) from the base plate. The gages were installed above the access door to minimize the effect to the stress distribution caused by the access panel opening on the shaft. The installation of the gages required the removal of the galvanizing over a region that is approximately one square inch in area at each gage location. A two part adhesive was used to install the gages. The adhesive consists of a Cyanoacrylate component that is applied to the surface as well as a catalyst that is applied to the back of the gage. After the gages were bonded to the pole shaft, microcrystalline wax was installed along with a layer of silicon to protect the gages from weathering and moisture. The galvanic protection to the shaft was restored using zinc spray paint following the removal of the gages.

3.2.2 Wind Measurement

The speed and direction of the wind was monitored using the Wind Monitor Model 05103 anemometer manufactured by Young. The anemometer consists of a four-blade helicoid propeller as shown in Figure 3.5. The anemometer provides DC voltage output ranging from 0 to 5 Volts for wind direction and AC voltage for the wind speed. An aluminum arm was fabricated to support the anemometer as shown in Fig. 3.5 The aluminum support was attached to the pole at a height of 35 ft (10.7 m), with stainless steel hose-clamp bands tightened around the pole. The support inclination can be adjusted by means of four pointed screws that bear on the pole, so that the anemometer can be aligned vertically. To minimize wind shielding of the anemometer by the pole, the support was designed to be twice as long as the diameter of the pole. The anemometer was oriented on the HMIP considering the prevalent wind activity in the area to further minimize shielding in the strongest wind direction for each location.

Fig. 3.5. Wind Monitor Model Young 05103, Helicoid Propeller Anemometer

Fig. 3.6. Setting up the anemometer on a pole (El Paso, TX)

Fig. 3.7. Solar panel and wireless antenna mounted on a pole (El Paso, TX)

3.2.3 Data Acquisition and Communication

The CompactRIO 9024 from National Instruments (NI) was used for data acquisition in the field. The system has an 800MHz processor, 512MB of RAM, and 4GB of Physical Memory. The strain gages were connected to a NI 9237 module on the CompactRIO in a quarter-bridge configuration whereas the voltage from the anemometer and battery were measured using a NI 9219 module. Measurements of the battery voltage provided valuable feedback on the power conditions during the winter months when the recharging abilities of the solar panel were lowered due to significant reductions in available daylight. An Airlink Raven X cellular modem from Sierra Wireless was used so that the DAQ could be remotely accessed through the GPRS/EDGE wireless network. The DAQ and the wireless modem were placed in a water resistant steel enclosure inside the shaft, through the existing access port.

3.2.4 Powering the System

A battery recharged by a solar panel was used to power the data acquisition system since the high voltage AC power supplied for the pole lights could not be used. To determine the nominal power of the solar panel, a calculation of the power consumption of the system was performed. The total power consumption, obtained by summing the maximum operating input power of the devices, was estimated to be 24 Watts (W). Considering that the solar panel can only charge the battery during the day, a factor of two was used. As such, the BP Solar BP350J, a 50 W nominal power panel 33" (84 cm) long, 21" (53 cm) wide, and weighing 13.2 lb (6 kg), was chosen. A custom

steel frame for the solar panel was fabricated to attach the panel to the HMIP as shown in Figure 3.7. The rack was clamped to the pole by means of two threaded bars. The panel was oriented facing south at an inclination of 30°, which is the approximate latitude in Texas. The battery chosen for the system is a flooded lead acid, deep cycle battery manufactured by Trojan. It has a nominal capacity of 130Ah (amp-hours), a weight of 67 lb (30 kg) and dimensions of 13.25" x 6.75" x 9.75" (34 cm x 17 cm x 25 cm). The battery was placed in a plastic enclosure inside the access door of the pole. The Morningstar Sunsaver 6 was the charge controller chosen, which has a solar rating of 6 Amps and a max load of 10 Amps. The charge controller has a load disconnect threshold of 11.5 Volts and a load reconnect of 12.6 Volts, and ensures that the battery is fully charged before it starts powering the system again.

3.3 Software

National Instruments LabVIEW was used to create a program for capturing, processing, and recording the data. The program captures data at 50 Hz (samples per second). The software incorporated several features including recording raw data as well as conducting a rainflow analysis for fatigue evaluation. The following subsections provide an overview of the features of the data acquisition program.

3.3.1 Rainflow Counting of Stress Cycles

A fatigue life assessment is typically based on the cumulative damage theory as presented in Miner (1945). The theory allows a complex stress history to be represented as a series of simple constant amplitude cycles. The number of stress cycles are usually estimated using the Rainflow Counting method which keeps track of the number of cycles within a preset series of stress ranges. In the rainflow method, the wide range of expected variations in the applied stress cycles is divided into a series of smaller increments. For example, if the cyclic stresses are expected to vary from 0 ksi to 10 ksi, a uniform increment in stress range can be selected such as 0.25 ksi. The stress range "bin sizes" would then be 0.25 ksi, 0.5 ksi, 0.75 ksi, etc. The Rainflow counting algorithm then keeps track of the number stress cycles within a given stress range over time. Figure 3.8 shows a simplified representation of the a variable stress history and the its Rainflow Counting.

In the literature many rainflow algorithms have been presented. The rainflow counting used in the program was presented in Downing and Socie (1982). By default, the program performs the rainflow analysis for each of the four strain gages every 30 minutes, using bin sizes of 5 microstrain and neglecting cycles smaller than two microstrain (equivalent to 0.06ksi)

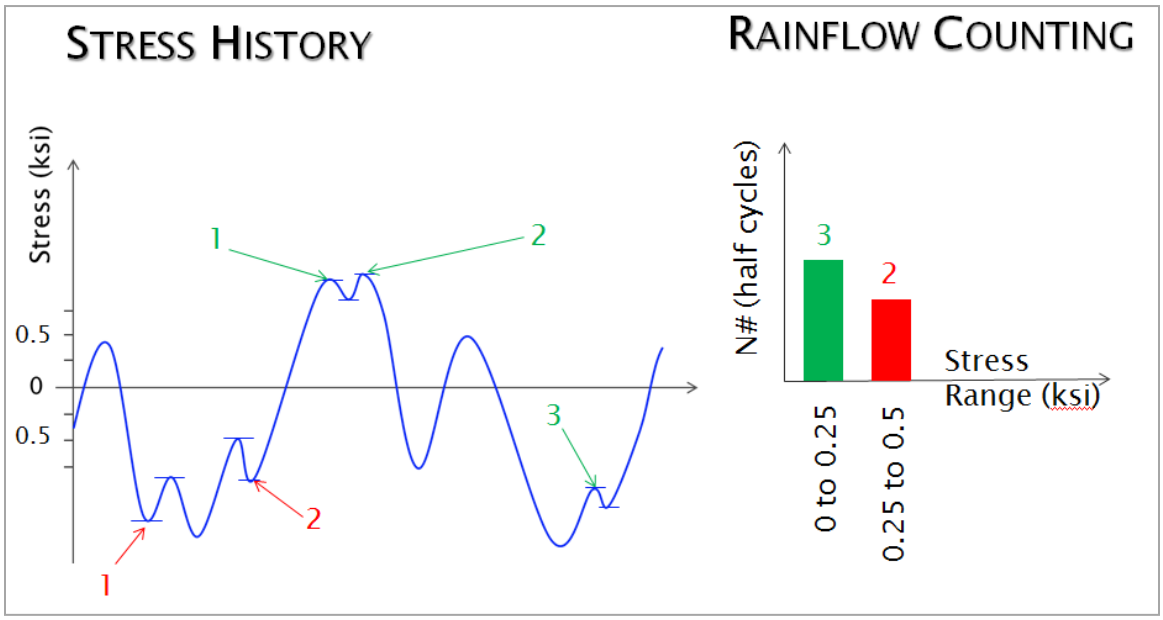

Fig. 3.8. Stress History and Rainflow Counting example

3.3.2 Event Capture

In addition to gathering rainflow stress range data, the program was also written to be triggered to gather raw data for a specified amount of time (usually 5 minutes) in the event that the wind exceeded specified threshold values. The raw data included strain values along with wind speed and direction. This data is useful to study the dynamic behavior of the pole as related to potential vortex shedding effects. After collecting a library of recordings, approximate relationships between wind speed and maximum stress can also be defined.

3.3.3 Voltage Measurement

Additional data that was monitored on the data acquisition system was the battery voltage, which provided valuable information on the performance of the system in terms of power. The instrumentation was installed during the summer months when there was significant sun exposure

to provide energy to the solar panels that recharged the battery. During the summer and early fall periods, solar exposure was sufficient to maintain the battery charge and keep the system running continuously. However, as the sunlight intensity diminished during the winter months, the solar panel could not recharge the battery fully. In addition, the colder temperatures in the winter reduced the overall capacity of the battery. These factors caused the system to turn off more frequently. If weather forecasts predicted storms (with higher winds), the readings of the battery voltage allowed the system to be turned off so that the battery could charge properly so that storm data was not missed. As expected, the performance of the system improved during the spring as the days became longer and the solar exposure increased.

3.3.4 Remote Access and Control

Fig.3.9 is a screenshot of the program interface for the remote control of the DAQ. The plot on the top right shows the real time values of the strain (in millistrain) measured by the four strain gages, named N-S-W-E. The Rainflow Information is provided in the lower right hand quadrant below that graph. The input parameters for the rainflow sampling consists of the length of over which the rainflow analyses is performed, the size of the bins in microstrain, the number of bins, and the minimum amplitude of strain cycles that should be considered in the rainflow analysis. The live readings from the anemometer are displayed in the bottom left corner. On the bottom right corner the control parameters for the triggering program used for the event capture. The parameters that can be specified include the wind speed that defines the triggering point for the event capture and also the duration of the event to be recorded.

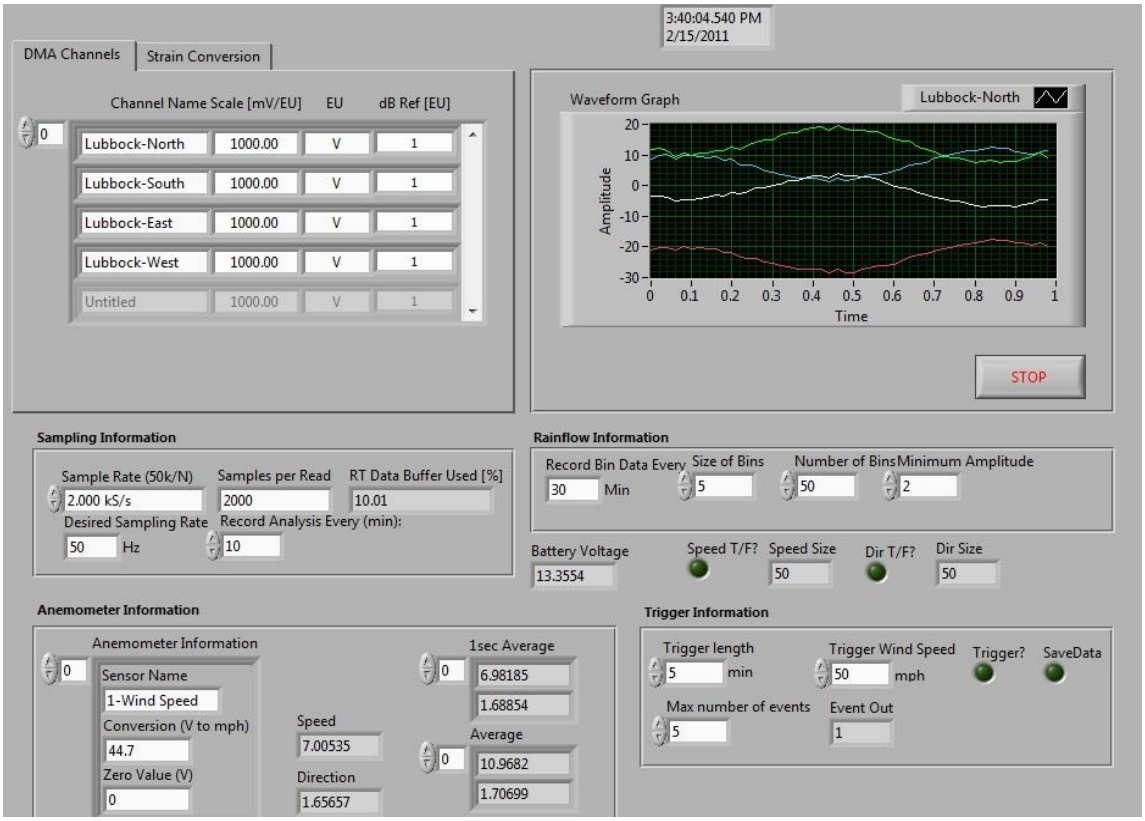

Fig. 3.9. Screenshot of the Instrumentation Program

Chapter 4 Background Information for Field Studies

4.1 Introduction

The data gathered from in-situ HMIP's provides valuable feedback on the actual performance of the poles. However, because of the wide variability of both pole geometry and site characteristics, the researchers considered information gathered from inspections and a database of weather history to select poles for instrumentation. This chapter provides an overview of the data that was considered in selecting candidate poles for instrumentation. The chapter has been divided into three sections. Following this introduction, an overview of data gathered from TxDOT inspections is provided. The data focuses on ultrasonic inspections that were conducted for crack identification and crack growth monitoring. The final section of the chapter provides an overview of the historical weather data for the candidate sites that were selected for field monitoring.

4.2 TxDOT Ultrasonic Inspections

In an effort to determine the severity and range of damage on existing HMIP's around the state, TxDOT initiated an effort to inspect the state's HMIP inventory. The main instrument used for the inspection was Ultrasonic Testing (UT) in which a pulse wave is introduced into the HMIP material through a transducer that also serves as the receiver as the signal is reflected back to the device. Cracks or defects in the material affect the amount of sound that is reflected back to the transducer. An experienced technician can use the measurements to identify and measure cracks in the material or welds. In common practice, transducers with a 45° angle working in a 2.0 to 2.5 MHz range are typically used. However because the initial galvanizing cracks were relatively small and difficult to detect using standard procedures, the UT inspections on the HMIPs were performed using a 3.5MHz, 70° transducer with a ½" diameter. The higher ultrasonic frequency increases the sensitivity of the measurements, and the interpretation of the results can be dependent on the experience of the technician.

Another non-destructive inspection method that was tested is magnetic particle testing in which a magnetic field is introduced into the region and iron filings are used to identify discontinuities (cracks) (Pool, 2010).

4.2.1 UT Results on Texas In-Service HMIPs

The data that was obtained in the UT tests on in-service poles provided insight into the condition of the states HMIP inventory. The results from these tests along with variations in the sight conditions around the state provided valuable data into the selection of poles that should be instrumented for long term monitoring. The UT results for 12-sided poles from around the state are summarized in Table 4.1. The inventory of poles were divided into two main groups consisting of 80 mph designs and 100 mph designs. Four different pole heights existed within each design wind speed: 100′, 125′, 150′, and 175′. Two different details were used between the shaft and the baseplate. Details designated as "TX" represent a connection with a full penetration weld with no external collar as outlined in Chapter 2, while those designated as "EC" had an external collar.

Table 4.1. TxDOT Ultrasonic Testing Results

	12 (sides)															
	80 (mph)								**100 (mph)**							
	100'		**125'**		**150'**		**175'**		**100'**		**125'**		**150'**		**175'**	
	TX	EC	TX	EC	TX	EC	TX	EC	TX	EC	TX	EC	TX	EC	TX	EC
#UT	7	3	1	3	3	36	8	17	9	0	3	26	4	17	8	23
#Cr	4	2	1	1	3	36	3	9	2	0	0	0	1	5	6	2
%Cr	57	67	100	33	**100**	**100**	38	53	22	0	0	0	**25**	29	75	9
D/T	79	79	90	90	104	104	97	97	68	68	66	66	77	77	75	75

In the table the row labeled #UT is the number of HMIPs that were inspected while the row with #Cr represents the number of poles in which cracks were found. The %Cr is the simply the percentage of the poles inspected in which cracks were found, while the row labeled D/T provides the ratio of the diameter at the base of the shaft to the shaft thickness. Previous observations have been made in the correlation between the D/T ratio and the likelihood for the HMIP to have cracks. This correlation can be demonstrated in the graph of the percentage of cracked poles versus the D/T ratio as shown in Figure 4.1 (Pool, 2010). The detail with the highest rate of cracking is the 80mph 150ft tall HMIP (100% cracking rate), which has also proved to have a poor performance in terms of fatigue. A high ratio between the diameter and the thickness could

indicate a potentially worse performance of the pole during the galvanization process. For a large diameter with a thin shaft it would appear that the temperature difference during the dipping phase of the pole in the molten zinc might create larger gradients between two sides of the pole, thus leading to higher thermal stress generation.

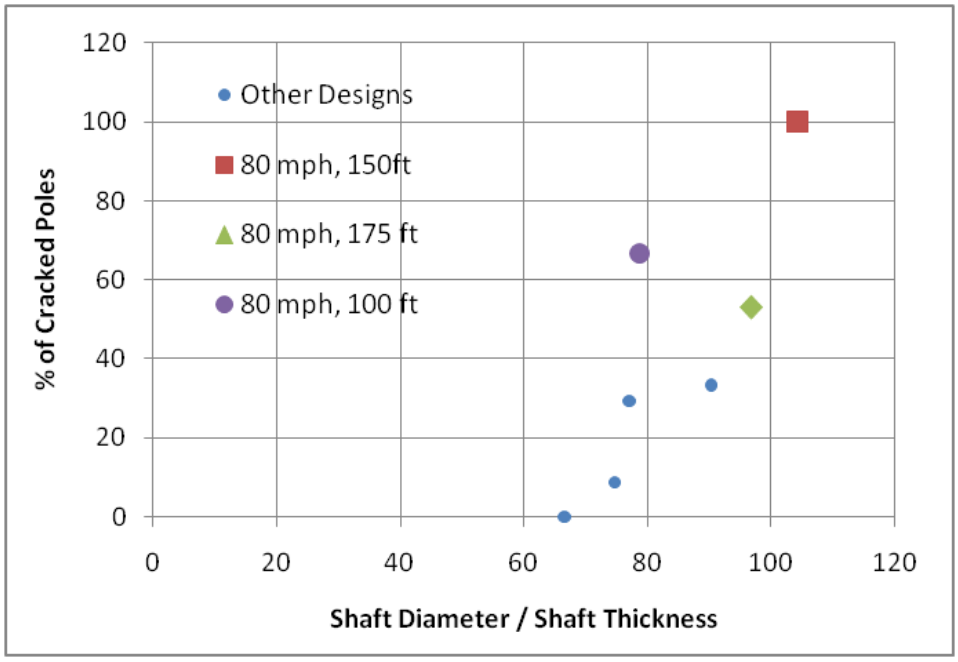

Fig. 4.1. TxDOT Ultrasonic Testing Results

4.2.2 Cracking on Instrumented HMIPs

Based upon the geographic location and environmental exposure, poles were selected in Austin, Corpus Christi, El Paso, and Lubbock for field instrumentation. The selected locations were well representative of the range of environmental exposure that HMIPs might be subjected to around the state. Ultrasonic testing inspections were performed on the specific poles so that the cracking condition of the poles was also known prior to instrumentation. The UT results are summarized in Table 4.2. The measured crack length in inches for each of the 12 bends is indicated in the table. A check mark for a given bend indicates that no crack was found. Although the poles in Lubbock and Corpus Christi had very little cracking; two poles in El Paso were selected since they had significant cracking. The El Paso poles were actually inspected on multiple occasions due to concerns about the cracks growing over time. One of the poles in El Paso was located on

IH 10 while the other pole was on US 54. The latest inspection the HMIP on IH10 in El Paso was found to have 11 out of 12 bends cracked, with a total crack length (summation of all the cracks lengths) equal to 32" which is almost 1/3 of the overall circumference of the base shaft. Considering three consecutive inspections of the IH10 pole in different times of the year, the amount of cracking observed was found to be inconsistent from the first to the second inspection. Since it is not physically possible that the cracking decreases with time, it is believed that this inconsistency was likely due to the following reasons:

- Ultrasonic Testing is a sensitive and operator-dependable measurement, especially when detecting microcracks such as those present in the welds. It is therefore possible that the accuracy of the readings from the technician could vary from one day to the other.
- It has been observed on small sections of the HMIP baseplate to shaft connection cut after fatigue testing (Figure 1.3), that cracks open and become more visible when the specimens are heated to a higher temperature. It is therefore possible that the ambient temperature had an effect, making the cracks more evident on the first inspection (conducted in August 2008), and making the cracks close and become less detectable in the second inspection (conducted in April 2009).
- The heat transmitted to the pole by sun radiation also causes a thermal gradient on the HMIP. The sunny side can be several degrees warmer than the shaded side. This gradient leads to a differential thermal expansion of the two sides of the pole, which causes the HMIP to bend as depicted in Figure 4.2. This effect is visible by looking up at the poles on sunny days. The second order moment generated by the bending may open the cracks on the sunny side, and close the cracks on the shaded side. Further investigation was carried out with a finite element model that is discussed in the next chapter. The model was used to quantify the bending moment at the base of the pole generated by this effect.

If the reason for the inconsistency of the UT measurements is a thermal mechanism, then the higher estimate of the crack length would be the most correct. If the difference is due to variability in the reading by the operator, an average of the multiple readings would be the most reasonable estimate. It would be interesting for TxDOT to report the ambient temperature and the shaft temperature on the sunny side for every UT inspection performed. This would be helpful in determining the nature of this change in measurements.

Table 4.2. UT results for the field-instrumented HMIPs

HMIP	1	2	3	4	5	6	7	8	9	10	11	12	Date	% of Bends cracked	TOT Crack length [in]
El Paso US-54	2.0	1.2	1.0	0.5	√	2.0	2.1	2.0	1.1	1.0	√	2.7	4/8/2009	**83**	**15.6**
"	2.0	1.2	1.0	0.5	√	2.0	2.1	2.0	1.2	1.0	√	2.7	6/15/2010	**83**	**15.7**
El Paso IH-10	√	√	2.6	*	2.3	2.2	2.7	3.2	2.7	2.7	2.7	2.7	8/18/2008	**75**	**21.1**
"	√	√	2.9	√	3.2	3.2	3.0	√	3.0	√	√	3.8	4/7/2009	**67**	**15.3**
"	0.8	√	3.7	1.0	3.3	3.2	2.7	4.0	3.3	3.0	2.9	4.0	6/14/2010	**92**	**31.9**
Lubbock[1]	√	√	√	√	√	√	√	√	√	0.9	√	√	-	**8**	**0.9**
Corpus Christi[2]	√	√	√	√	√	√	√	√	√	√	√	√	-	**0**	**0**

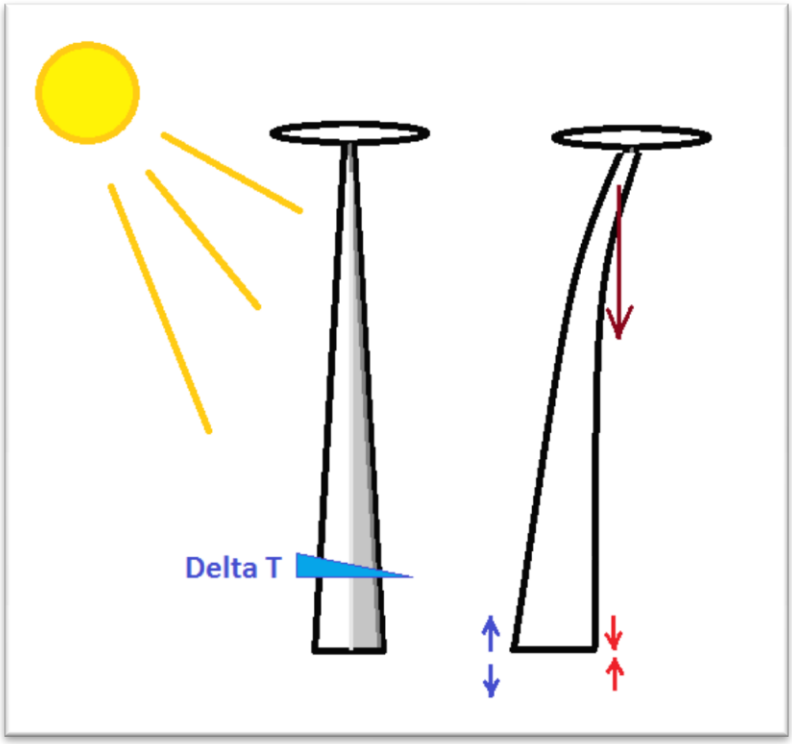

Fig. 4.2. Schematic representation of differential heating due to sun radiation heating of the HMIP

[1] 100 mph wind speed design with external collar

[2] 100 mph wind speed design with full penetration weld (Texas detail)

* small spot crack

4.2.3 UT results of the HMIP specimens load tested in previous research phases

Ultrasonic tests were also performed on HMIPs specimens before being load tested at Ferguson Structural Engineering Laboratory in the previous phases of the project. Table 4.3 shows the results from the UT inspections on the specimens. The ultrasonic inspections were carried out by a TxDOT technician, with the same procedure used for the in-service HMIPs. All the poles reported in the table are 12 sided, 150ft tall designed for 80mph wind speed. The difference is that some of the poles had the external collar connections, while others did not. On the right end column the number of cycles to failure from the load test performed at a stress range of 12ksi is shown. The specimen that showed the worst performance had a Texas standard shaft-to-baseplate connection, with the full penetration weld and no external collar. It seems that within HMIPs featuring the same connection detail the amount of initial cracking has an impact on the fatigue performance. As expected, the specimen that had larger initial cracks showed the poorest performance.

Table 4.3. UT results on HMIP specimens before load testing

HMIP #, Station	External Collar	Galvanized	% of Bends cracked	TOT Crack length [in]	Cycles to Failure @ 12ksi
33-3-12-TXEC-SG-A	Yes	Yes	17	5.00	No failure
33-3-12-TXEC-SG-B	Yes	Yes	25	8.00	No failure
33-3-12-TX-SG-A	**No**	**Yes**	**83**	**11.00**	**81326**
33-3-12-TX-VG-A	No	Yes	25	5.00	358228
33-3-12-TX-VG-B	No	Yes	33	4.63	358228
33-3-12-TX-SG-B	No	No	0	0	No failure

The crack data from these previous experiments combined with the number of fatigue cycles to failure are useful for predicting the fatigue performance for the instrumented HMIPs. Indeed, if there is a correlation between the initial cracking conditions and the fatigue performance, comparing the UT results for the HMIP instrumented to the load tested specimens it will give an idea of expected fatigue performance. The HMIP on US54 in El Paso, for instance, had initial cracks prior to the field tests that were similar to specimen 33-3-12-TX-SG-A, highlighted in bold in the table. The laboratory specimen had 83% of the bends cracked and a total crack length of 11", which is a little less than the length of approximately 15" measured on the El Paso US 54

HMIP. It could be then assumed that the pole would have shown a similar performance under the same loading conditions. The pole on IH 10 had an even larger amount of cracking at the shaft to baseplate connection, with cracks on 92% of the shaft bends and a total crack length of about 30". This HMIP was removed from service in July of 2011, and will be fatigue tested at Ferguson Structural Engineering Lab using the same setup used for the previous investigations. This test will demonstrate the impact of severe cracking on the fatigue performance of the pole.

4.3 Wind Historical Records

There are a number of organizations that archive meteorological data including statistics on the wind historical records. These organizations make the data available to public. The following sources provide wind historical data that can be used for various sites:

- National Climatic Data Center (NCDC), a US governative agency that offers the world's widest archive of meteorological data.
- Weatherunderground, a private company that owns 19000 weather stations across the US and makes its information accessible through its website www.weatherunderground.com.
- Texas Commission on Environmental Quality (TCEQ), the environmental agency for the state of Texas

The wind historical records were helpful in selecting pole locations for instrumentation. One of the major goals of the field instrumentation was to gain a measure of wind induced stresses in the pole. Higher wind speeds will create larger stresses in the poles. In addition, the propensity for vortex shedding and the various dynamic modes are sensitive wind speed. Therefore, reviewing the historical wind records were important in selecting sites that might result in significant wind exposure for the instrumented HMIPs.

Tables 4.4 and 4.5 show the average and the maximum wind speed measured in the past in the three cities that were selected for HMIP instrumentation. The right end column shows the time length of the reference data. The average yearly wind speed in Lubbock and Corpus Christi is around 12 mph, while in El Paso the average wind speed is almost 9 mph. On the other hand El Paso had the highest measured gust of 86mph compared to 85 mph for Lubbock and 67 mph for Corpus Christi.

Table 4.4. Average Wind speeds in the Instrumented HMIP locations (NCDC)

	JAN	FEB	MAR	APR	MAY	JUN	JUL	AUG	SEP	OCT	NOV	DEC	V average	Recorded Period [yr]
CORPUS CHRISTI, TX	12	12.9	14	14.3	12.8	11.7	11.5	11	10.4	10.4	11.7	11.6	**12**	60
EL PASO, TX	8.3	9.1	10.9	11	10.3	9.3	8.3	7.7	7.6	7.5	8	7.9	**8.8**	60
LUBBOCK, TX	12	13.2	14.6	14.7	14.2	13.6	11.4	10.1	10.5	11.2	11.7	11.8	**12.4**	53

Table 4.5. Maximum gusts speeds in the HMIP locations (NCDC)

	JAN	FEB	MAR	APR	MAY	JUN	JUL	AUG	SEP	OCT	NOV	DEC	V MAX	Recorded Period [yr]
CORPUS CHRISTI, TX	52	60	54	67	60	61	49	48	61	53	60	54	**67**	60
EL PASO, TX	86	60	69	66	55	69	63	48	62	53	54	61	**86**	60
LUBBOCK, TX	59	64	77	71	74	85	72	59	58	52	63	64	**85**	53

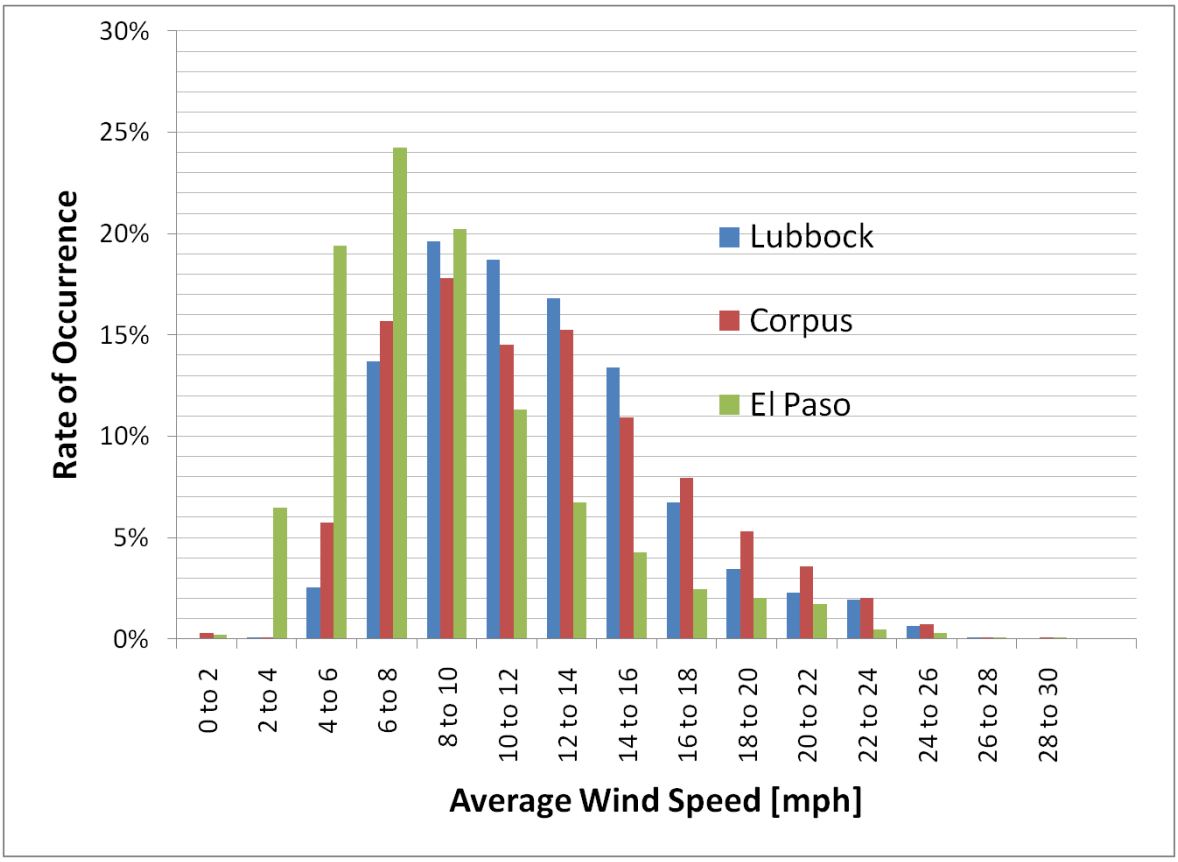

Fig.4.3. Rate of occurrence of the daily average wind speed at the HMIP Locations

Figure 4.3 is a plot of the rate of occurrence of the daily average wind speeds in the last 3 years. For El Paso the wind speed with the highest rate of occurrence is from 6 to 8 mph, while for Lubbock and Corpus Christi the wind speed with the highest rate is from 8 to 10 mph. Lubbock and Corpus Christi are more likely to have sustained wind (10 to 20 mph) on an average basis.

Another useful source of information for the instrumentation layout are "wind roses" that consist of radial plots that show the probability distribution of the wind in terms of speed and direction. This information can be used to position the anemometer on the pole to minimize wind shielding in the direction that is most likely to have the prevailing wind. Figure 4.4 shows that Corpus Christi has a prevalent wind action happening in the South-East direction, while Lubbock has a prevalent wind happening from the South direction. The El Paso plot shows wind activity in almost all the directions with peaks at North and South-East. It can also be seen that in El Paso strong wind events (higher than 20mph) from the West are prevalent.

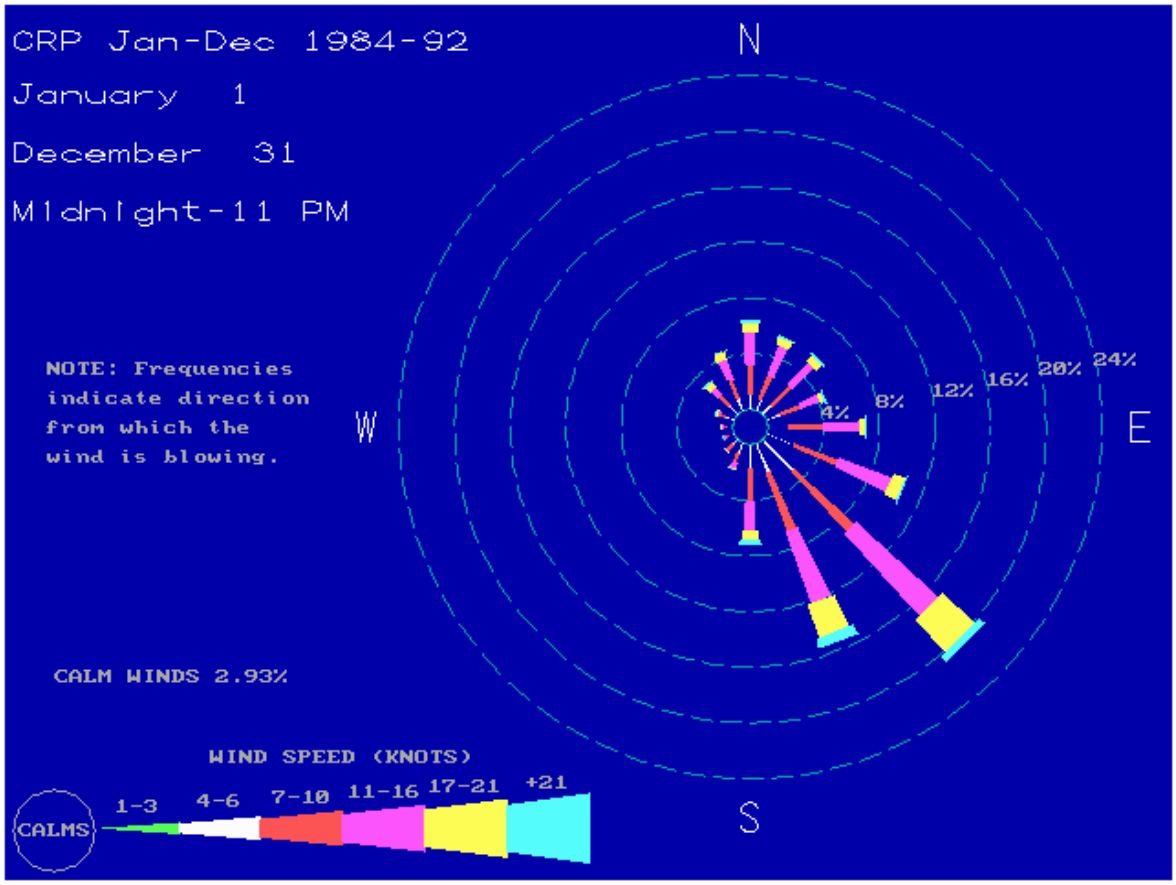

*Fig. 4.4.*Yearly wind rose for Corpus Christi (Texas Commission on Environmental Quality)

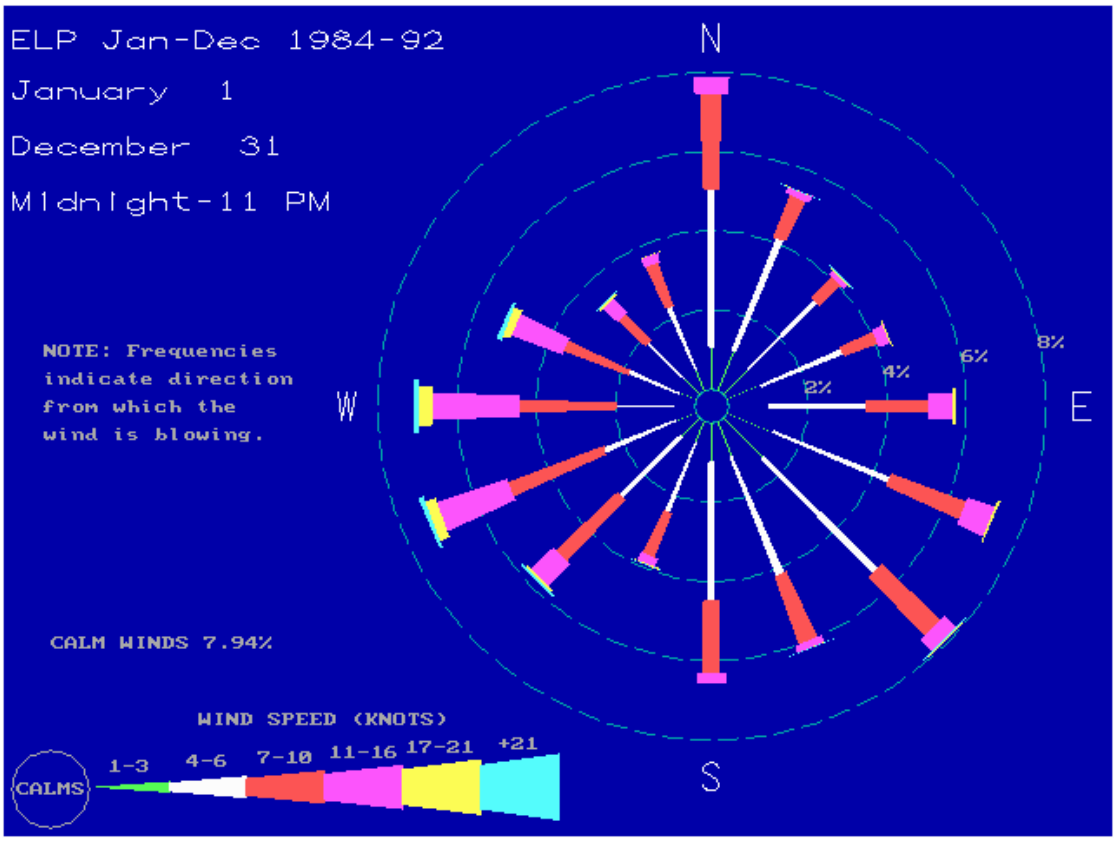

Fig. 4.5. Yearly wind rose for El Paso (Texas Commission on Environmental Quality)

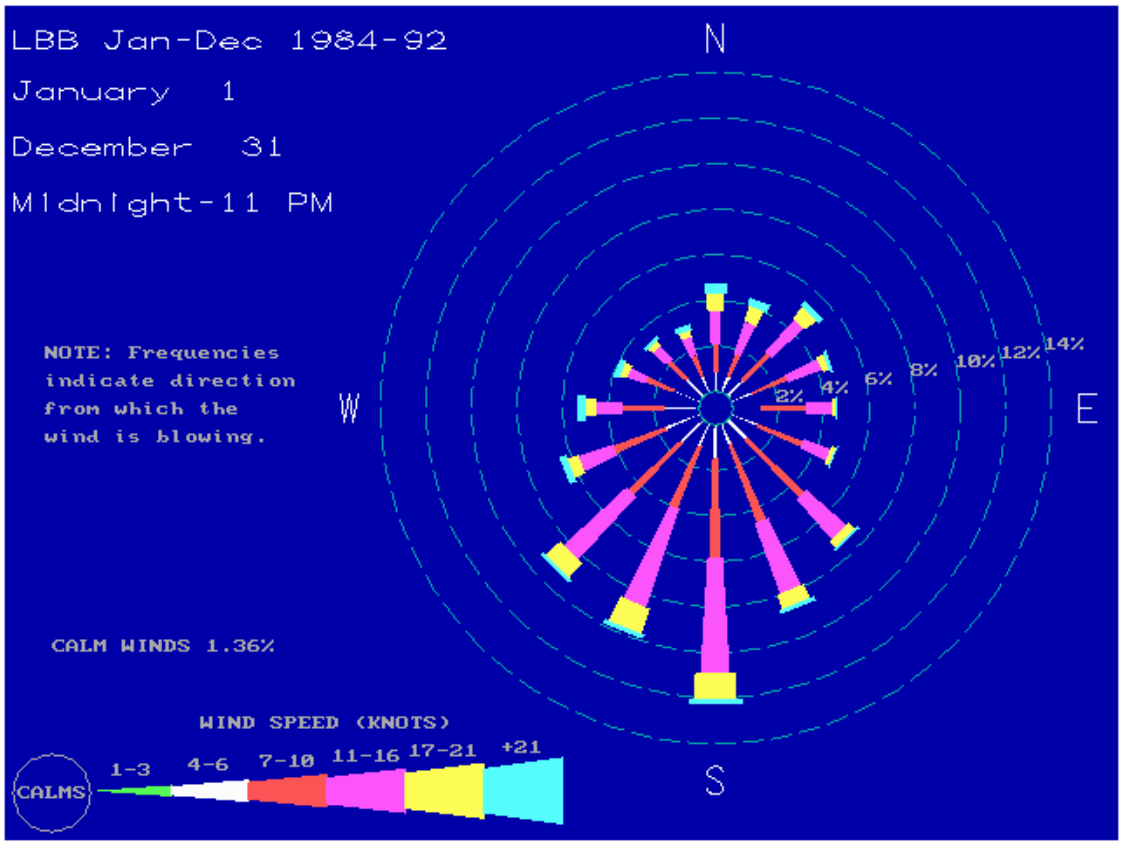

Fig. 4.6. Yearly wind rose for Lubbock (Texas Commission on Environmental Quality)

4.4 Summary

Significant background information was used for identifying the poles that should be instrumented for field monitoring. The data included ultrasonic testing that identified cracks in the welds between the shaft and the base plate of the HMIP as well as wind historical records. The wind historical records provided valuable data on the average wind speeds in each site as well as the maximum gusts that have occurred at each site. The data also provided an indication of the prevailing wind direction for use in positioning the anemometer to avoid wind shielding from the HMIP. The UT results from the poles from around the state provided insight into the pole geometries that had the largest probability of cracking from the galvanizing. For each pole that was instrumented, the UT results showed the degree of cracking that was present. While this data was not necessarily used in the selection of all of the instrumented poles, in the case of the El Paso pole on I10, the data was used since it was desired to see if the damage was escalating based upon severe wind exposure.

Chapter 5 Data Analysis

5.1 Supporting Finite Element Modeling (FEM)

In an effort to complement the field measurements, two linear elastic models were created to support the data analysis. The models include a simple cantilever beam model and a shell element model. The beam model was developed to simulate the dynamic behavior of the high mast pole, while the shell element model of the pole base section was put together to investigate the influence of the anchor bolts on the stress distribution. Both the models were developed using the structural analysis commercial software SAP2000 Nonlinear. The following two subsections provide an overview of the computer models as well as the results that were used to assist in the data analysis from the field work.

5.1.1 Beam FEM

To match the taper of the HMIPs, the beam model was composed of non-prismatic beam elements, with a point mass on the top to model the lighting apparatus. The total weight of the HMIP is approximately 14300 lbs., including 12500 lbs. for the pole and 1800 lbs. for the lighting apparatus at the top. The model is restrained from translation and rotation at the ground to simulate the fixed end condition of the cantilever poles. The model was used to conduct a modal analysis to determine the natural period for the first three modes of the structure as shown in Fig.5.1.

The bending moment diagram along the length of the pole was determined for each natural mode as shown in Fig.5.2. This information was used to determine the ratio between the stress measured in the field using the strain gages located 76" (193 cm) from the base and the nominal stress at the base. A node in the finite element model was positioned at the strain gage location to provide the value of the moment at the strain gage location. The FEM moment shape corresponding to the respective first, second, and third modes shows that the stress at the base of the HMIP are 5%, 11%, and 23% greater than the stress at the strain gage location. These values were used to adjust the strain gage measurements to determine the nominal stress at the base.

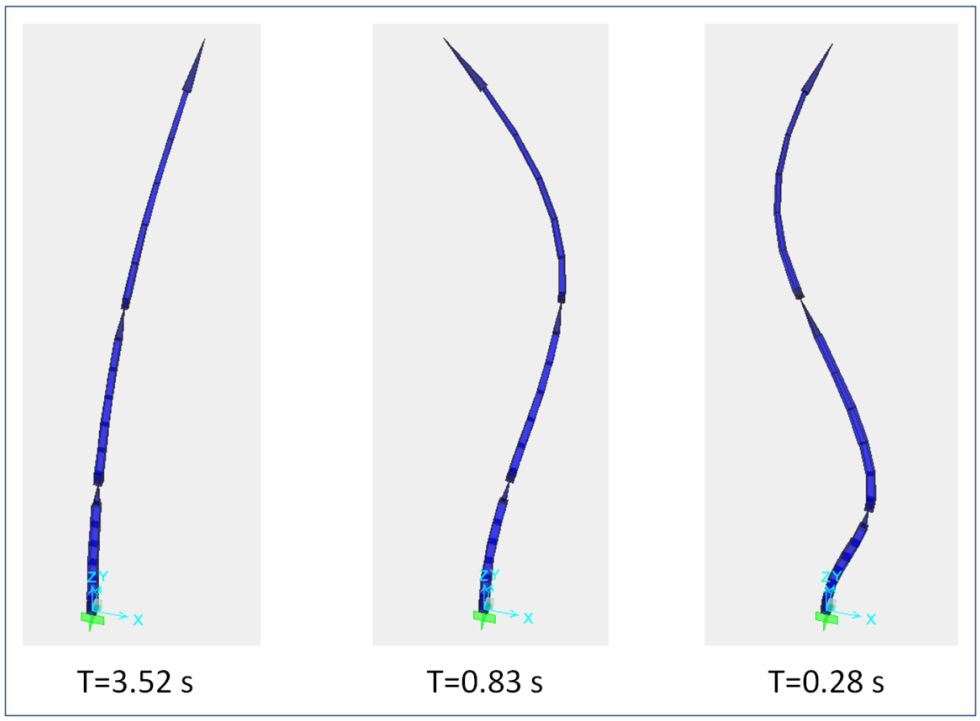

Fig.5.1. Natural Periods of the HMIP from the Finite Element Model

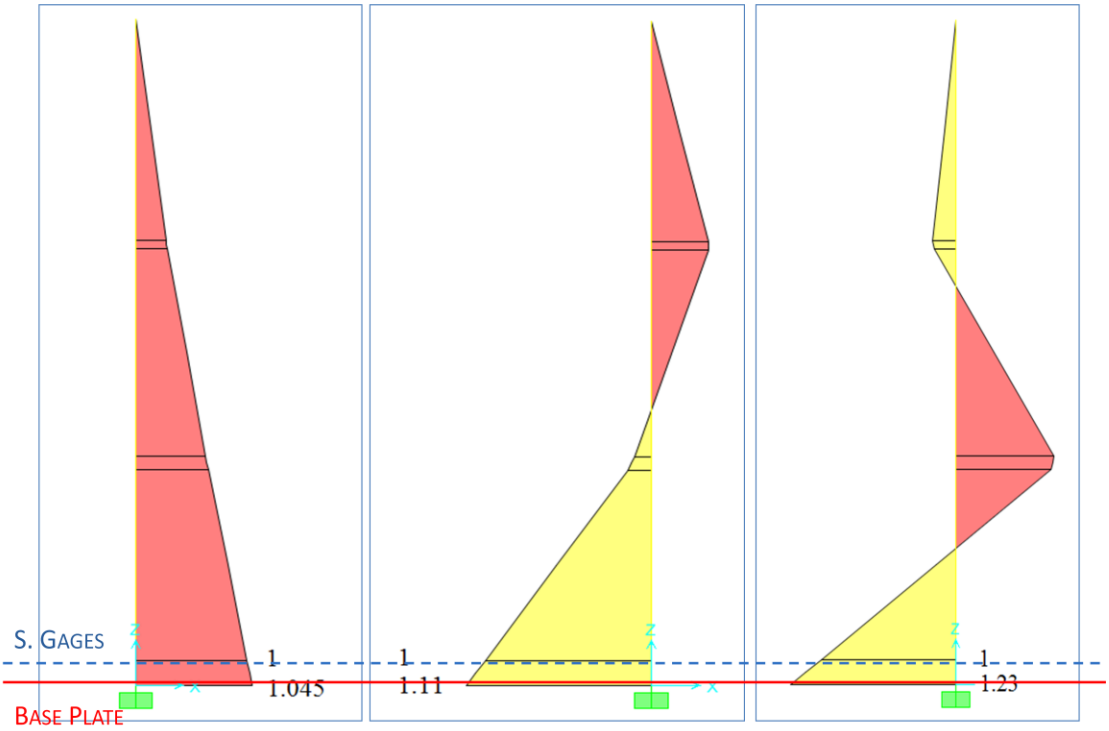

Fig.5.2. Bending moment shapes for the natural modes of the HMIP

The natural frequencies calculated by the modal analysis were used to determine the wind speeds that could potentially cause vortex shedding. Recalling the equation presented in section 2.3:

$$U_{Lock-in} = \frac{f_n \cdot D}{S_t} \qquad \text{(Eq.5.1)}$$

Where, $U_{Lock-in}$ is the wind velocity for vortex shedding lock-in

D is the diameter of the cross section

S_t is the Strouhal number,

The above equation is intended for prismatic sections. To use the expression on the tapered HMIP, an the diameter of the HMIP at 2/3 of the total height was used to approximate an equivalent prismatic section, which is also the location that an equivalent wind push was located. For the poles being studied, the diameter at 2/3 of the total height was 16". The Strouhal number was taken as 0.15, as suggested by AASHTO for a multisided section. Table 5.1 shows the values of the vortex shedding critical wind speed calculated for the first three natural modes.

Table 5.1. HMIP calculated natural frequencies and periods

	I MODE	**II MODE**	**III MODE**
$\boldsymbol{f_n}$ **[Hz]**	0.28	1.20	3.57
$\boldsymbol{U_{Lock-in}}$ **[mph]**	1.7	7.4	21.6

As noted in the discussion of the data acquisition system, event capturing was used to gather data for very high wind speeds or behavior for other conditions. Event capturing was used to investigate the behavior of the pole in presence of the wind speeds shown in Table 5.1, to understand if there is any vortex shedding effect on the HMIPs. The frequency analysis of the recorded strain was used to evaluate the accuracy of the model in predicting the natural period of the structure. This is discussed in subsection 5.2.2.

The model was also used to evaluate the deformation of the HMIP under a temperature gradient as explained in section 4.2.2. To determine a suitable value for the temperature gradient between the sunny and the shaded side of the pole, measurements were taken on a pole shaft throughout

the day using an infrared thermometer. The largest temperature difference recorded was 30F which occurred on on a spring day at approximately 10AM. The ambient temperature at this time was 60 F, and the sun radiation heated the steel surface on the sunny side to above 90F. Since the temperature difference was measured close to the bottom section of the pole, the gradient was calculated by dividing the gradient by the bottom shaft diameter of 33". The resulting temperature gradient of 0.9 F/in was then applied to the frame elements of the model, and a second- (P-Delta) order large displacement analysis was conducted. The coefficient of linear thermal expansion used was set to $6.5 \times 10^{-6}\ {}^{\text{in}}/_{\text{in F}\cdot}$

The analysis results show a displacement of 10" at the top of the pole. The value of the second-order moment generated by the structural weight at the base of the pole was computed to be 43 k-in. Whether such a moment could affect the results of the UT inspections will be confirmed in the next phase of the project. The HMIP in El Paso on IH10 has been removed from service and will be fatigue tested at Ferguson Structural Engineering Lab. It will be easy to apply such a bending moment on the specimen once set up in the loading frame. Multiple UT inspections can then be performed with the moment applied in the opposite direction to determine the impact on the readings.

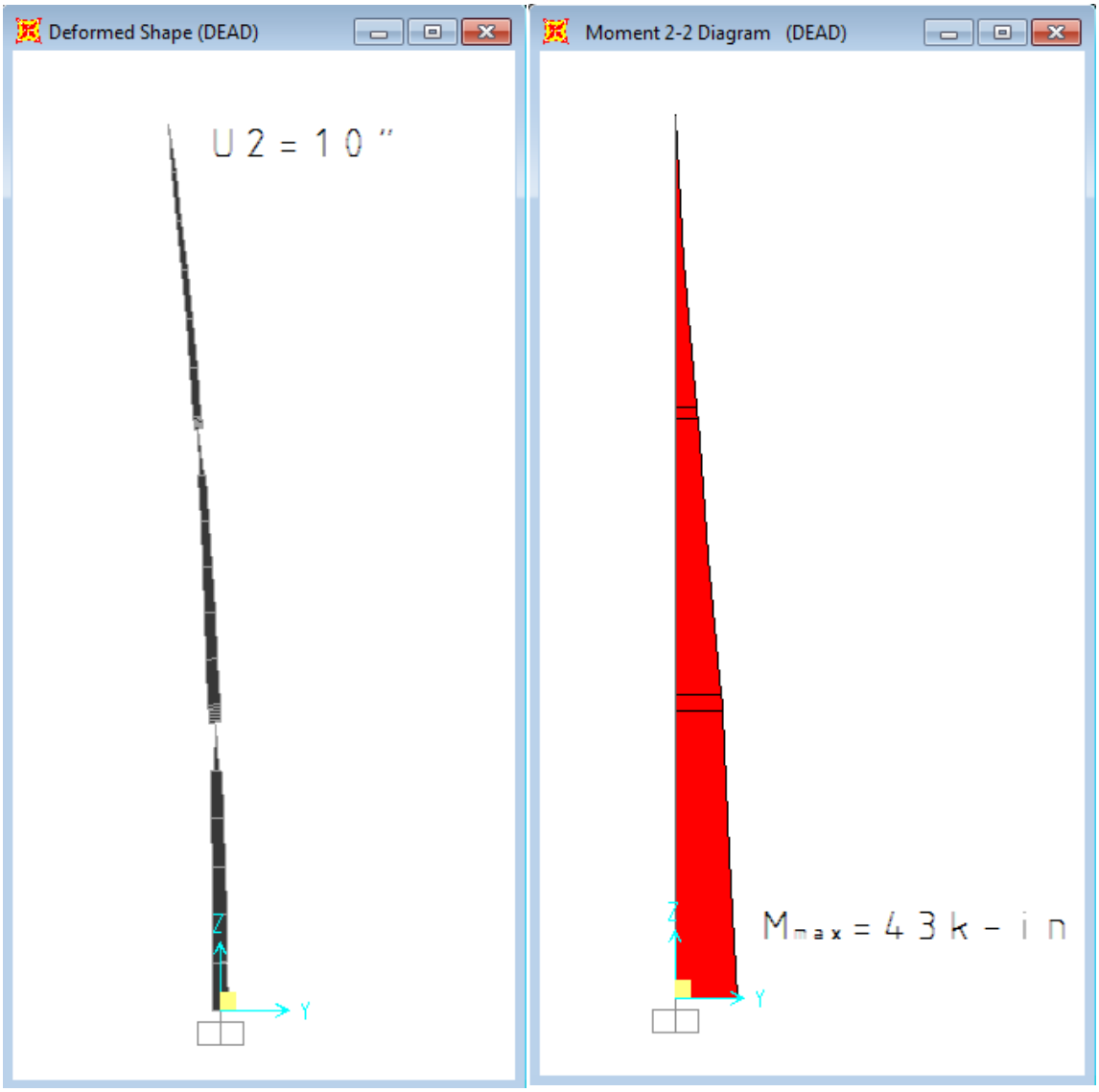

Fig.5.3. Displacement shape (left) and Moment diagram (right) due to sun temperature gradient and P-delta effects

5.1.2 Shell FEM

In some in HMIP pole installations, the anchor bolts are not properly tightened or the nuts are even missing. The impact of the improper anchor installations on the stress conditions at the base is not well understood. A three-dimensional finite element analytical model was therefore created to evaluate the impact on the stress concentration factor (SCF) with differing support conditions. The model represents a 10 ft (3 m) long section with a 3" (76 mm) thick base-plate that was restrained at the base with 10 anchor bolts. The access door opening was also modeled to obtain an indication of influence on the stress distribution. The section was subjected to a concentrated bending moment applied at the top. The moment is applied through 12 rigid beam elements connected to each shaft bend as depicted in Fig.5.4.

Multiple simulations were run on the model taking out some supports in an effort to model the lack of anchor bolts on the pole behavior. The value of the stress at the most critical bend of the shaft was then compared to the value from the analysis with the full anchor bolt connection. The value of the stress to be compared was the average stress in the shell element in the vertical direction (S22) at the most critical bend. Table 5.1 shows the results of this parametric study.

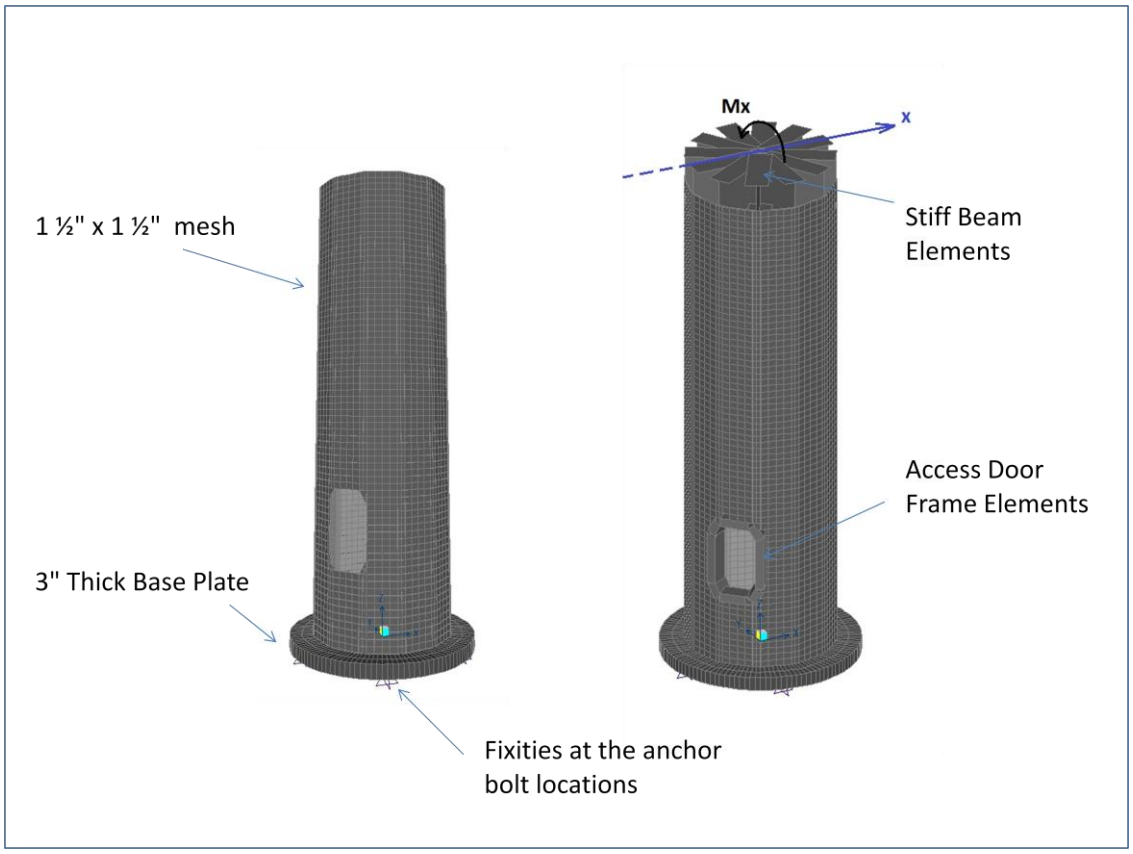

Fig.5.4. Shell Finite Element Model

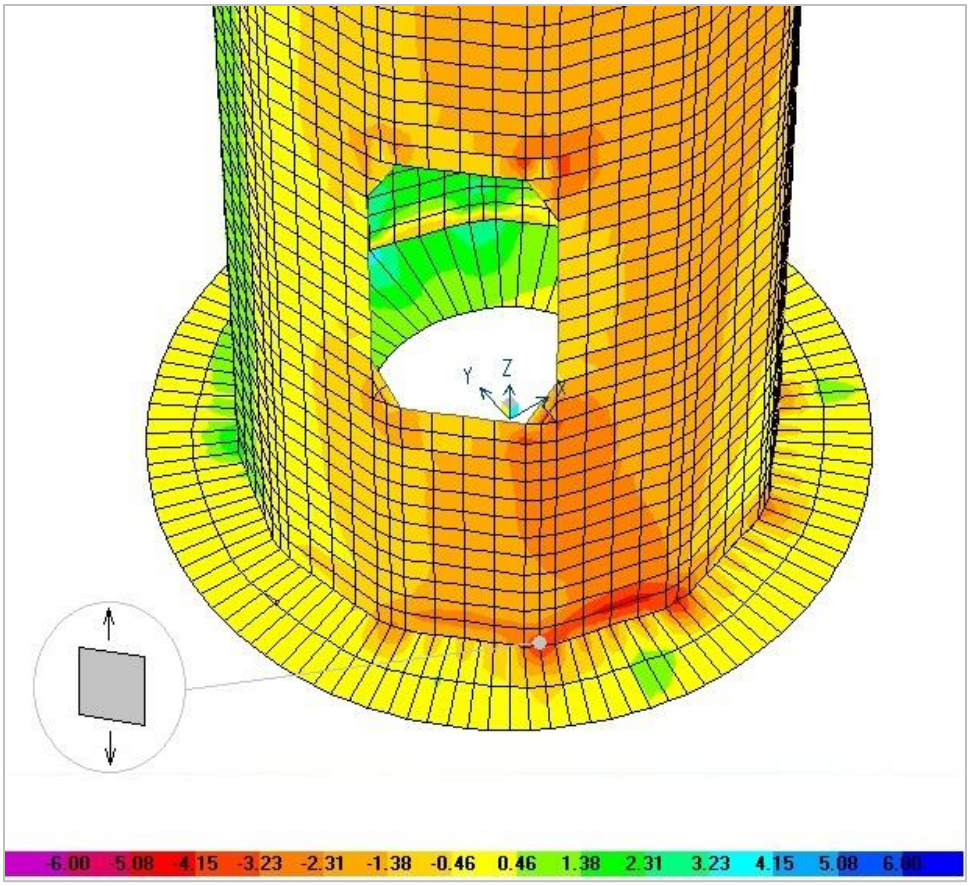

Fig.5.5. Shell stresses S22 [ksi]

Table 5.2. Influence of anchor bolts on fatigue life

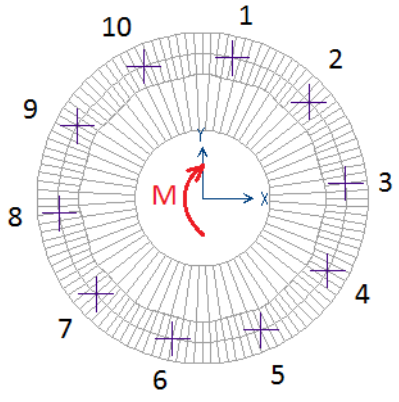	**MISSING SUPPORTS QT, (#ID)**	**STRESS (ksi)**	**STRESS RATIO**	**FATIGUE LIFE REDUCTION**
	- , -	4.55	1.0	1.0
	1, (#5)	4.76	1.05	1.1
	2, (#5 #7)	5.24	1.15	1.5
	3. (#4 #5 #7)	5.54	1.22	1.8

The values on the right end column of the table represent a measure of how the fatigue life of the HMIP was affected with a reduction in the number of anchor bolts. This factor was calculated assuming that the fatigue life is proportional to the stress range to the power of three, as stated by Miner (1945). Miner's theory is discussed in Section 5.2.

The positive effect of a higher number of anchor rods on the fatigue life of the HMIP had been pointed out in previous studies (Warpinski, 2006, Rios, 2007, and Stam, 2009). Stam (Stam, 2009) also investigated this problem in a three-dimensional FEM study. He investigated anchorages with 8, 10 and 12 rods distributed symmetrically, concluding the higher number of bolts not to be significantly improving the fatigue performance when the base plate was thick, such as the 3" plate present in the HMIPs considered in this work. However, in the application discussed in this section, the anchor bolts were not symmetrically placed around the HMIP, thereby simulating a condition of improper tightening or missing nuts on the anchor bolts. Such a situation, creates a different stress distribution, with higher concentrations at the hotspots.

The problem has also been investigated in a field study part of the research reported by Warpinski, 2006. During the pluck test (described in Section 2.3.1), some anchor bolts were loosened to simulate improper installation. With just one nut loosened, an increase of stress was noticed in the vicinity of the loosened anchor point. It needs to be pointed out that the base plate thickness of the HMIP under consideration was only 1.25" thick, which makes the stress distribution more susceptible to change with the number of anchor points.

5.2 Event Capture Analysis

This section focuses on the data gathered from the event capture feature of the data acquisition system that was discussed in Section 3.3.2. A triggering program was used to capture real time records of strain and the corresponding wind speed and direction at a frequency of 50Hz. The recording started when the wind speed exceeded a specified threshold. A library of 5 minute long events was captured at wind speeds ranging from 0 to 50 mph during the period of instrumentation. Many records were taken at wind speeds that could potentially cause vortex shedding, in the 7mph range and 20mph range as discussed in the previous section.

5.2.1 Data Observation

Figure 5.6 shows a graph of a 10 second record for an event with a wind speed ranging from 30 to 50mph. The wind speed shown is averaged over a three second period, while the stress is averaged over a one second period. The average wind direction during the recording was 237 degrees (W-S-W). The plot shows the stress calculated on the east side of the pole, which is a measure of the pole bending in the East-West direction. From the recording it can be seen that the HMIP is shaking with a period that is approximately 3.5 seconds, with a 7 ksi stress range. This indicates that, at high wind speeds, the first mode is the primary mode that is excited, and that the wind effect is prevalently buffeting, exciting the pole in the direction of the wind rather than transversally.

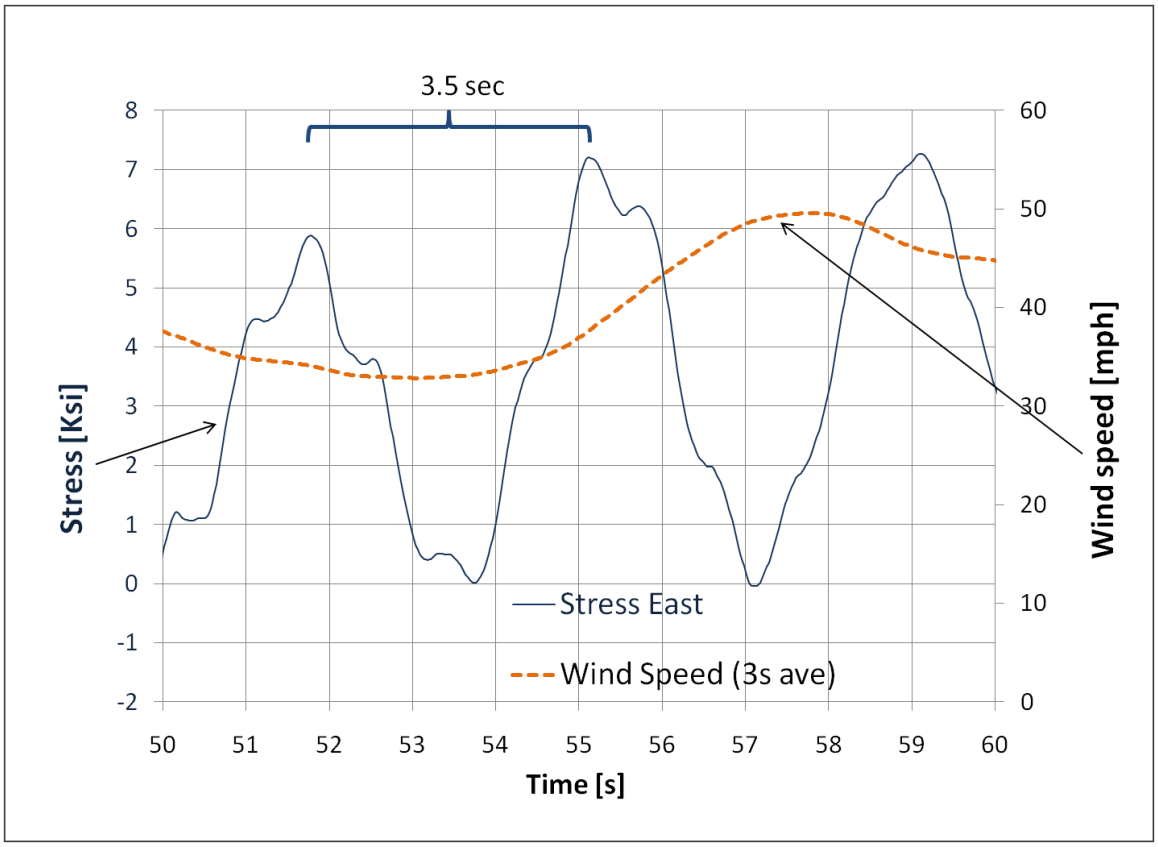

Fig. 5.6. Event recorded on the El Paso US-54 pole at a 50mph wind speed

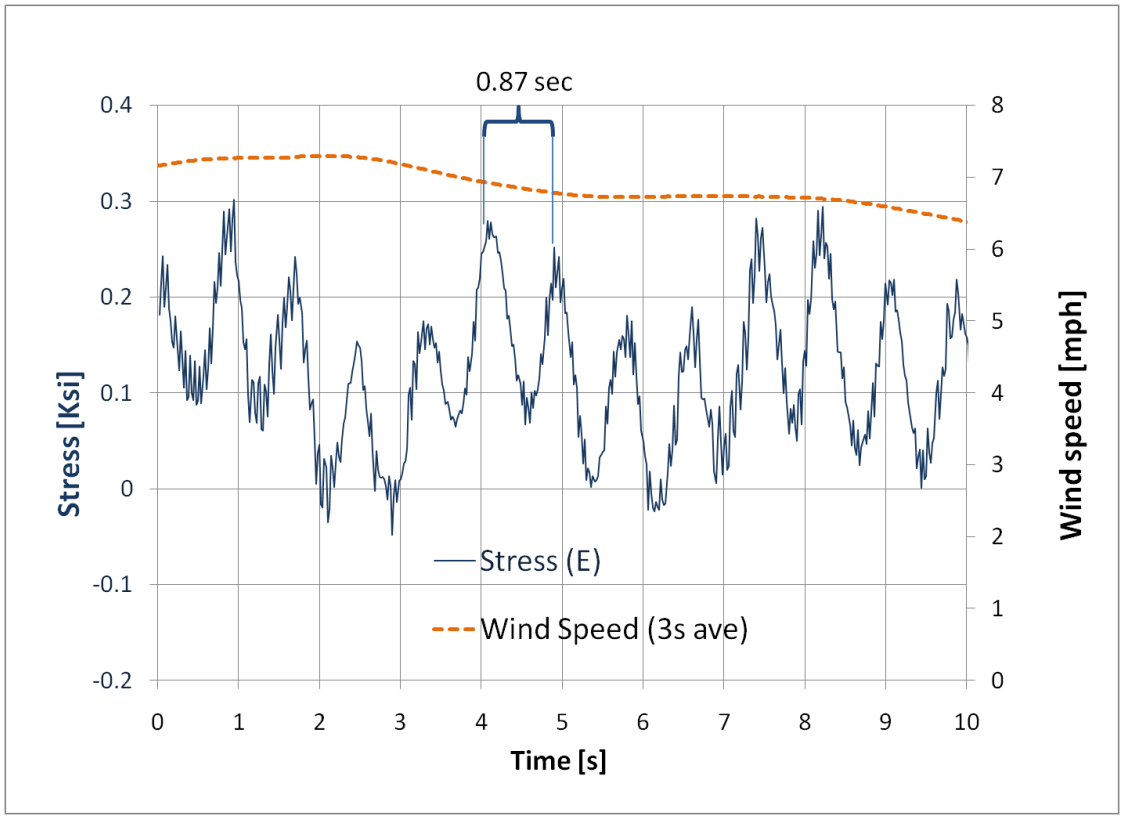

Fig. 5.7. Event recorded on the El Paso US-54 pole at a 7 mph wind speed direction S-S-W

Figure 5.7 shows a graph of a 10 second event record for a 7 mph wind speed. The average wind direction during the recording was 200 degrees (S-S-W). The wind speed is averaged over a three second period, while the stress is averaged above 0.2 seconds. From the recording it can be seen that the HMIP is shaking with a period that is approximately 0.87 seconds, with a 0.2 ksi stress range. This is an indication of vortex shedding exciting the second mode of the structure. This is consistent with the observations from Warpinski (2006) that was discussed in Section 2.4. The difference is in the amount of stress generated in the pole, which in this case remains below 1.5 ksi compared to those reported by Warpinski of values as large as 4 ksi for the vortex-shedding second mode induced vibrations (MTC, 2007).

Figure 5.8 shows an event recorded on the Lubbock pole with a 25 mph wind and a direction 300 degrees (W-N-W). The plot shows the stress measured by the North strain gage, which is measuring mostly cross wind swinging. The strain contains first mode vibrations mixed with a small number of third mode cycles. The period was approximately 0.28 seconds, and had

amplitudes smaller than 0.2 ksi. The third mode vortex shedding induced vibration in the measurements in this study cause small stress variations and are judged not to contribute significantly in the fatigue damage of the pole. This is consistent with the findings from previous studies (MTC, 2007).

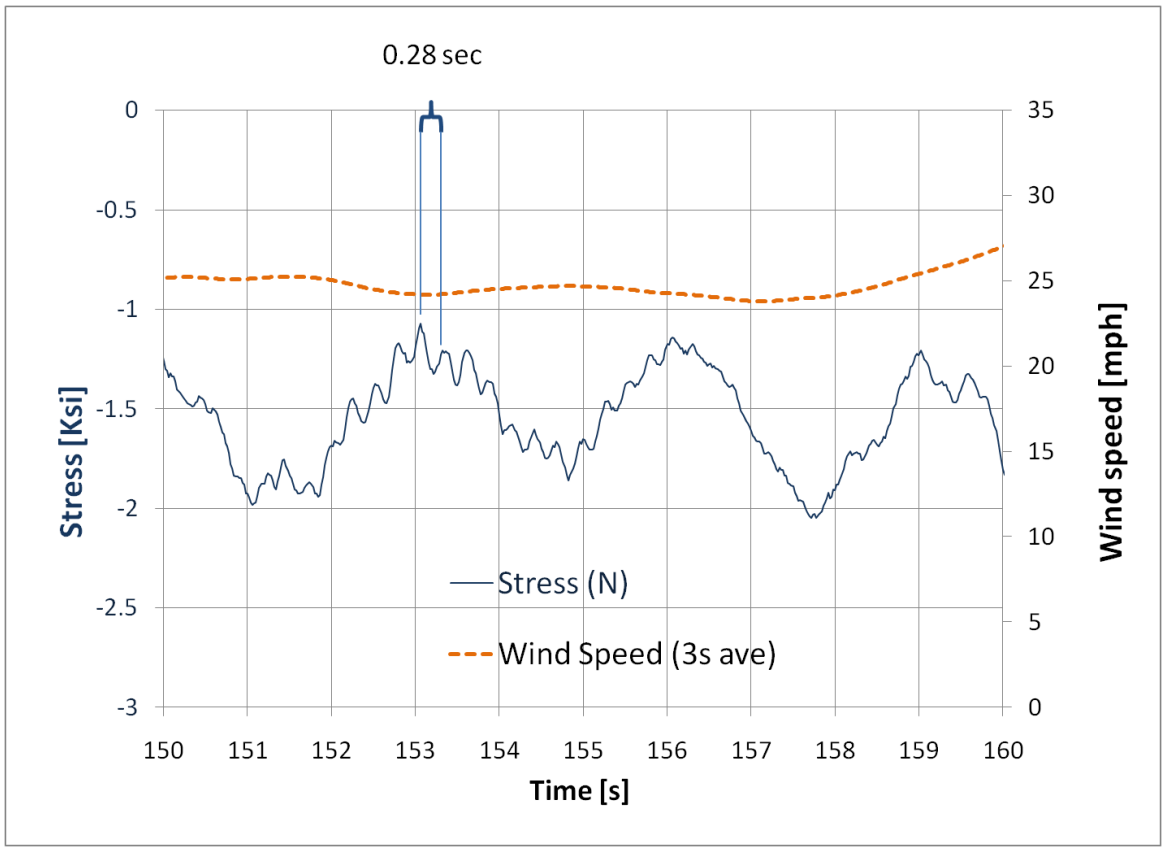

Fig. 5.8. Event recorded on the Lubbock pole at a 25 mph wind speed, direction W-N-W

From the observation of the data it can be concluded that the first and second modes are mostly involved in the excitation of the structure. The first mode excitation occurs at a high wind speed that can cause considerable stress in the structure, but are less likely to occur on an average basis. The second mode induced vibrations have a lower stress range and happen at a lower wind speed and are therefore more common.

Considering the wind activity at the locations where the HMIPs were instrumented, it has been shown that the wind speed with the highest probability of occurrence is approximately 8 mph for El Paso and 11 mph for Corpus Christi and Lubbock. Observing an event with an average wind speed close to 10 mph provides an indication of the average dynamic response of the HMIP. From Figure 5.9 it can be seen that the response is a combination of first and second modes, with stress ranges of roughly 0.2 ksi for the first mode and less than 0.1 ksi for the second mode.

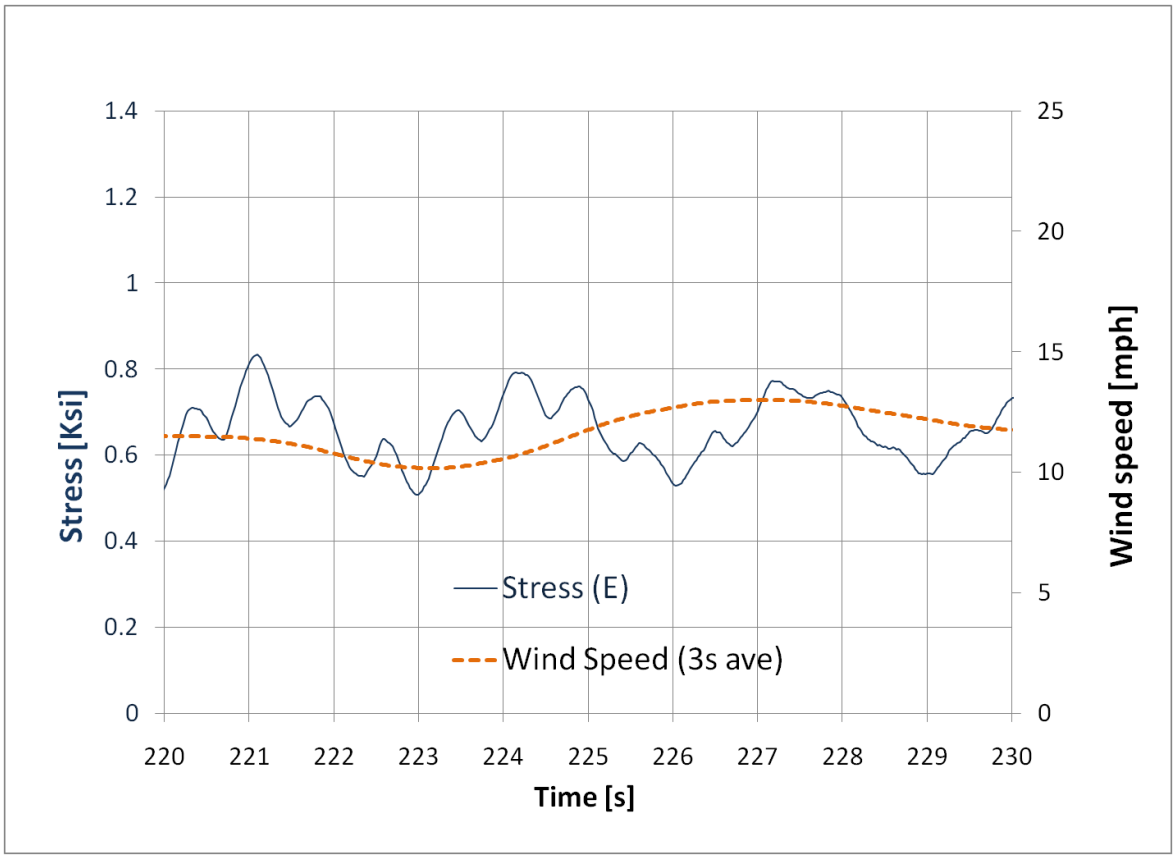

Fig. 5.9. Event recorded on the Lubbock pole at a 10 mph wind speed, direction S-W

Further evaluation will be done to determine how much each of the first and second modes contribute to the fatigue damage of the pole.

5.2.2 Frequency Analysis

This section presents an analysis of the event capture data based on frequency content. The analytical tools used for this analysis are mainly the Fast Fourier Transform (FFT), and the Root Mean Square (RMS).

The FFT indicates an algorithm that produces a Discrete Fourier Transform (DFT) of a generic signal that is the representation of the signal itself in a frequency domain rather than in the time domain. The FFT performs the calculation with a smaller number of operations than the classic DFT, making it suitable for a computational use. More information about the FFT procedure can be found in the literature [e.g. Clough & Penzien, 1994; Paz, 1997; Lynn & Fuerst, 1998].

The root mean square (RMS) of the FFT allows the representation of the acquired time history signal in the frequency domain but keeps the same physical quantity of the signal on the Y-axis. For example, if the strain-time history is investigated, strain is graphed on the Y-axis and frequency is graphed on the X-axis while if stress-time history is investigated, stress is graphed on the Y-axis and frequency is graphed on the X-axis. The general expression of the cumulative RMS is:

$$RMS(f^*) = \sqrt{\int_{f=0}^{f=f^*} FFT(f)} \qquad \text{(Eq.5.2)}$$

The Fourier spectrum for a typical strain record is shown in Figure 5.10. The frequency is reported on the horizontal axis, and the Fourier amplitude is graphed on the vertical axis. The peaks correspond to the first three modes of vibration of the HMIP. Comparisons between the frequencies obtained from the FFT of the strain record and the frequencies calculated with the finite element model are shown in Table 5.3. The comparison shows that the FEM was very accurate for the first two modes with less than 2% difference, while the third mode had a 12% difference.

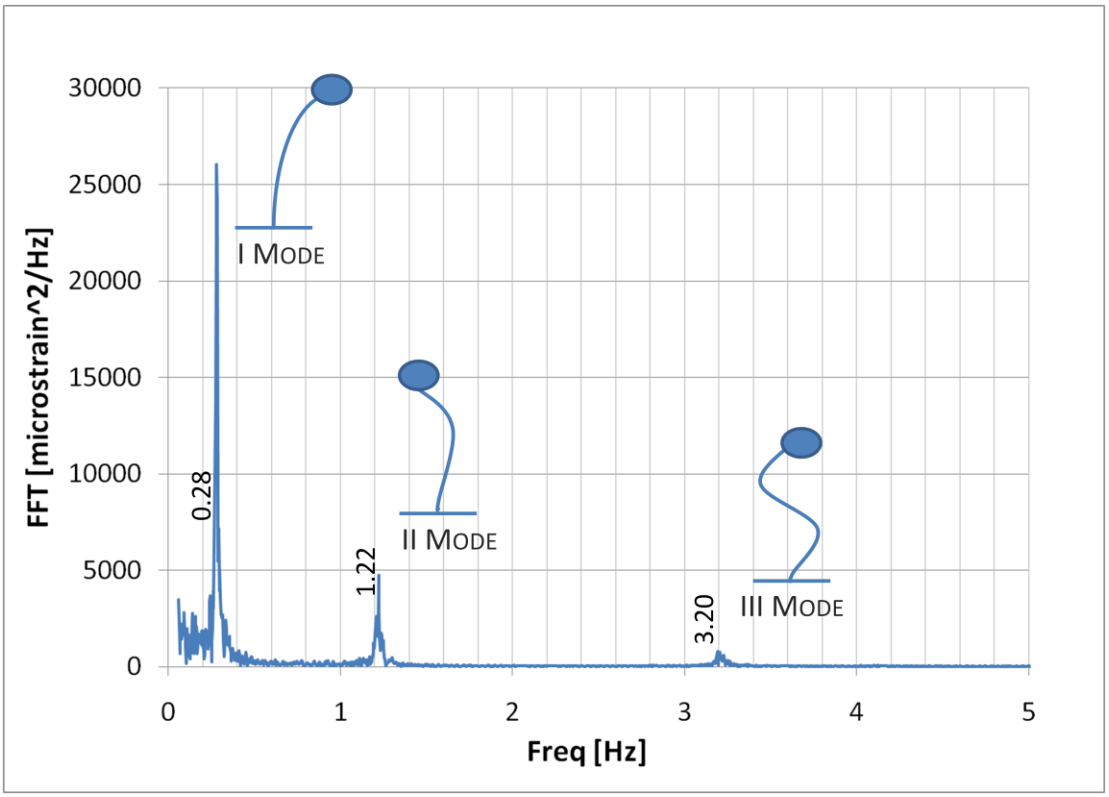

Fig. 5.10. Fourier Spectrum of a strain gage record

Table 5.3. Comparison between the FEM frequencies and FFT frequencies

	f_n FEM [Hz]	f_n FFT [Hz]	Difference [%]
I MODE	0.28	0.28	-
II MODE	1.20	1.22	2
III MODE	3.57	3.20	12

It is also interesting to note that the natural frequencies are similar to the ones calculated in the Iowa Study for the poles in Sioux City (see section 2.5). Despite the different design, the poles have similar dynamic properties, with frequencies differing only to 10% from one to the other. The Iowa poles had indeed the same height (150 ft), the same cross sectional shape (12 sides), but a much thinner baseplate (1.25" vs. 3" for the Texas HMIP) and a smaller base shaft diameter (28.5 " vs. 32.625 ") than the HMIP considered in this study.

Table 5.4. Texas HMIP natural frequencies vs. Iowa HMIP natural frequencies

	TEXAS f_n (FFT) [Hz]	IOWA f_n (FFT) [Hz]	Difference [%]
I MODE	0.28	0.31	10
II MODE	1.22	1.34	10
III MODE	3.20	3.33	4

Figure 5.11 shows the strain FFT (Y-axis on the right) together with the cumulative RMS (Y-axis on the left). The RMS has a monotonic positive trend. The graph starts from zero with a steep slope, which represents the static push of the wind, and for each natural frequency has a step that represents how much each mode contributes in terms of strain. In the plot it can be seen that for the record processed, the first mode contributed the most with roughly 10 microstrain cycles, while the second mode had less than 5 microstrain cycles and occurred with a really small strain range.

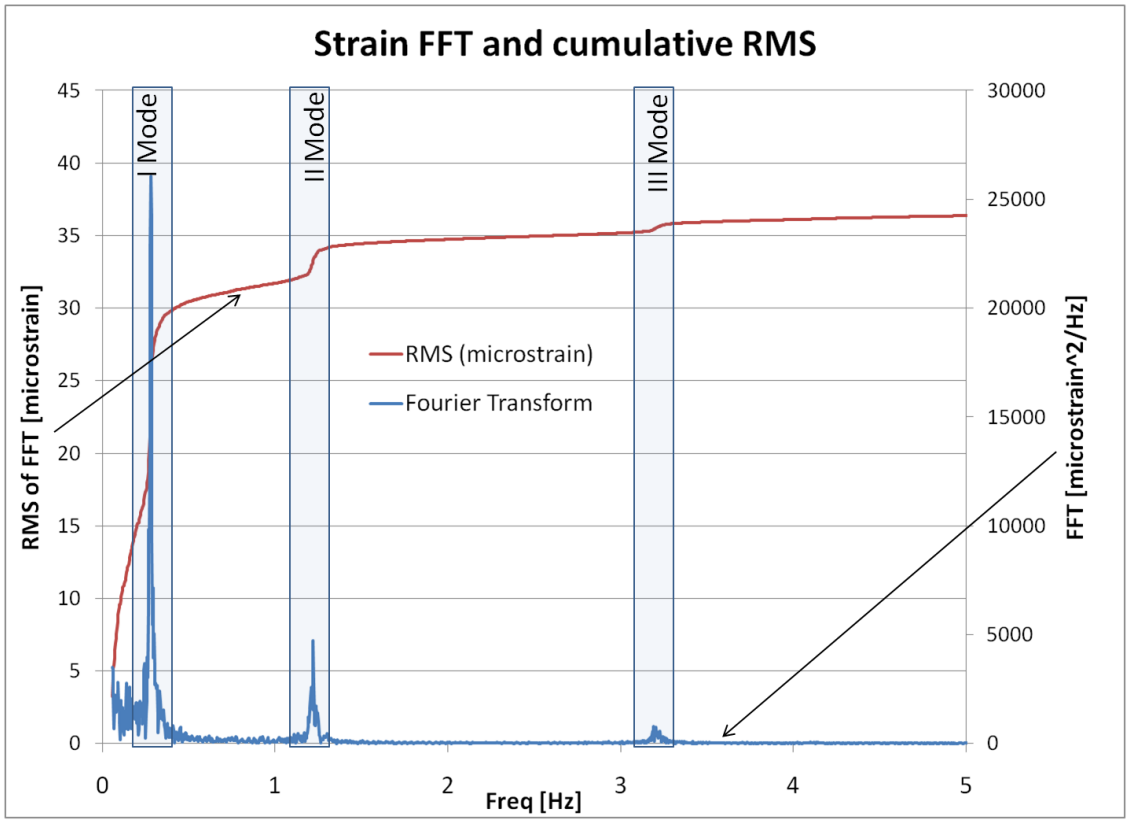

Fig. 5.11. Fourier Spectrum (FFT) and cumulative RMS of a strain gage record

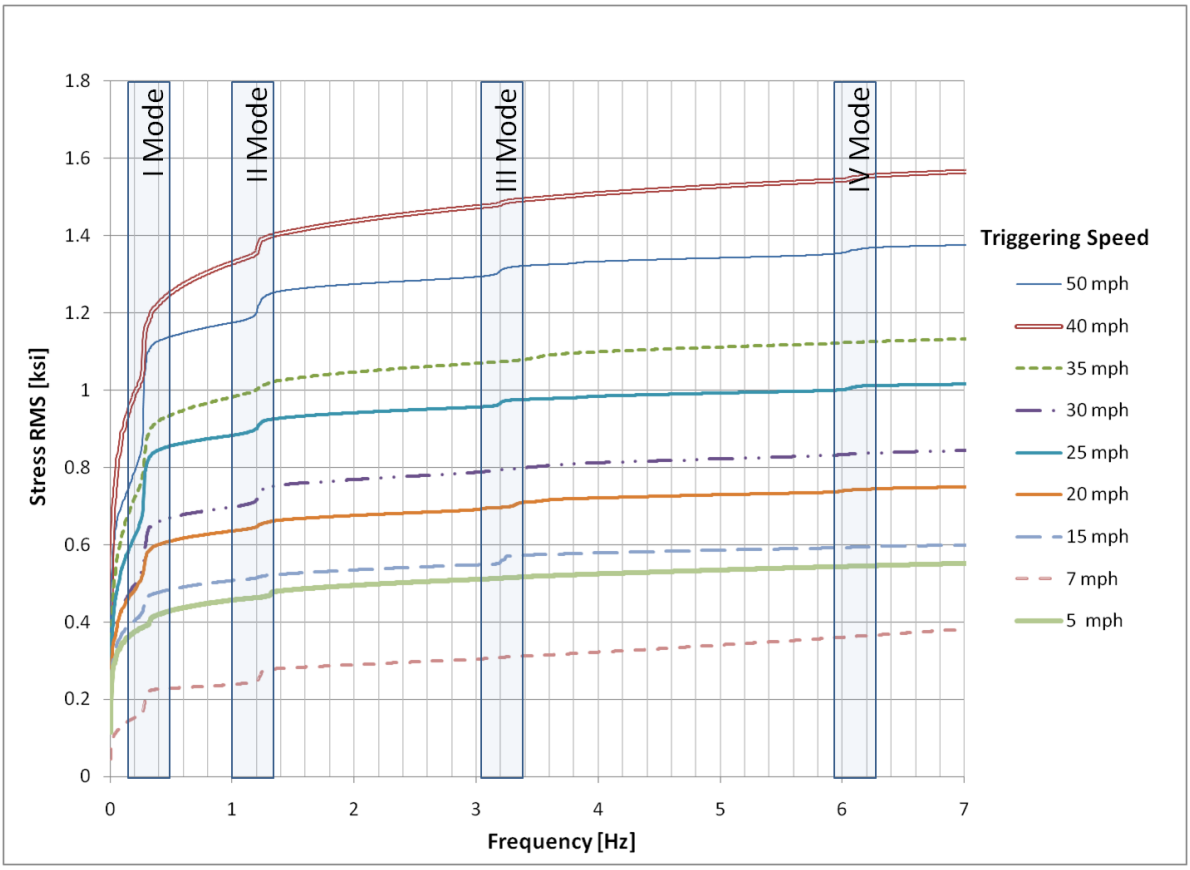

Fig. 5.12. Cumulative RMS of stress records at different triggering wind speeds

Figure 5.12 shows the cumulative RMS of stress records vs. frequency at different wind speeds. From the plot it can be seen that the static wind push generates more stress than the natural vibratory modes at the high wind speeds. Also it can be noticed that, among the natural modes, the first mode contributes the most to the excitation of the pole in terms of stress. The third and fourth modes do not contribute significantly. The second mode stress range is comparable to the first mode induced stress range when the wind speed is close to the critical vortex shedding speed.

The analysis results discussed in Section 5.1.1 can be used to modify the stresses measured at the strain gage locations to the estimate the stresses at the base plate connection. Considering that both the first and second modes contribute to the fatigue damage of the pole, an increment for the measured stress to compute the nominal stress at the base should be between 4.5% and 11%.

Theoretically, the increment should be differentiated depending on the level of stress considered. For low stress cycles, which mostly happen in the 6 to 9 mph wind speed range where the second mode vortex shedding has some effect, an increment of 11% should be applied. While for higher wind speeds that have been shown to excite the first natural mode, the increment should be 4.5%. It was decided to simply apply an average increment of 7% to all the stress levels which makes the nominal stress at the connection ($\sigma_{nominal}$):

$$\sigma_{nominal} = 1.07 \times \sigma_{gage} \qquad \text{(Eq.5.3)}$$

Where σ_{gage} is the stress measured by the strain gages.

5.2.3 Wind Speed to Stress Correlation

This section focuses on the relationship between wind speed and the stress measured on the poles. Figure 5.13 shows data points for multiple events captured on all the poles, together with approximate expressions of the static wind push as suggested by AASHTO (Section 2.3.4), and a second-order polynomial regression of the data points. For each data point, the x-axis coordinate is the maximum wind speed (averaged over 3 seconds) measured during a 5 min event, and the y-axis coordinate is the maximum measured stress from the four strain gages. No distinction was made to see whether the stress was measured transversally or parallel to the wind direction in this plot.

The calculations for the equivalent wind push with the AASHTO equations were carried out considering a simplified shape of the HMIP (Fig.5.14). The lighting ring was modeled as a rectangle with a width equal to the ring diameter (63") and a height of 11", in such a way to cover the same surface area as the lighting apparatus. The AASHTO procedure for the calculations of the equivalent static push was presented in Section 2.3.4.

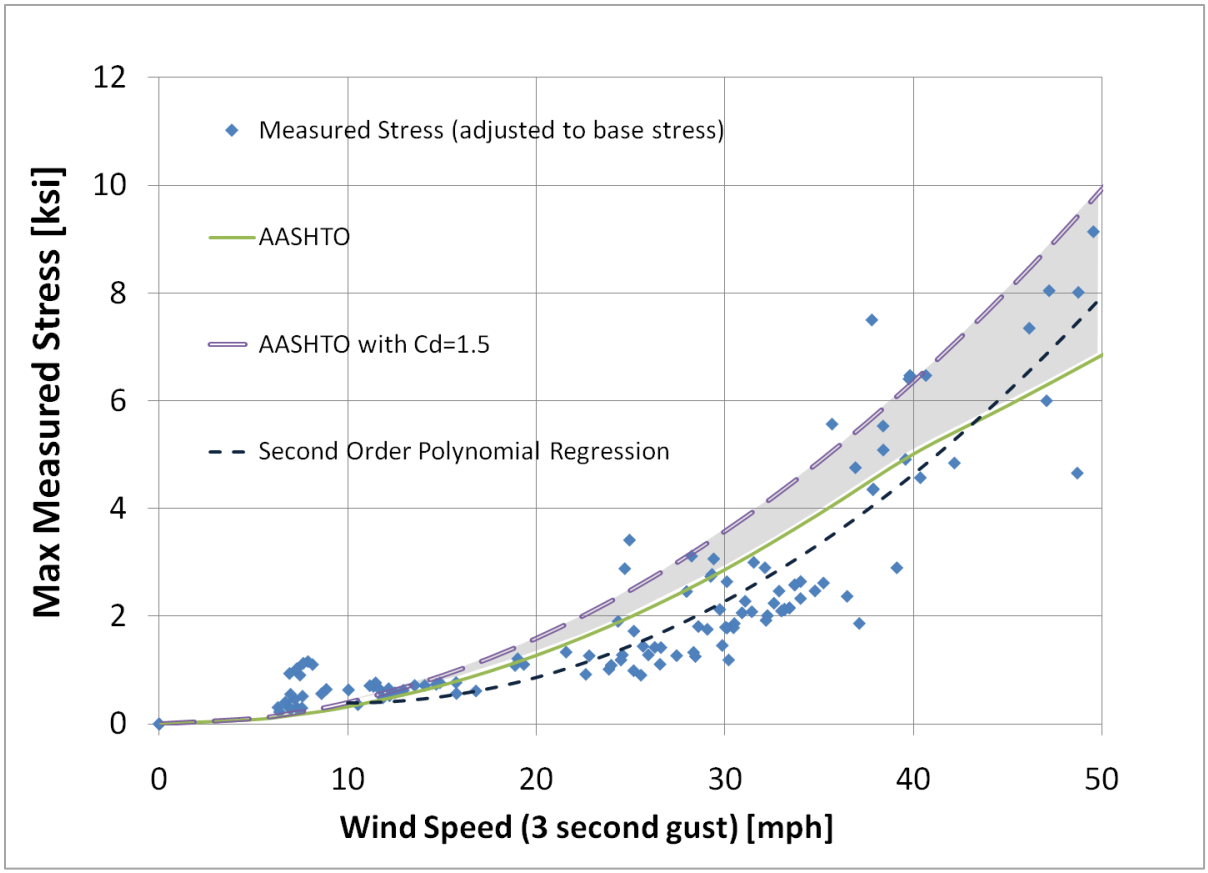

Fig. 5.13. Max measured Stress vs. 3 second wind speed

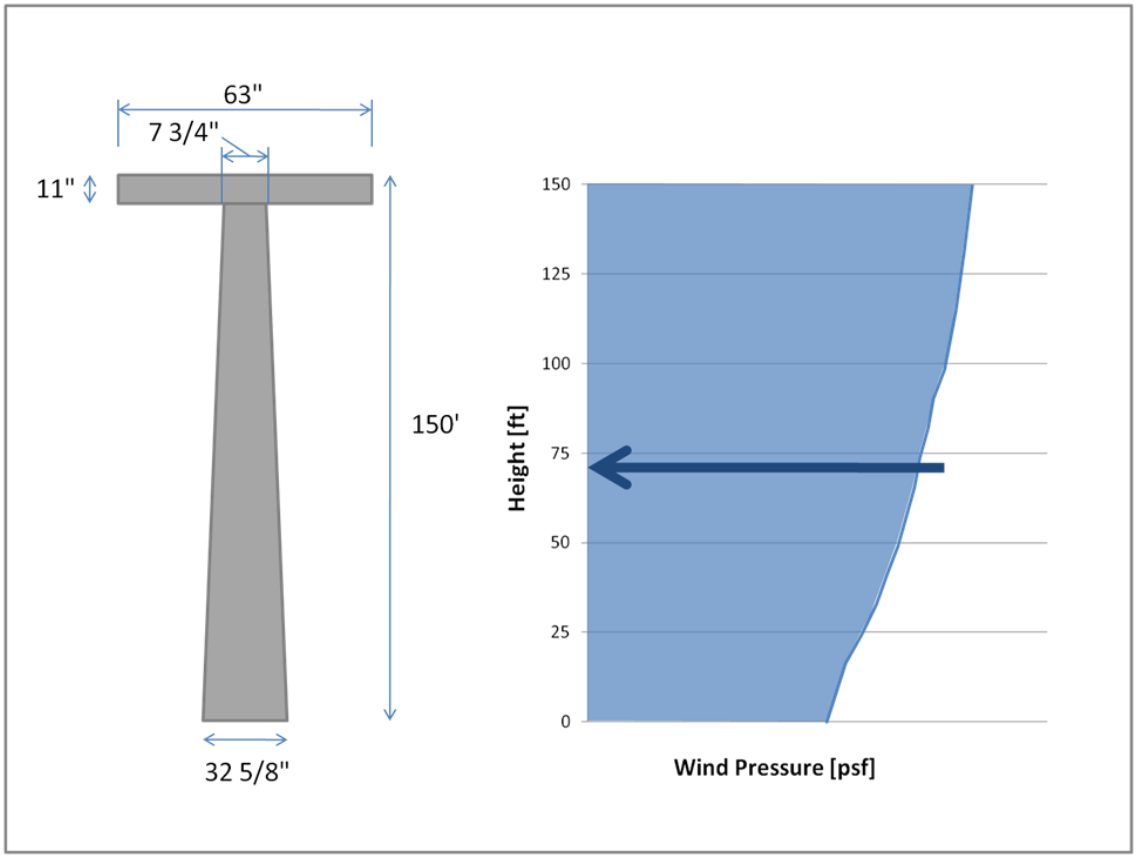

Fig. 5.14. Simplified model for the equivalent wind push

AASHTO suggests the height and exposure factors K_z to account for the variation of the wind speed along the height from the ground. The value of the exposure factor is equal to 1 at a height of 33 ft, which is the typical height at which weather stations are located, and thus wind speed data are available. The exposure factor has a minimum of 0.87 at the ground level and goes up to 1.37 at 150 ft from the ground.

For the gust effect factor the minimum value of 1.14 was used, while for the drag coefficient two options were chosen:

- C_d, as shown in Fig.2.9, specified by AASHTO for a dodecagonal section (solid line)
- C_d = 1.5, which is the average value measured in the wind tunnel testing performed in the Iowa study (MTC,2007), as shown in Figure 2.11 (doubled dash line)

The pole cross wind surface was then divided in sections along the length and for each section the equivalent wind pressure P_i was computed. The bending moment at the base of the pole is then computed as:

$$M_{Base} = \sum P_i \cdot A_i \cdot h_i \qquad \text{(Eq.5.4)}$$

Where P_i is the equivalent wind pressure at the section – i

A_i is the area of the section - i

h_i is the height of the centroid of the section - i.

In Figure 5.12, it can be seen that the AASHTO equivalent push expression with a drag coefficient is higher than the same expression with the drag coefficient suggested by AASHTO. It can also be seen that the recorded data fit the trend of the two curves well and stayed below the AASHTO prediction.

It can also be seen that for events with wind speed below 10 mph the stress in the structure is higher than the static push predictions. This is because the vortex shedding effect locks in the structure second mode of vibration in that range of wind speeds. This seems to be consistent with what has been observed in the Iowa study, although relatively minor vortex shedding induced stresses can be observed.

A plot of the maximum measured stress range and the corresponding average wind speed over a 1 minute period is shown in Figure 5.15. The plot shows a comparison with stresses measured at the Iowa HMIP (Connor, Hodgson 2006) (Warpinski, 2006). It can be seen that from a wind speed of approximately 7mph the induced stresses on the Iowa HMIPs are as high as 2 ksi, while the stresses measured in this study are below 1 ksi. It seems then that this HMIP is less subject to vortex shedding excitation. This is mainly due to a higher taper of the shaft and a larger cross sectional diameter.

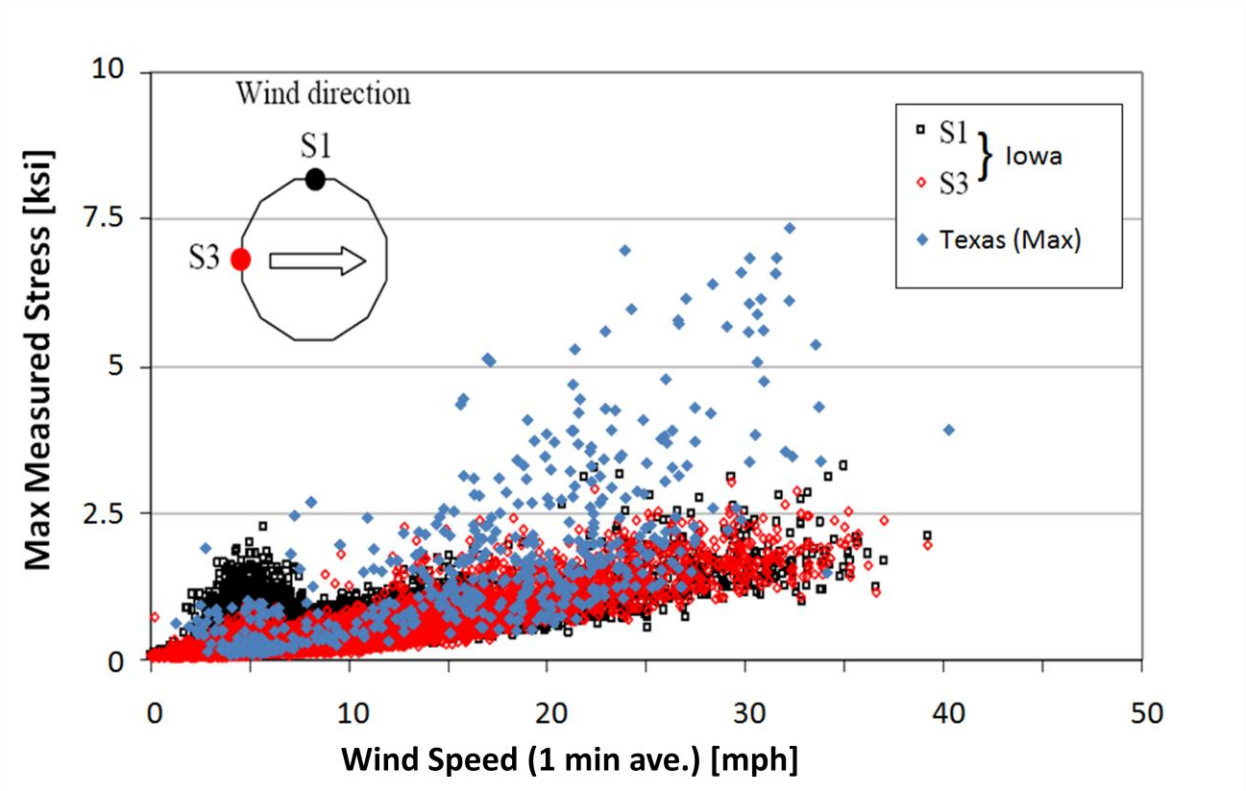

Fig. 5.15. Max measured Stress vs. 1 minute wind speed

Generally it can be stated that the trend of the data points follows a monotonic second order polynomial curve, which means that wind push from buffeting is the prevalent mechanism for the pole.

5.3 Fatigue Assessment with Rainflow Data

This section focuses on the procedure for the fatigue life estimate using the field stress data. The rainflow counting of the stresses provide an indication of the load paths that each pole experienced during the monitoring period. Assuming that each pole will experience the same load path in the future, an estimate of the fatigue life of the poles can be made using the cumulative damage theory as expressed by Miner (1945). The following subsection provides an overview of the cumulative damage theory.

5.3.1 Cumulative Damage Theory

Miner's rule states that the damage resulting from a certain stress range is proportional to the number of cycles that fall in that stress range. The rule can be expressed by the following equation:

$$\sum \frac{n_i}{N_i} = 1 \qquad \text{(Eq.5.5)}$$

Where n_i is the number of cycles at the stress range i

N_i is the number of cycles that would cause failure at the stress range i.

The rule does not consider sequence effects and the average stress of the cycle, both of which have been seen to affect the fatigue life (NSBA, 1998). The fatigue life estimates obtained using this method have a high variability, but they do constitute a good measure of the fatigue performance for the poles, and thus of the hazard of a potential collapse for fatigue.

Miner also stated that a stress path composed by loading cycles of different range can be transformed into a simple load path of constant amplitude. This equivalent stress amplitude S_{Re} can be calculated as:

$$S_{Re} = \left[\sum \gamma_i \cdot S_{Ri}^3\right]^{1/3} \qquad \text{(Eq.5.6)}$$

Where S_{Ri} is the stress range of the bin *i* in the rainflow counting

γ_i is the ratio of the number of cycles of the bin *i* and the total number of cycles $^{n_i}/_{\sum n_i}$.

The number of cycles to failure is calculated as:

$$N_{fail} = A \cdot {S_{Re}}^{-3} \qquad \text{(Eq.5.7)}$$

Where S_{Re} is the equivalent stress amplitude as defined in Eq. 5.1

A is a constant that depends on the fatigue performance of the detail under consideration.

AASHTO defines different 7 different fatigue categories as listed in Table 5.5. The best fatigue category is A and the worst performance is category E'. For each category a value of *A* is specified as indicated in Table 5.5.

Table 5.5. AASHTO *A* values for the fatigue performance

AASHTO FATIGUE CATEGORY	A	B	B'	C	C'	D	E	E'
A [x 10^8 ksi^3]	250.0	120.0	61.0	44.0	44.0	22.0	11.0	3.9

Once the value of *A* is defined, the estimate can then be computed as:

$$Expected\ Life\ [yr] = \frac{N_{fail}}{n_{eq}} \times \frac{\#\ days\ of\ data\ record}{365} \qquad \text{(Eq.5.8)}$$

Where N_{fail} is the number of cycles to failure as previously defined

n_{eq} is the equivalent number of cycles measured during the instrumentation time

$\#\ days\ of\ data\ record$ is the time length of the data set available.

It is clear that the longer the period of instrumentation, and thus the data set, the more realistic the prediction will be. Wind activity can indeed vary depending on the season, being generally higher in the spring time.

5.3.2 Definition of the fatigue performance

Defining the correct fatigue coefficient *A* for the HMIPs is of key importance in the process of assessing the expected fatigue life. The detail used in the HMIP under consideration is a full penetration groove welded between the tube and the transverse plate connection, welded from both sides (without backing bar). This detail is categorized as E by the AASHTO specifications. Category E therefore provides a good representation of the resistance for an un-cracked pole. However, micro-cracks due to galvanizing have been found to reduce the resistance (Pool, 2010). It is reasonable to assume the connection is an AASHTO category E′, the lowest category.

A more accurate estimate of the resistance comes from using the cyclic load test results. A library of six tests performed on 33" (84 cm) diameter 12-sided poles is available for comparison (Pool, 2010; Stam, 2009). Test results are available for poles without cracks, poles with initial micro-cracks, as well as poles repaired with "field repair" and "shop repair" procedures. The plot in Figure 5.16 shows the results of the laboratory fatigue tests in the previous research work. The solid red circle dot represents the design that is more critical, and that is under consideration in this study. A way to determine the *A* coefficient based on the performance showed in the load test is to draw a line on the plot that passes through the data point (Figure 5.14). The expression of the *A* coefficient then becomes:

$$A = N \cdot {S_{Re}}^3 = 81{,}326 \cdot 12^3 = 1.4 \times 10^8\ ksi^3 \qquad \text{(Eq.5.9)}$$

Two estimates were made for the HMIP. The first estimate assumed AASHTO category E', and the second estimate assumed the same capacity of the pole tested in the laboratory. Although not presented in this thesis, two additional specimens will be fatigue tested in this research study. One of the specimens is the base section of the pole on IH10 in El Paso, which will be taken out of service and shipped to Ferguson Lab. Multiple ultrasonic inspections performed on this pole within the last two years have found that the pole has cracks in 11 out of 12 of the shaft bends and that the cracks are growing with time. This test will give the best estimate of fatigue resistance for other poles in service that present this type of cracking.

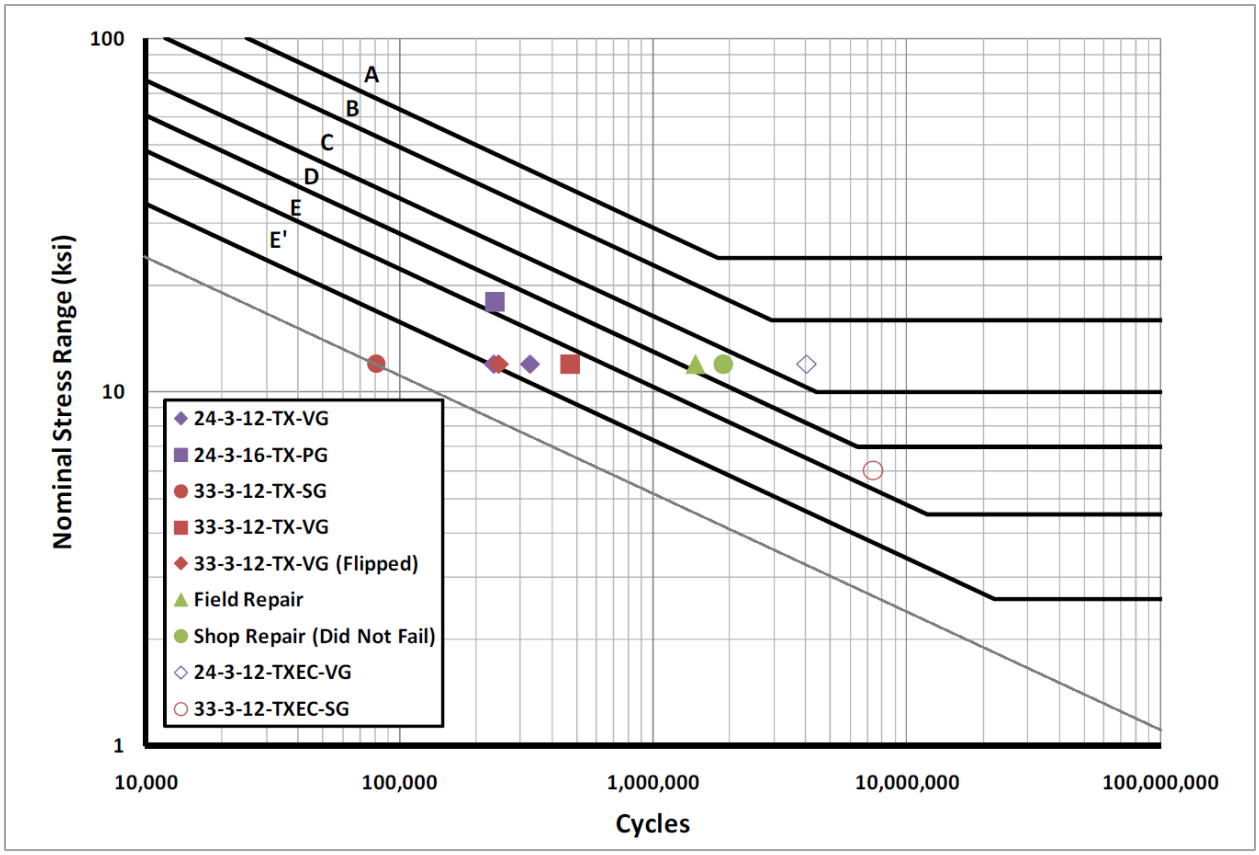

Fig. 5.16. Definition of the Fatigue Performance of a cracked HMIP based on load test results

5.3.2 Estimates of the fatigue life

From an observation of rainflow counting data (Fig.5.17) it can be seen that the pole on US54 is the one with the most number of cycles for relevant level of stress. It is also the one that had the most reliable instrumentation system in terms of continuity, and had the longest period of recoded data. In the wintertime when the sun exposure was the shortest, the system showed a good recharging behavior.

Most of the cycles for all the poles happen in the low stress range, smaller than 2 ksi. This means that low stress cycles have a strong impact in the fatigue damage computation. The process of counting stress cycles for fatigue damage evaluation uses a process referred to as rainflow counting. In the procedure, Small stress cycle increments are defined so that cycles within a certain range can be counted in a "bin". For example, if a "bin" size of 0.25 ksi is selected, stress ranges would be counted in 0-0.25 ksi, 0.25-0.5 ksi, 0.5-0.75 ksi, and so on. To understand how

much every bin contributes to the damage of the structure a plot of $\gamma_i \cdot S_{Ri}^3$ versus S_{Ri} can be done (Fig. 5.18). It can be seen that for all the locations instrumented, the peak damage happens at stresses below 1 ksi. The plot decreases quickly past 1 ksi for the El Paso IH-10 and Corpus Christi HMIPs, while for the Lubbock and El Paso US-54 HMIPs cycles up to 3 ksi still possess a significant contribution. As mentioned above, the US-54 instrumentation has been operating the longest, ensuring a continuity of operation even in the winter months. The rainflow counting from El Paso US54 represents the most reliable measure of the stress path exciting the structure on an average basis.

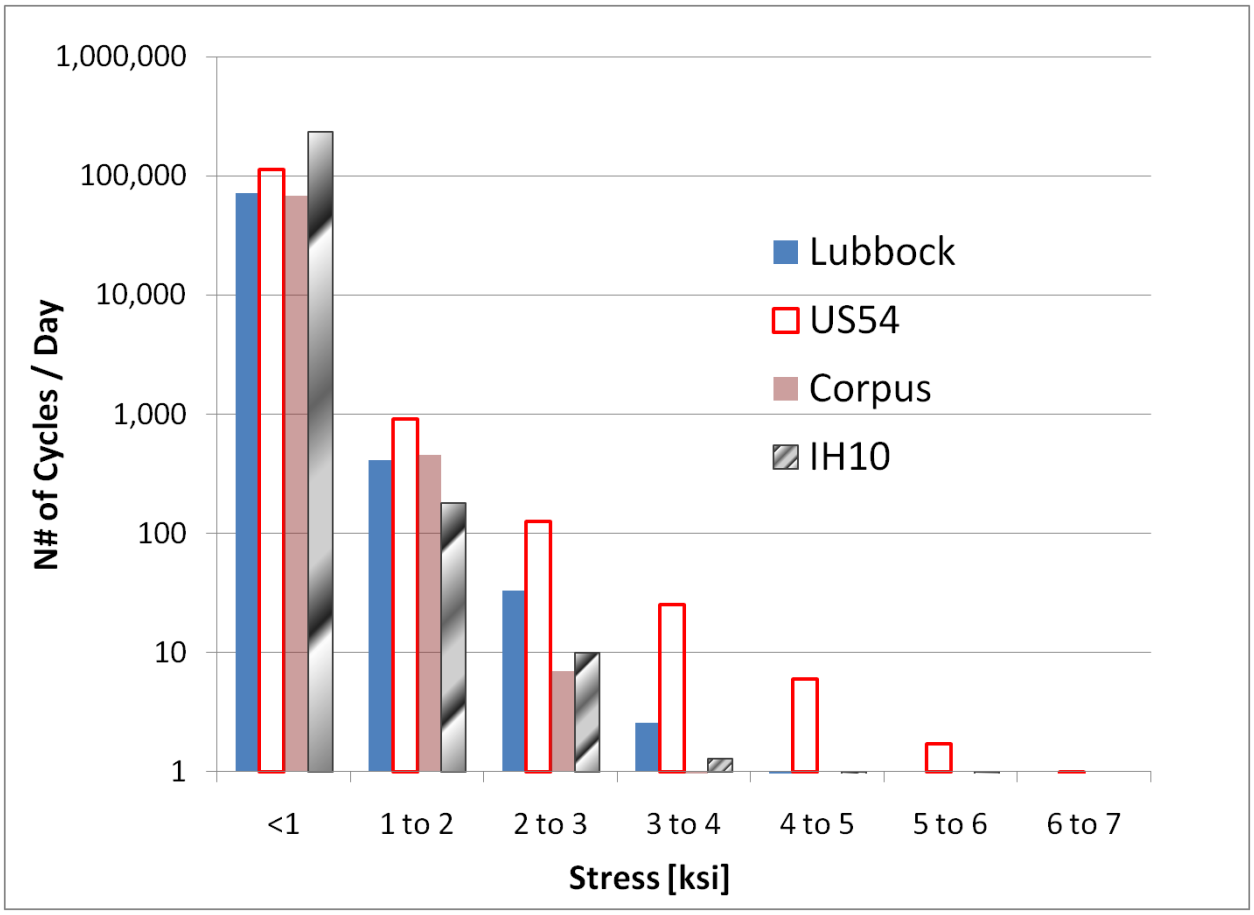

Fig. 5.17. Rainflow Counting per day of record.

The rainflow counting was programmed to discard strain cycles smaller than 2 microstrains, which corresponds to a stress level of 0.006 ksi. These really small cycles can indeed be considered noise rather than actual strain measurements. AASHTO specifies a value of constant

amplitude limit stress (ΔF) for each fatigue category. This value is a lower bound threshold for the stress, below which cycles are not considered to cause cumulative fatigue damage in the structure. For this specific case, since the performance of the HMIP with initial cracking is relatively low, below every category specified by AASHTO, and because the structure is subject to low stress cycles, it is not easy to determine a fixed value for ΔF. Therefore, rather than use a fixed limit, increasing values of ΔF have been employed, discarding bins lower than a specified amount from the fatigue life calculations. The following tables show the calculations of the expected fatigue life for the poles instrumented at varying constant amplitude limit stresses. The life estimate named "Cracked" (right end column) is computed using the load test performance, with a value of $A = 1.4 \times 10^8\ ksi^3$. The plot in Figure 5.19 shows how the fatigue life estimate ("cracked") for each HMIP changes depending on the constant amplitude limit stress used. A general rule to choose the appropriate limit is to take the value for which the curve changes slope and starts growing rapidly. From the curves it is not easy to detect such a change. The El Paso US-54 HMIP is the only pole that shows a sudden change in slope, happening between 0.4 and 0.5 ksi. It was then decided to use a constant amplitude limit stress equal to 0.5 ksi. The rows corresponding to that stress limit have been highlighted in the tables (0.44 ksi). In many field studies stress ranges below 0.5 ksi are often used as a limit below which stress cycles are considered noise.

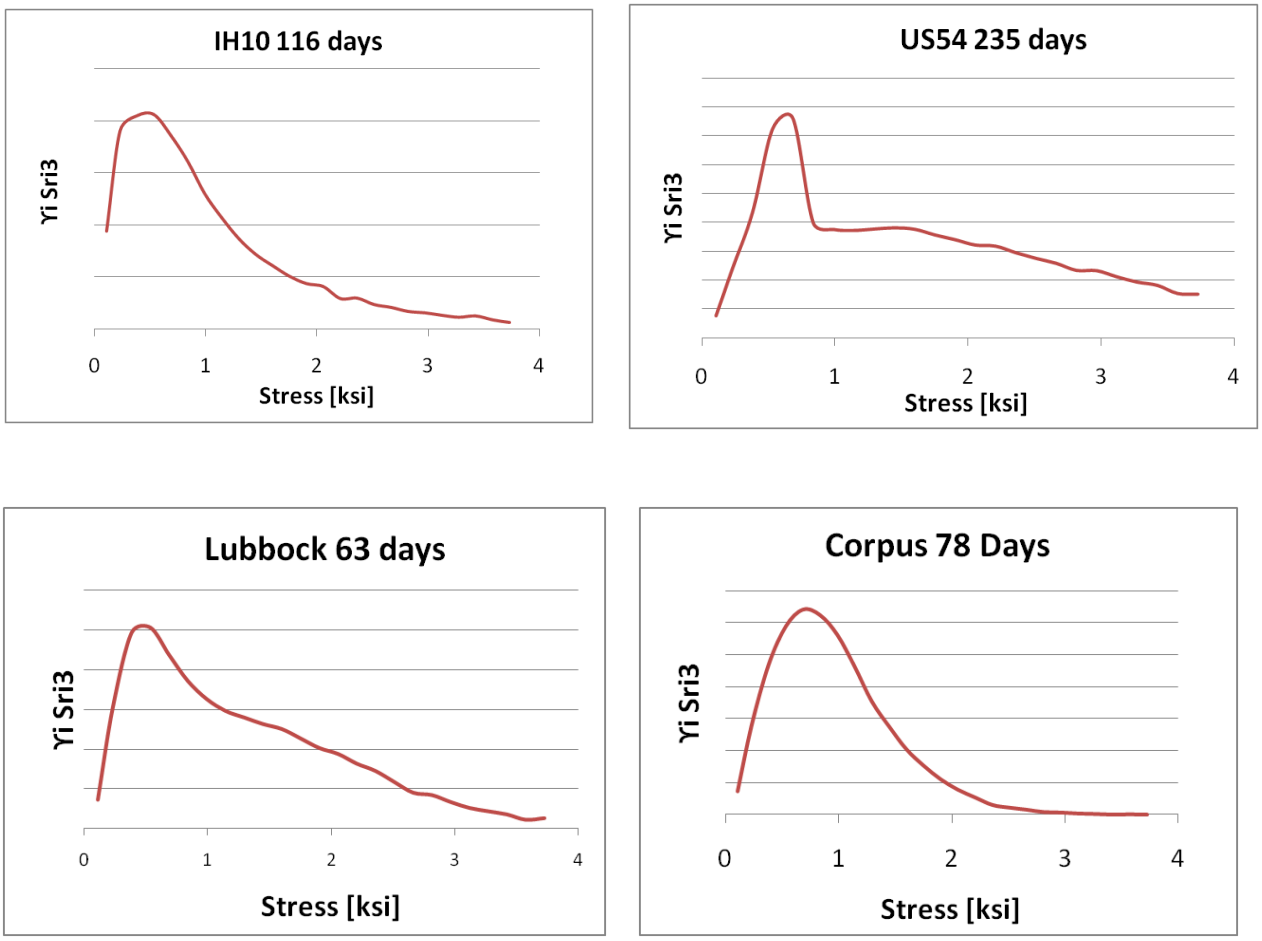

Fig. 5.18 Fatigue damage contribution of each stress range

Table 5.6. Fatigue life estimates for the El Paso US-54 HMIP

Constant Amplitude Limit Stress	(Σ Yi Sri3)1/3	Neq	Nfail	Life (E')	Life (Cracked)
[ksi]	[ksi]			[yr]	[yr]
0.06	0.48	26912148	3927155184	94	34
0.15	0.67	9971072	1466940218	95	34
0.30	0.86	4587909	692701796	97	35
0.44	**1.04**	2466757	391186904	**102**	**36**
0.59	1.29	1175145	203469967	111	40
0.74	1.62	538548	103169929	123	44
0.89	1.82	355735	72175559	131	47
1.03	2.01	251379	54009991	138	49
1.18	2.18	184064	42001140	147	52
1.33	2.36	137214	33411133	157	56
1.48	2.53	103273	26977139	168	60

Table 5.7. Fatigue life estimates for the El Paso IH-10 HMIP

Constant Amplitude Limit Stress	(Σ Yi Sri3)1/3	Neq	Nfail	Life (E')	Life (Cracked)
[ksi]	[ksi]			[yr]	[yr]
0.06	0.22	26912148	39413277120	461	165
0.15	0.42	9971072	5802153301	520	186
0.30	0.67	4587909	1457954886	610	218
0.44	**0.86**	2466757	683363484	**700**	**250**
0.59	1.06	1175145	370106495	825	295
0.74	1.25	538548	222819185	982	351
0.89	1.45	355735	142891048	1176	420
1.03	1.65	251379	97385906	1401	501
1.18	1.84	184064	69611570	1661	593
1.33	2.03	137214	51992336	1952	697
1.48	2.22	103273	40155822	2283	815

Table 5.8. Fatigue life estimates for the Lubbock HMIP

Constant Amplitude Limit Stress [ksi]	(Σ Yi Sri3)1/3 [ksi]	Neq	Nfail	Life (E') [yr]	Life (Cracked) [yr]
0.06	0.39	26912148	7203595397	275	98
0.15	0.72	9971072	1184167453	297	106
0.30	0.93	4587909	545654065	331	118
0.44	**1.15**	2466757	290050655	**376**	**134**
0.59	1.35	1175145	176943586	426	152
0.74	1.54	538548	119930302	480	171
0.89	1.71	355735	87415503	539	193
1.03	1.87	251379	66929661	609	217
1.18	2.02	184064	52771435	692	247
1.33	2.17	137214	42531759	795	284
1.48	2.33	103273	34687446	926	331

Table 5.9. Fatigue life estimates for the Corpus Christi HMIP

Constant Amplitude Limit Stress [ksi]	(Σ Yi Sri3)1/3 [ksi]	Neq	Nfail	Life (E') [yr]	Life (Cracked) [yr]
0.06	0.39	26912148	7.34E+09	295	105
0.15	0.53	9971072	2.98E+09	299	107
0.30	0.69	4587909	1.32E+09	317	113
0.44	**0.85**	2466757	7.21E+08	**352**	**126**
0.59	1.00	1175145	4.41E+08	410	146
0.74	1.15	538548	2.88E+08	499	178
0.89	1.30	355735	1.98E+08	631	225
1.03	1.46	251379	1.41E+08	831	297
1.18	1.62	184064	1.03E+08	1122	401
1.33	1.77	137214	78411439	1534	548
1.48	1.93	103273	61034730	2148	767

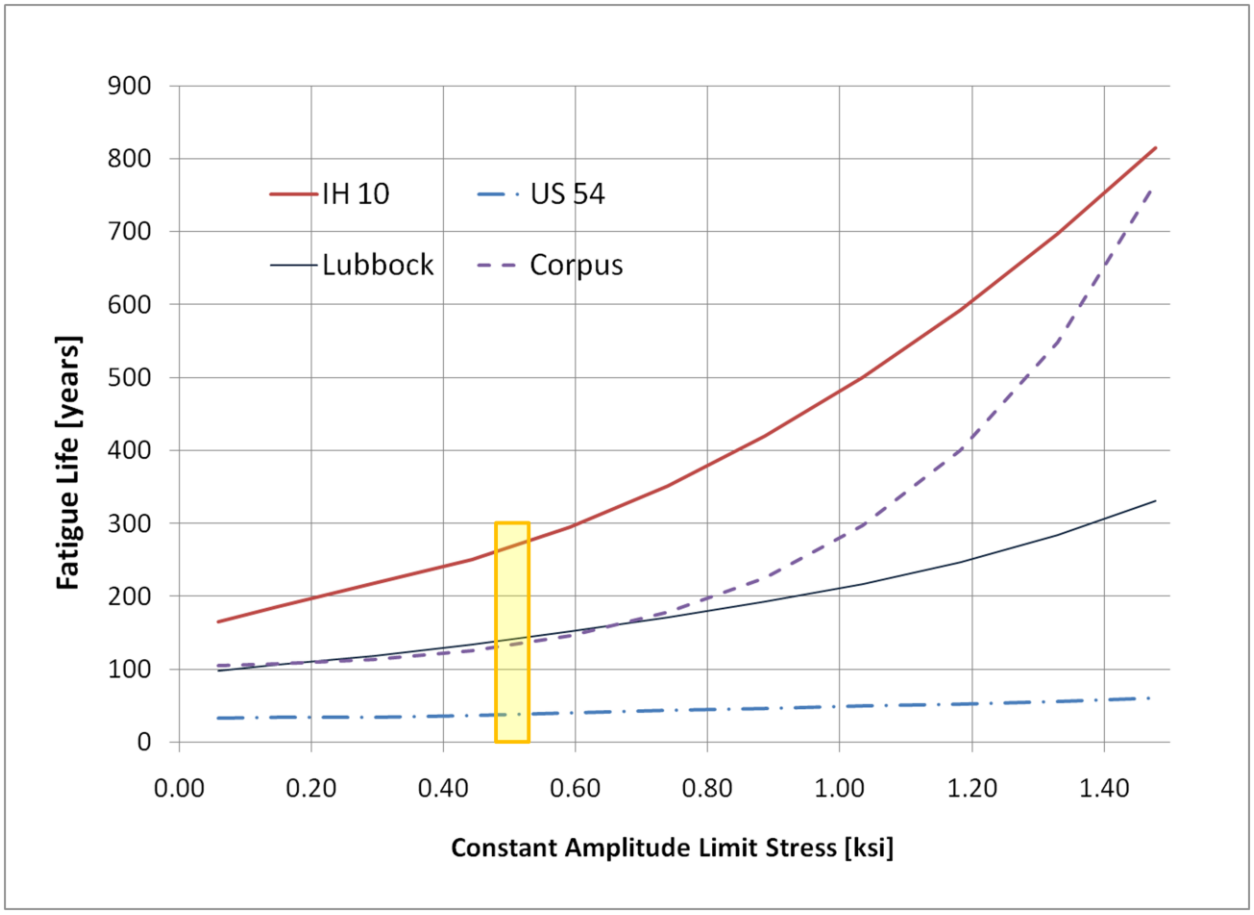

Fig. 5.19. Fatigue Life Estimate (cracked) as function of the Constant Amplitude Limit Stress for the instrumented HMIPs

5.4 Modification to the estimate due to short term measurement

This section suggests a modification to the fatigue life estimate to account for the fact that measurements have not been taken throughout a whole year. The main issues of discontinuity in the measurements were due to a low recharging power provided by the solar panels during the winter months. The powering performance of the systems is discussed in the next section.

The following plots represent for each location instrumented the number of days of measured data for each month (right axis), together with the average monthly wind speed at that location (left axis). The El Paso US-54 instrumentation setup was installed in May 2010, together with the El Paso IH-10 instrumentation, which was removed in September 2010 to be transferred to Lubbock. Both the instrumentation setups in El Paso showed a good performance in terms of continuity and charging power during the period of operation. The Corpus Christi and the Lubbock instrumentations, on the other hand, showed a poor performance during the wintertime.

It is useful to observe what the average wind speed was during the days of operation as opposed to the other months of the year. Indeed the fatigue life estimate is carried out with the assumption that the stress history measured during the instrumentation period represents the same level of stress that the structure will experience in the future. For this assumption to be acceptable, the average wind activity during the monitoring period has to be close to the average yearly wind activity.

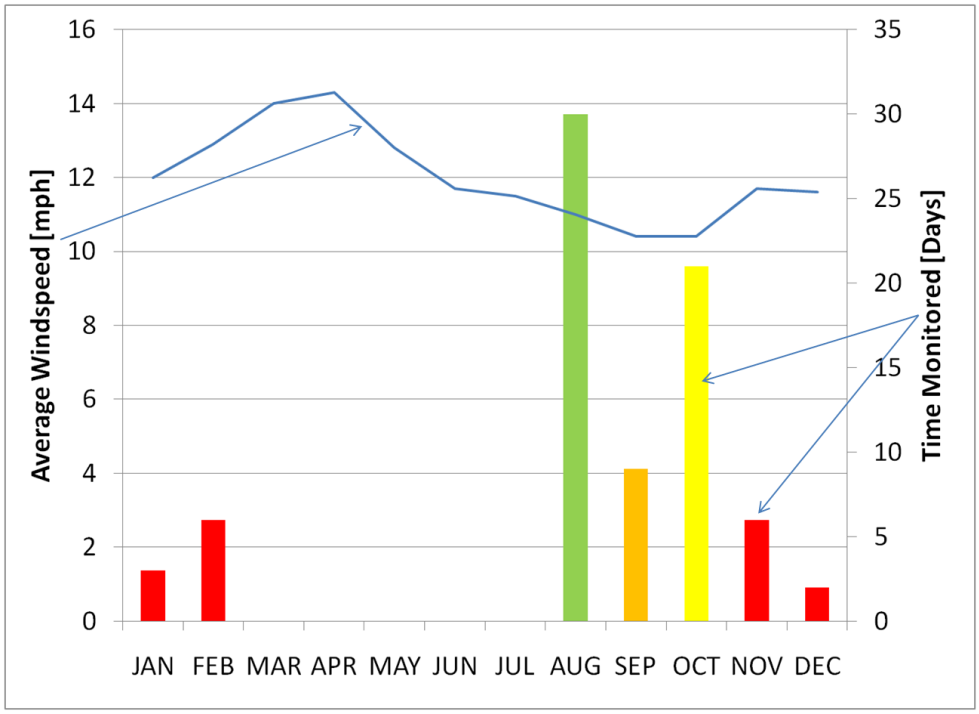

Fig. 5.20. Days of Operation and Average Monthly wind speed for the Corpus Christi HMIP

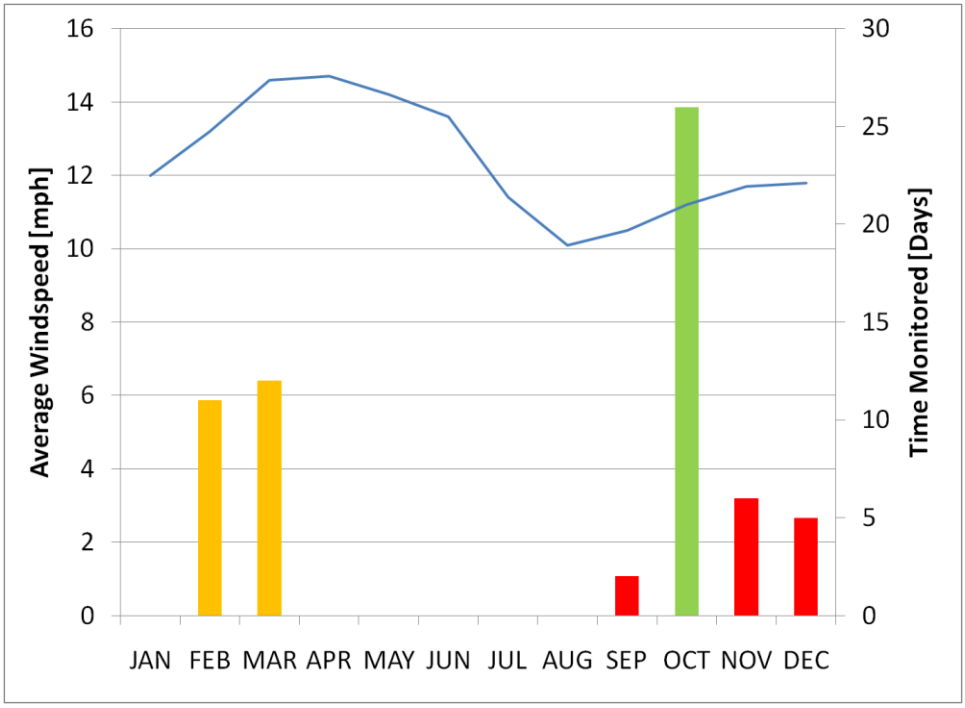

Fig. 5.21. Days of Operation and Average Monthly wind speed for the Lubbock HMIP

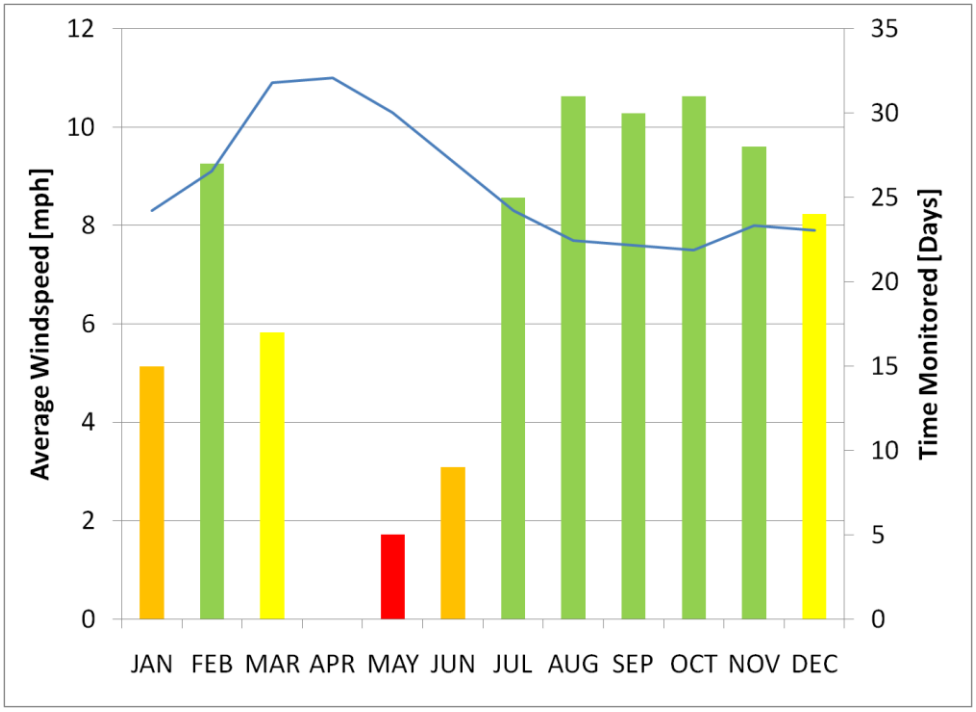

Fig. 5.22. Days of Operation and Average Monthly wind speed for the El Paso US-54 HMIP

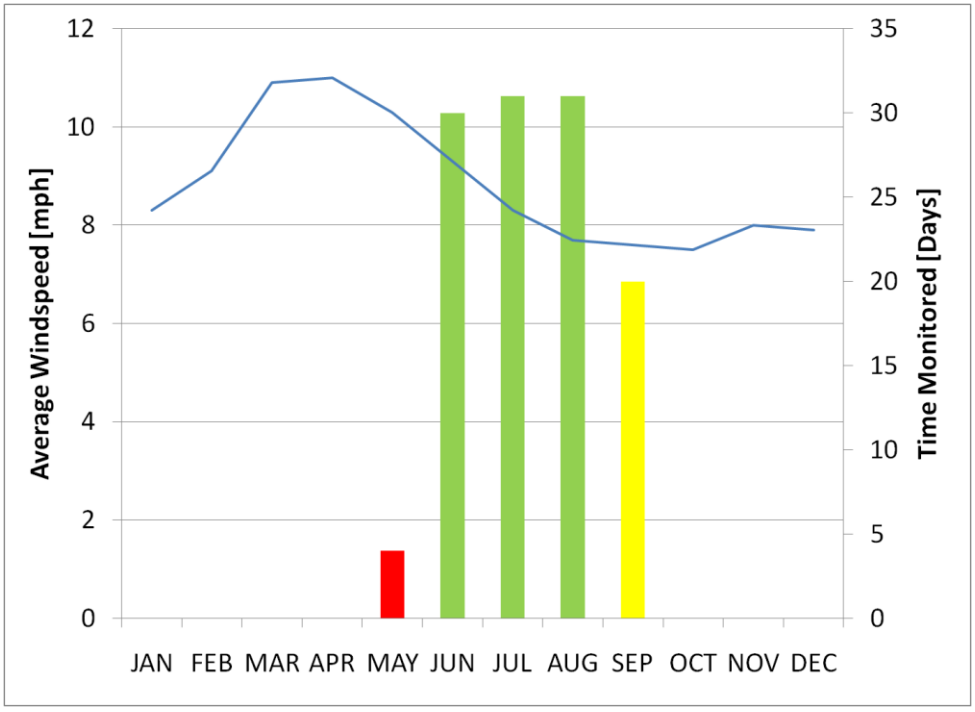

Fig. 5.23. Days of Operation and Average Monthly wind speed for the El Paso IH-10 HMIP

The modification to the fatigue estimate was carried out considering the average wind speed during the instrumentation period for each pole (V_{inst}) and the average wind speed throughout the year (V_{year}). Qualitatively, if the average wind speed during the instrumentation is lower than the average wind during the whole year, it is assumed that the measurements underestimate the excitation effect on the HMIPs. Recalling the data plot shown in Figure 5.12, the relationship between the stress and the wind speed has been seen to be following a monotonic trend, and that the vortex shedding effect does not have a strong impact on the low speeds. For this reason a stress correction factor is calculated using the AASHTO equivalent static push expression (solid line in Figure 5.12). The stress correction factor is calculated as the ratio of the two stresses obtained inputting V_{year} and V_{inst} in the AASHTO equation. It seems reasonable to assume that this stresses could represent the average stress cycles that the HMIPs are subjected to, under an average wind.

The next step is to modify the fatigue life prediction. Recalling Miner's rule, the expression of the number of cycles to failure, is a function of the stress range to the power of three. The correction for the fatigue life is then obtained by elevating the stress correction factor to the power of three. The fatigue life reduction factors for each location calculated with these assumptions and listed in Table 5.10. It can be seen that the fatigue life estimate for the Corpus Christi location should be reduced by 70%. This big reduction is due to the fact that the rainflow counting available for that location where measured when the wind activity was low. The fatigue estimate for Lubbock should be reduced by only 5%, because the average wind speed during the instrumentation period is close to the yearly average wind speed.

Table 5.10. Modification of the fatigue life estimate for short term monitoring period

	V_{year}[3] [mph]	V_{inst} [mph]	Stress Correction Factor	Fatigue Life Reduction Factor
CORPUS CHRISTI	12.0	11.0	1.19	**1.70**
EL PASO - US54	8.8	8.3	1.12	**1.39**
EL PASO - IH10	8.8	8.3	1.11	**1.36**
LUBBOCK	12.4	12.3	1.02	**1.05**

[3] Source www.weatherunderground.com

Based on these coefficients, the fatigue life estimates previously calculated are modified (Table 5.11). These estimates could represent the expected fatigue life for all the HMIPs with the critical design (12 sided section, 150ft tall, 80 mph design wind speed, and without external collar) that are in service in the same locations. The fatigue life calculated assuming AASHTO category E' would be appropriate for HMIPs with a limited amount of cracking, while the estimate using the load test resulting capacity (cracked) would be appropriate with poles having extended cracking. From these numbers it can be seen that the El Paso US54 pole has the highest potential for fatigue failure. All the other locations reported values that are higher than 50 years, which is the typical design life for these poles, thus they are less likely to encounter a fatigue failure. These estimates represent a good measure for the fatigue failure hazard of this type of HMIPs. It can be said that HMIPs located in the El Paso area, presenting cracking at the base connection should be considered for a replacement or a repair. One of the reasons why the El Paso area could be more critical for the fatigue performance of these poles is that the average windspeed throughout the year has a peak of occurrence in the 6 to 8 mph range (Fig. 4.3). In this location the II mode vortex shedding could have a bigger impact on the excitation of the structure, causing the HMIPs in that area to experience more cycles than the ones in other locations.

Table 5.11. Modification of the fatigue life estimate for short term monitoring period

Location	**Fatigue Life (E')** [years]	**Fatigue Life (Cracked)** [years]
EL PASO - US54	73	**26**
EL PASO - IH10	515	**184**
LUBBOCK	358	**128**
CORPUS CHRISTI	207	**74**

Chapter 6 Conclusions

6.1 Introduction

This thesis documented a research investigation on the fatigue performance of high mast illumination poles. The work presented is part of a larger study that has included laboratory tests, monitoring the behavior of HMIP sections during galvanizing, computational studies, and monitoring of HMIPs in the field. The primary focus of this thesis was the field monitoring of existing HMIPs in the state of Texas and a small portion of the computational studies. Measurements of stress and wind speed on high mast illumination poles where used to determine the dynamic behavior under wind loading and to estimate their remaining fatigue life. Chapter 2 of the thesis provided a summary of background information from previous studies on the subject. In Chapter 3 a description of the instrumentation used for the field monitoring was provided. Chapter 4 showed preliminary data regarding the HMIP locations. In Chapter 5 the observation of the measured data, a study on the dynamic behavior of the poles, the fatigue life estimate, as well as the supporting finite element models were discussed. This final chapter presents the conclusions for this research work.

6.2 Finite Element Analyses

The computational studies presented in this thesis consisted of results from a modal analysis from a finite element model of the poles subjected to wind and gravity loading. Two models were used consisting of a line element model and a shell element model. The support conditions of the poles consisted of restraints from translation and rotation at the base of the HMIP.

- The modal analysis performed on the frame cantilever model of the HMIP provided good estimates for the natural periods of the poles. The comparison of the computed natural periods with the Fourier spectrum of the measured stresses showed that the error was less than 10% on the third natural mode.
- The second order bending moment at the base connection generated by differential heating on the HMIP was computed to be 43k-in.

- The analysis performed on the shell finite element model showed that the support conditions can affect the stress concentration at the shaft to base plate connection of the HMIP, in such a way that the fatigue life can reduce by a factor of 1.8.

6.3 Field Monitoring Data

- Vortex shedding takes place at a wind speed close to 7 mph, exciting the second natural mode. The maximum nominal stress range at the pole connection caused by vortex shedding is less than 1 ksi. When compared to the HMIP designs in other states, the TXDOT pole geometry has a higher taper of the shaft, which mitigates the effect of vortex shedding on the structure.
- The El Paso pole on US-54 was found to have a remaining fatigue life lower than the design life, which is 50 years. Observing the recording from weather stations in El Paso it was observed that the average daily wind speed is close to 7 mph.
- The fatigue life estimate showed that the equivalent stress amplitude for all the HMIP locations was close to 1ksi.
- Both vortex shedding and buffeting contribute to the fatigue damage of the poles.

6.4 Future Work

- The fatigue testing that will be performed on the HMIP taken out of service from the El Paso, IH-10 location will provide an indication of the fatigue performance of a pole that is heavily cracked in the field. This information will allow another estimates of the fatigue life for the poles instrumented.
- Considering that the equivalent stress measured on the poles was close to 1 ksi, the new load testing should be performed with a lower stress amplitude than what was used in the previous phases. The minimum stress amplitude that could be used will be controlled by the time required to reach the expected number of cycles to failure at the maximum loading frequency that the hydraulic actuators can deliver.
- From the inspection of the cracks after the fatigue test of this pole it will be possible to determine if the cracks were growing in the field as it seems to be from the multiple

Ultrasonic inspections performed. The cracks will be cut open to determine whether their nature is fatigue or thermal, from the galvanizing process.

6.5 Recommendations to HMIP Owners

- An important aspect of proper HMIP installation is that the top and bottom anchor nuts on the baseplate are properly tightened and tack welded, because that has been found to affect the fatigue life of the poles.
- Based on the results of the fatigue life estimates it is recommended that a replacement or a repair of the poles that are found to be heavily cracked should be considered by the owners.

Appendix A: Texas Department of Transportation's Standard Plans for High Mast Illumination Poles

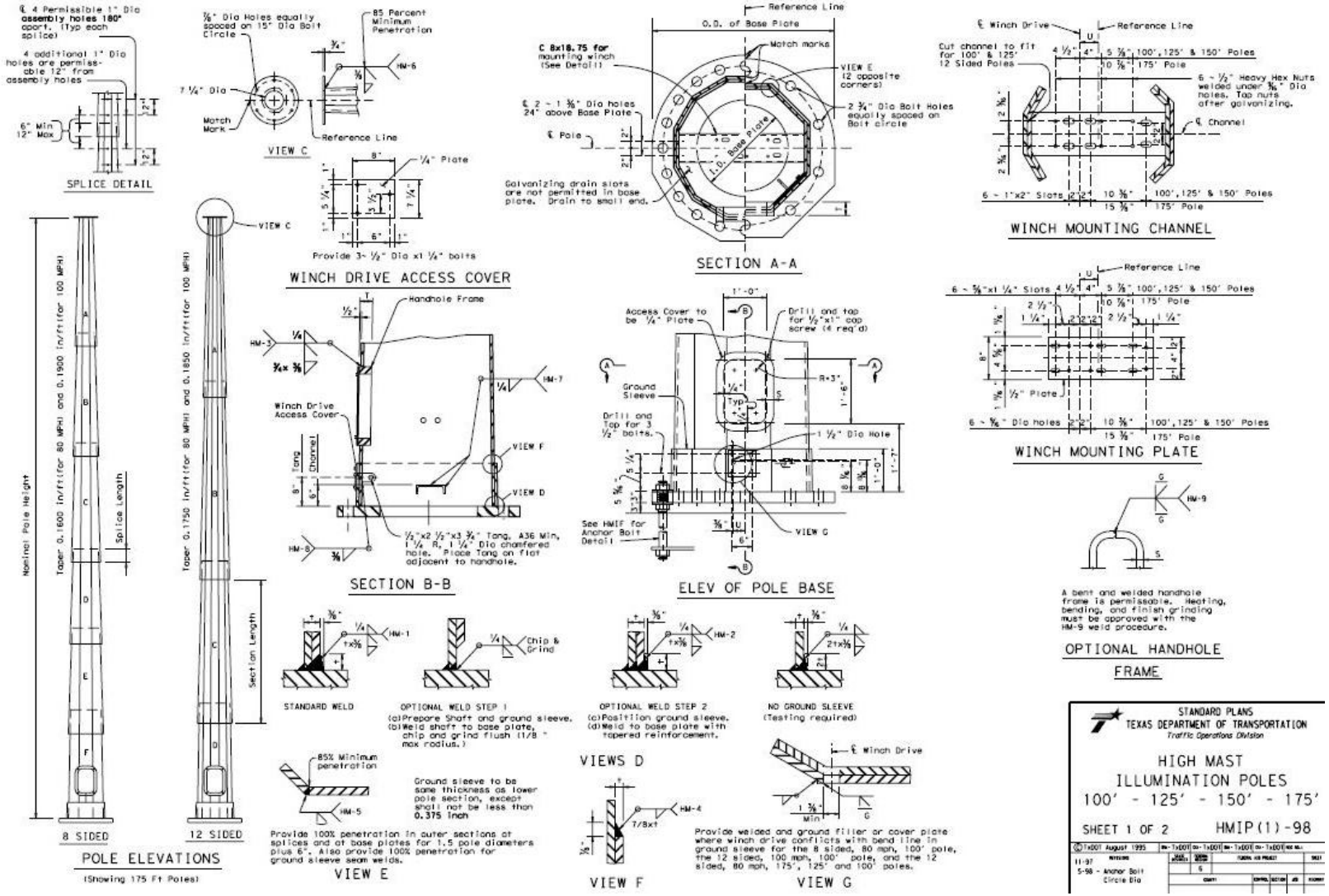

STANDARD PLANS
TEXAS DEPARTMENT OF TRANSPORTATION
Traffic Operations Division

HIGH MAST ILLUMINATION POLES
100' - 125' - 150' - 175'

SHEET 1 OF 2 HMIP(1)-98

©TxDOT August 1995 | 8x-TxDOT | 8x-TxDOT | 8x-TxDOT

11-97 REVISIONS
5-98 - Anchor Bolt Circle Dia

TABLE OF VARIABLE POLE DIMENSIONS

	Ht (ft)	Section	8 SIDED POLE Diameter (Inches) Bottom	Diameter (Inches) Top	Thickness (Inches)	Length (feet)	Splice (Inches)	12 SIDED POLE Diameter (Inches) Bottom	Diameter (Inches) Top	Thickness (Inches)	Length (feet)	Splice (Inches)
80 MPH DESIGNS	175	A	13.083	7.750	.250	33.33	19	16.792	7.750	.250	51.67	24
		B	17.792	12.205	.375	34.92	25	24.858	15.817	.313	51.67	36
		C	22.250	16.583	.375	35.42	32	32.625	23.583	.313	51.67	48
		D	25.375	20.948	.438	27.67	36	36.250	31.175	.375	29.00	~
		E	28.375	23.895	.500	28.00	41					
		F	31.250	26.703	.500	28.42	~					
	150	A	13.083	7.750	.250	33.33	19	16.792	7.750	.250	51.67	24
		B	17.792	12.205	.375	34.92	25	24.858	15.817	.313	51.67	36
		C	22.250	16.583	.375	35.42	32	32.625	23.583	.313	51.67	~
		D	25.375	20.948	.438	27.67	36					
		E	28.375	23.895	.500	28.00	~					
	125	A	13.083	7.750	.250	33.33	19	16.792	7.750	.250	51.67	24
		B	17.792	12.205	.375	34.92	25	24.858	15.817	.313	51.67	36
		C	22.250	16.583	.375	35.67	32	28.250	23.583	.313	26.67	~
		D	25.375	20.948	.438	27.67	~					
	100	A	13.083	7.750	.250	33.33	19	16.792	7.750	.250	51.67	24
		B	17.792	12.205	.375	34.67	25	24.625	15.817	.313	50.33	~
		C	22.250	16.583	.375	35.67	~					
100 MPH DESIGNS	175	A	14.208	7.875	.313	33.33	20	17.433	7.875	.375	51.67	25
		B	19.792	13.142	.375	35.00	28	25.747	16.173	.438	51.75	37
		C	25.250	18.473	.438	35.67	36	33.750	24.176	.438	51.75	49
		D	29.000	23.680	.500	28.00	42	37.375	31.995	.500	29.08	~
		E	32.625	27.210	.563	28.50	47					
		F	36.125	30.631	.563	28.92	~					
	150	A	14.208	7.875	.313	33.33	20	17.433	7.875	.375	51.67	25
		B	19.792	13.142	.375	35.00	28	25.747	16.173	.438	51.75	37
		C	25.250	18.473	.438	35.67	36	33.750	24.176	.438	51.75	~
		D	29.00	23.680	.500	28.00	42					
		E	32.625	27.210	.563	28.50	~					
	125	A	14.208	7.785	.313	33.33	20	17.433	7.875	.375	51.67	25
		B	19.792	13.142	.375	35.00	28	25.747	16.173	.438	51.75	37
		C	25.250	18.473	.438	35.67	36	29.125	24.176	.438	26.75	~
		D	29.00	23.680	.500	28.00	~					
	100	A	14.208	7.875	.313	33.33	20	17.433	7.875	.375	51.67	25
		B	19.792	13.142	.375	35.00	28	25.500	16.173	.375	50.42	~
		C	25.250	18.473	.438	35.67	~					

Diameters are measured across the flats.

TABLE OF VARIABLE BASE DIMENSIONS

	Ht (ft)	O.D. (Inches)	I.D. (Inches)	Bolt Cir (Inches)	No. Bolts	S (Inches)	T (Inches)	U (Inches)
		8 SIDED POLE						
80 MPH DESIGNS	175'	47	22	41	16	2.00	3.75	4.50
	150'	44	18	38	12	2.00	4.00	3.50
	125'	41	16	35	8	2.00	4.50	3.50
	100'	37	14	31	6	2.00	5.00	3.50
		12 SIDED POLE						
	175'	50	24	44	12	1.75	3.50	3.50
	150'	47	22	41	10	1.75	3.50	2.50
	125'	42	18	36	8	1.75	3.75	2.50
	100'	38	13	32	6	1.75	4.00	2.50
		8 SIDED POLE						
100 MPH DESIGNS	175'	52	27	46	20	1.75	3.50	4.50
	150'	49	23	43	16	1.75	4.00	3.50
	125'	45	21	39	12	1.75	4.50	3.50
	100'	40	17	34	10	1.75	4.50	3.50
		12 SIDED POLE						
	175'	52	27	46	16	1.75	3.25	3.50
	150'	50	25	44	12	1.75	3.50	2.50
	125'	46	22	40	10	1.75	3.75	2.50
	100'	42	19	36	6	1.75	4.00	2.50

NOTE: Base Plate may be round or with 8 or 12 equal segments matching the pole.

GENERAL NOTES:

Design conforms to AASHTO Standard Specifications for Structural Supports for Highway Signs, Luminaries, and Traffic Signals and Interim Revisions thereto. The Design Wind Speed is 80 mph or 100 mph.

The required design height and wind speed shall be as shown elsewhere in the plans.

Each pole section, top flange plate and base plate shall be permanently marked on the reference line. The required mark locations are shown on the baseplate, top plate, and foundation plan details. These marks shall be used in pole assembly and erection alignment. The reference line and anchor bolt orientation shall be parallel to roadway centerline unless otherwise shown on Lighting Layouts.

STANDARD PLANS
TEXAS DEPARTMENT OF TRANSPORTATION
Traffic Operations Division

HIGH MAST ILLUMINATION POLES 100' - 125' - 150' - 175'

SHEET 2 OF 2 HMIP(2)-98

DN: TxDOT	CK: TxDOT	DW: TxDOT	CK: TxDOT

REVISIONS	DIST.	COUNTY	HIGHWAY NO.	SHEET
5-98 - Anchor Bolt Circle Dia	6			

COUNTY	CONTROL	SECTION	JOB	HIGHWAY

References

1. American Association of State Highway and Transportation Officials, AASHTO Standard Specifications for Structural Supports for Highway Signs, Luminaries and Traffic Signals, Fourth Edition, AASHTO, Washington, D.C., 2001.

2. American Society of Civil Engineers, Minimum Design Loads for Buildings and Other Structures. ASCE7-10, 2010.

3. Anderson, T.H., Fatigue Life Investigation of Traffic Mast-Arm Connection Details, M.S. Thesis, Department of Civil Engineering, The University of Texas at Austin, August 2007.

4. Chang, B., Phares, B.M., Sarkar, P.P., and Wipf, T.J., Development of a Procedure for Fatigue Design of Slender Support Structures Subjected to Wind-Induced Vibration, Transportation Research Record: Journal of the Transportation Research Board, No. 2131, Transportation Research Board of the National Academies, Washington, D.C., 2009, pp. 23–33. DOI: 10.3141/2131-03

5. Clough, R.W., Penzien, J., Dynamics of Structures, Third Edition, Computers and Structures Inc., Berkeley, CA, 2003.

6. Connor, R.J., Hodgson, I.C., Field Instrumentation, Testing, and Long-Term Monitoring of High-Mast Lighting Towers in the State of Iowa, Pennsylvania Department of Transportation Final Report, November 2006

7. Downing, S.D., Socie, D.F., Simple Rainflow Counting Algorithms, International Journal of Fatigue, Volume 4, Issue 1, pp. 31-40, 1982.

8. Fisher, J.W., Kulak, G.L., and Smith, I.F.C., A Fatigue Primer for Structural Engineers, NSBA/AISC, Chicago, IL, 1998.

9. High Mast Illumination Poles. Standard Plans, Texas Department of Transportation (TXDOT), August 1995.

10. Kinstler, T.J., Current Knowledge of the Cracking of Steels During Galvanizing. GalvaScience LLC, Springfield, Alabama, 2006

11. Koenigs, et al., Fatigue Resistance of Traffic Signal Mast-Arm Connections. Texas Department of Transportation, Research Report 4178-2, Center for Transportation Research, August 2003.

12. Lynn, P., Fuerst, W., Introductory digital signal processing with computer applications, Second Edition, John Wiley, 1998.

13. Miner, M.A., Cumulative Damage in Fatigue, Journal of Applied Mechanics, pp. 159-164, 1945.

14. Pool, C.S., Effect of Galvanization on the Fatigue Strength of High Mast Illumination Poles, The University of Texas at Austin, Master's Thesis, 2010.

15. Rios, C.A., Fatigue Performance of Multi-Sided High-Mast Lighting Towers. M.S. Thesis, Department of Civil Engineering, The University of Texas at Austin, May 2007.

16. Stam, A.P., Fatigue Performance of Base Plate Connections Used in High Mast Lighting Towers. M.S. Thesis, Department of Civil Engineering, The University of Texas at Austin, May 2009

17. Warpinski, M.K., The Effect of Base Connection Geometry on the Fatigue Performance of Welded Socket Connections in Multi-sided High-mast Lighting Towers, Department of Civil Engineering, Leigh University, May 2006

Vita

Luca Magenes was born in Pavia, Italy. After completing his Bachelor's in Civil Engineering at The University of Pavia in 2008, he enrolled in the University of Texas at Austin to pursue a Master's Degree.

Contact: luca.magenes@gmail.com

This thesis was typed by the author.